Thermal Modeling of Shape Memory Alloy Wire Actuators for Automotive Applications

by

Huilong Ma

A thesis
presented to the University of Waterloo
in fulfillment of the
thesis requirement for the degree of
Master of Applied Science
in
Mechanical Engineering

Waterloo, Ontario, Canada, 2010

Author’s declaration

I hereby declare that I am the sole author of this thesis. This is a true copy of the thesis, including any required final revisions, as accepted by my examiners.

I understand that my thesis may be made electronically available to the public.

Abstract

Shape Memory Alloy is an amazing material, which can "remember" and return to its original shape when heated due to its temperature dependent phase transformation. Shape Memory Alloy wire has significant potential for application in the automobile industry due to its high ratio of energy / weight and silent actuation. However, a dependable method to measure the operating temperature of SMA wire and a reliable heat transfer model to characterize the dynamics of the SMA wire limit its widespread use in the automobile industry. This thesis presents a detailed description of the work performed to develop a reliable method for determining surface temperature of current carrying SMA wires and the development of a heat transfer correlation for natural convection cooling of heated SMA wires. The major findings of the research are as follows:

When a spot welded thermocouple measures the temperature of a current carrying SMA wire, there is a "spurious voltage" ΔV added to the thermo electro-motive force (EMF) of the thermocouple as a result of a voltage drop across the two points of contact that the thermocouple wires make with the SMA wire. This leads to an erroneous temperature reading that can be higher or lower than the actual temperature depending on the direction of current flow. When the carrying current is reversed in direction, the "spurious voltage" becomes $-\Delta V$ allowing a correct temperature reading to be obtained by averaging the readings based on opposed current flow.

A two-step spot welding procedure for attaching thermocouples to SMA wire can eliminate the influence of the "spurious voltage" in the temperature reading. By spot

welding the thermocouple wires onto the SMA wire one by one, the thermocouple lead offset is eliminated and the thermocouple provides an accurate point source reading.

Infrared thermal imaging can be a good supplement in the experiment to monitor errors in temperature readings from thermocouples. Due to the curvature of the SMA wire, the temperatures of the locations on the SMA wire that are the closest to the infrared camera represent the temperature of the SMA wire. So a line analysis across the SMA wire on the software "ThermaCAM" is required to determine the temperature of the SMA wire by infrared thermal imaging and the highest temperature on the line is the temperature of the SMA wire.

A new natural convective heat transfer correlation comprising the inclination angle φ is developed based on experimental results, which can be used to predict the temperature of a SMA wire given its diameter and inclination angle.

The comparisons show that the new correlation agrees with existing correlations in a vertical orientation and for small Rayleigh numbers ($0.001 < Ra_D < 0.05$) in the horizontal orientation. The correlation developed in this work for horizontal orientation tends to overestimate values of Nusselt numbers as predicted in other correlations when the Rayleigh number is high ($0.05 < Ra_D < 0.6$). It is speculated that this overestimation can be attributed to a temperature distortion associated with thermocouple measurement at or near ambient pressure conditions.

Acknowledgements

I would like to express my sincerely appreciation to Professor Richard Culham (MME) and Professor Robert Gorbet (ECE) for giving me the opportunity to work on this project and valuable directions in my work. I also want to thank Professor Pete Teertstra (MME) for sharing his extensive experience in laboratory techniques, which is a very important part of my work. I would also like to thank all those who provided training, advice and guidance throughout the course of my program.

Dedication

To all of my family members, for their warm support.

To everybody I worked with in this project, from whom I learnt.

Table of Contents

List of Figures

List of Tables

Nomenclature

A	area, m^2
A_s	surface area, m^2
C_p	constant pressure specific heat, $kJ/(kg \cdot K)$
D	characteristic length, m
d	diameter of SMA wire, m
e	emissive power (usually with a subscript), W/m^2, without a superscript e is usually the exponential function
g	gravitational acceleration, m/s^2
Gr_D	Grashof number
h	convective heat transfer coefficient, $W/(m^2 \cdot K)$
i	radiation intensity, $W/(m^2 \cdot sr)$
i_λ	spectral radiation intensity, $W/(m^2 \cdot \mu m \cdot sr)$
I	electric current, A
k	thermal conductivity, $W/(m \cdot K)$
L	length, m
l	length, m
M	molar mass, $kg/kmol$
Nu_D	Nusselt number
P	pressure, Pa
Pr	Prandtl number
q	energy flux, energy per unit area and per unit time, W/m^2
q_o	radiosity, W/m^2
q_i	incident heat flux, W/m^2
Q	heat transfer rate, W
Q_{conv}	heat transfer rate through convection, W
Q_{cond}	heat transfer rate through conduction, W
Q_{rad}	heat transfer rate through radiation, W
R	gas constant, $kJ/(kg \cdot K)$
Ra_D	Rayleigh number
R_u	universal gas constant, $kJ/(kmol \cdot K)$

T temperature, *K*

T_m mean temperature, *K*

T_s surface temperature, *K*

T_{ss} steady-state temperature, *K*

T_∞ ambient temperature, *K*

V electric voltage, *V*

Z compressibility factor

Greek Letters

β volumetric expansion, *1/K*

ε emissivity

θ zenithal angle, *rad or degree*

λ wavelength, μm

μ dynamic viscosity, *kg/(m·s)* or $N{\cdot}s/m^2$

ν kinematic viscosity, = μ/ρ, m^2/s

ρ density kg/m^3

ρ liner resistance of wire, Ω/m

ρ reflectivity

σ Stefan-Boltzmann constant, 5.67 x 10^{-8} $W/(m^2{\cdot}K^4)$

φ azimuthal angle, *rad* or *degree*

φ inclination angle, *rad* or *degree*

Chapter 1

Introduction

1.1 Background

Shape Memory Alloys (SMAs) are amazing and unique materials. After being deformed, they can "remember" and recover their original shape when the temperature is increased. According to Otsuka and Wayman (1998) **[1]**, Arne Olander was the first who observed the pseudo elastic behavior of the Au-Cd alloy in 1938. Kurdjumov and Khandros **[2]** conducted experiments on CuZn and CuAl alloys and introduced the concept of thermo elastic martensitic transformation to explain the reversible transformation of martensite. The real breakthrough in the research and the application of shape memory alloys is the discovery of NiTi by Buehler *et al.* **[3]** in 1963. The term "NiTiNOL" was named after that in memory of their works in Naval Ordnance Laboratory (NOL). Since that time, a series of new shape memory alloys were investigated and adopted in commercial applications. In 1971, Cryofit, the first SMA material, was used to join titanium tubing on the U.S. Navy / Grumman F-14A **[4], [5]**. The NiTiNb systems were widely used in nuclear reactors to repair battle damage **[6]**. High Temperature SMA (HTSMA), such as TiPd, TiPt and TiAu, which possess transformation temperatures greater than 100 ^{0}C, were developed in earlier 1970's **[7]**. In 1999, Miyazaki *et al.* **[8]** improved NiTiCu alloys. The improved fatigue life and low cost of this new material made it suitable for a wide variety of engineering applications.

There are other types of SMA besides NiTi, such as: CuZnAl, CuAlNi, CuAlMn, CoNiAl, NiMnGa, etc.

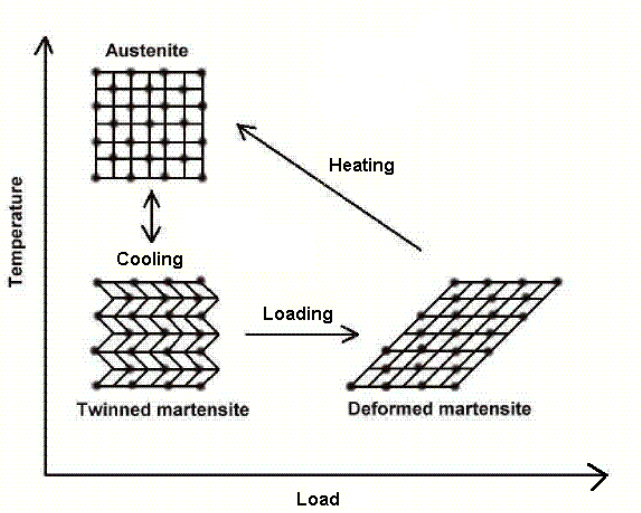

Figure 1-1 Microscopic Diagram of the Shape Memory Effect

Two major characteristics of shape memory alloys are shape memory and pseudo-elasticity. Studies of micro structure shows: SMA has two different temperature-dependent crystal structures (or phases). One is martensite which exists at low temperature; the other is austenite that exists at higher temperature. The austenite is usually called the parent phase. It is the two different phases and a solid to solid phase transition that gives rise to these special characteristics of SMA. As shown in **Figure 1-1[9]**, at low temperature, SMA exists in the twinned martensite form. When a load is applied to the SMA, it undergoes a macroscopic shape change and its micro structure changes to the deformed martensite in which its molecules are no longer twinned. When being heated, a reverse phase transformation (from detwinned martensite to austenite) occurs which leads to a complete shape recovery. Cooling of the SMA causes the

formation of twinned martensite again with no associated shape change is observed. This process is called shape memory effect (SME).

For many years, shape memory alloys have been a good choice for engineers and other designers who apply the shape memory effects to convert thermal energy into mechanical work. They have a variety of applications in aerospace, medicine and transportation. In aerospace, they have been used in the Smart Wing program and the Smart Aircraft and Marine Propulsion System demonstration (SAMPSON) **[10],** Rotorcraft **[11]** and the low-shock release mechanism in satellites **[12]**. In the field of medicine, SMAs can be used in Orthodontic applications, Cardiovascular applications, Orthopedic applications and Surgical Instrument applications. In transportation, SMAs have been used for applications ranging from impact absorption to sensing and actuation, such as: deployment of a protective panel; actuating blinds that cover the fog lamp to prevent damage; and SMA spring-actuated valves to adjust the oil level in the gearbox **[13]**.

1.2 Motivation for the Current Work

Shape memory alloy (SMA) actuators can be an ideal substitution for more traditional actuators (e.g., magnetic solenoid) due to their unique "shape memory" property. Low cost, light weight, scalable and having a high power/weight ratio, these actuators are promising in a variety of mechanical systems, particularly in the automotive industry. The grill of the louver in front of a car, for instance, can be opened and closed using the shape memory alloy thus enabling you to control the aerodynamics of a car. Springs made from shape memory alloys can be used as sensor-actuators in pressure control valves or oil cooler bypass valves in automatic transmissions. Shape memory alloys can

even be designed to capture heat energy from engine exhaust gases via an electric generator and transfer that energy to recharge batteries for hybrids or next generation electric vehicles. With more and more scientists and engineers investigating this material, shape memory alloy components are becoming increasingly popular for automotive applications.

1.3 Problem Statement

SMA actuators rely on a reversible, thermally-driven phase transformation which occurs as the alloy temperature is cycled between approximately 30 ^{0}C and 100 ^{0}C. The difference in mechanical properties of the two material phases can be used to do mechanical work. Notably, the NiTi SMA commonly used for actuation has a relatively high electrical resistivity, enabling the design of electro-mechanical actuators using SMA. An actuator design typically comprises a biased wire made of SMA, which contracts in the presence of an electrical current, and expands as it cools when the current is removed. The actuator behavior can be roughly divided into the thermo-electric heating response which converts electrical to thermal energy and generates the phase transformation, and the thermo-mechanical phase transformation which causes the motion.

A good numerical thermo-electrical model of SMA wire is very important to protect this material from overheating, while achieving maximum performance. The thermo-electrical process starts from Joule heating when a current passes the SMA wire, undergoes heat exchange with environment and eventually obtains heat equilibrium. This process may be incorporated with a phase transformation when the SMA wire

temperature goes above the transition temperature T_{As} at which martensite changes to austenite. In the whole process, the temperature of the SMA wire increases from the room temperature along a power curve, probably hesitates when phase transformation occurs, and in the end reaches a balanced temperature. In order to accurately model the thermo-electrical behavior of SMA wire, it is necessary to develop a reliable technique to measure the temperature of SMA wire and to understand clearly the mechanisms whereby the SMA wire exchanges heat with the environment.

This work is divided into two parts. The first part focuses on the efforts to experimentally investigate appropriate temperature measurement techniques, and the development of reliable thermocouple-based methods. The measurements are developed for the validation of thermo-electric models for SMA wire heating in the laboratory, so a reasonable level of accuracy and precision is desirable. In addition, the eventual approach may also be used in direct temperature measurement in an end application, for direct temperature control of the SMA actuator. In the second part, the existing natural convective heat transfer correlations of different orientations were studied and analyzed. Due to differences in experimental conditions, these existing correlations are not applicable to the design condition stipulated for this work; however they provide useful information for the development of new heat transfer models.

1.4 Overview

In chapter 2, different available methods of temperature measurement will be reviewed. The studies of temperature measurement in different categories from researchers will also be analyzed, that include: invasive, non-invasive and semi-invasive methods. The

knowledge about temperature measurement will be used to develop experimental methods to measure the temperature of SMA wire. After this, the existing heat transfer correlations for natural convection from slender cylinders will be reviewed. Methods for determining the applicable Rayleigh number (*Ra*) and Nusselt number (*Nu*) range, the fluid type, and the diameter of the cylinder will be examined. The review helps to determine if these correlations can be applied in this work directly or they can only be the reference to a new correlation.

In chapter 3, infrared thermal imaging will be studied. The basic principle of thermal radiation and the structure of the IR camera will be reviewed. The problems that occur when using an IR camera to find out the temperature of SMA wire will be investigated, such as: the emissivity of SMA wire; the correct location to determine the temperature of SMA wire; and the verification of the IR camera.

In chapter 4, the two step spot welded thermocouple will be introduced. This includes: the problems encountered when deploying spot welded thermocouple to measure a current carrying wire; the theory of the effective voltage of a thermocouple; and a series of experiments that result in the improved two step spot welded thermocouple.

Chapter 5 will discuss the experimental method to examine the effect of other parameters on convection and to determine a new heat transfer correlation, which includes: the overview of the experiment, the SMA wire setup on fixture, the experiment setup diagrams, the experimental equipments, the experiment procedures and the uncertainty errors in the experiment.

Chapter 6 presents the results and discussion of the experiments and consists of three sections. In the experimental data reduction section: the experimental data are processed

and presented in tables and figures. Based on these figures, a new convective heat transfer correlation is developed in the second section. A comparison of the new correlation to existing correlations in the horizontal and vertical orientations are performed and discussed. In the last section, three examples are used to demonstrate how to predict the temperature of SMA wire through the new correlation.

Chapter 7 gives the conclusions and recommendations.

Chapter 2

Literature Review

Shape Memory Alloy materials are becoming more prevalent in many engineering applications such as switches and actuators as a low cost alternative to more elaborate and complex systems. As new materials are developed with unique thermophysical properties, it is imperative that measurement techniques be developed that allow for accurate and reliable assessment of these properties. In certain instances new measurement procedures may need to be prescribed where there has been little activity in the past, however, in many instances a review of the open literature will provide valuable insight into procedures that can potentially be adapted to temperature measurement in current carrying SMA wires. The following review is a non-exhaustive examination of measurement techniques commonly used to determine surface temperatures of objects with relatively small characteristic length scales, such as wires and thin films. In addition, the literature review will examine empirically derived heat transfer correlations that have been developed for natural convection heat transfer from similar objects such as wires and circular cylinders.

2.1 Review of Temperature Measurement

The topic of temperature and temperature measurement has garnered much attention over the past several centuries. Although fundamentally simple in its concept, temperature measurement can be challenging, especially when trying to isolate localized temperature fields over small domains, such as wires and ribbons with characteristic

lengths in the sub-millimeter range. For these micro-scale applications, conventional methods of temperature measurement often do not provide satisfactory results, primarily due to effects of scale such as lead losses and contact resistance in contact methods, and domain resolution in non-contact methods.

Typically temperature cannot be measured directly relying instead on measuring the effects of some other physical phenomena and then relating this to temperature. Even our most fundamental methods of temperature measurement such as a thermometer (volumetric expansion of a fluid), a thermocouple (Seebeck voltage induced in a couple of dissimilar metals) or resistance temperature detector (resistance change) depend on indirect methods of temperature detection. By the nature of contact between the medium of interest and the device, Childs **[14]** classified the various temperature measurement techniques into three categories: invasive; semi-invasive and non-invasive.

The purpose of this work is to determine SMA temperatures either directly or indirectly as the wire is transitioned through the austenitic/martensitic transformation regimes. Measurement constraints include accurate measurement of surface temperature at multiple points on SMA wires in the range of 0.3 – 1.0 *mm* diameter, with a current flow of up to 1.5 *A* and a temperature ceiling of approximately 150 ^{0}C. The following review describes several potential measurement techniques and critically examines their applicability to the measurement constraints listed above.

2.1.1 Invasive Temperature Measurement Methods

As the name implies, invasive techniques include a wide variety of measurement techniques where the detector or the transducer is in direct contact with the medium of

interest thereby "invading" the measurement field. In most situations, the act of measurement influences the measurement parameter of interest. Examples of invasive methods include: liquid-in-glass thermometers, bimetallic strips, thermocouples, resistance temperature detectors and gas thermometry.

2.1.1.1 Thermometers

Standard tube or capillary thermometers use a calibrated relationship between volumetric expansion of a fluid and heat input to determine temperature over a nominal range of interest. Typical fluids used in capillary tube thermometers include mercury or organic liquids such as alcohol.

Bimetallic thermometers rely on the fact that materials expand at different rates as they are heated. By attaching two dissimilar metals together to form a composite strip, a strain is introduced into the strip upon heating which can be calibrated to provide a measure of temperature. While these devices are not as accurate as thermocouples or RTDs and they do not readily lend themselves to temperature recording, they have found wide spread use in devices used to control temperature levels **[15]**.

Gas thermometry provides an accurate means of measuring temperature but tends to be a specialist activity and is usually confined to standards laboratories and cryogenic applications. The use of gas thermometry in applications requiring a high measure of certainty has been detailed by several other researchers including, Steur **[16]**, Steur and Pavese **[17]**, and Edsinger and Schooley **[18]**. Gas thermometers are generally not commercially available.

Unfortunately, thermometers do not generate data that are easily recorded or transmitted and they cannot easily be used to make spot or point measurements, effectively restricting their use for measuring temperatures in SMA wires and ribbons.

2.1.1.2 Thermocouples

Thermocouples are a common choice for temperature measurement because of their self-energization, low cost, robust nature and wide temperature range. Measurement accuracy is typically not as good as RTDs or thermistors but "as received" accuracies of 0.75 – 2.0 ^{0}C are typical and accuracies of 0.25 – 0.5 ^{0}C can be achieved with minor calibration corrections.

Like other solid bodies and surfaces, SMA wires and ribbons face the same problems when measuring their temperatures as Michalski *et al.* **[19]** described in their *Theory of the Contact Method.* They pointed out that temperature measurement of a solid surface has a series of possible errors that could contribute to deviations between a measured temperature and that of the undisturbed object. These errors include: *temperature distortion error* of the solid surface when introducing a probe; *contact thermal resistance error* between the solid surface and the probe; and *conduction thermal resistance error* in the probe. From the reviews below, we can conclude that choosing probes as thin as possible and making good thermal contacts between the solid surface and the probes can minimize all these systematic errors in temperature measurement of SMA wires and ribbons.

In respect to these three main errors: temperature distortion error, contact thermal resistance error, influence of current on thermocouple readings and system error of

thermocouple thermometry, numerous research initiatives have been conducted and the following methods have been proposed to eliminate or control these effects.

Temperature Distortion Error

Robertson **[20]** improved a surface temperature probe by utilizing a heater and a differential temperature measurement to control the heater so as to minimize the temperature gradient along the probe and temperature distortion on the surface as well.

Nakabeppu and Suzuki **[21]** developed an active method for temperature measurement with sub-micron resolution and a thermal feedback system. Similar to Robertson, this method can keep a sensor at the same temperature as the target by using a differential thermocouple and an electrical heater.

Ishihara *et al.* **[22]** investigated the measurement of surface temperature of burning solid using micro thermocouples. They found that the decrease in indicated surface temperature (temperature distortion) due to heat conduction through the leads was as large as 100 *K*, depending on the wire diameter, burning rate and lead wire angle.

Shaukatullah and Claassen **[23]** reviewed the effect of thermocouple size and attachment method on the measurement of surface temperature. They concluded that thermocouple wires with small diameter cross sections and low thermal conductivities are better for minimizing errors due to heat losses through the wires.

From the above works, we can see that several procedures can be used to minimize the temperature distortion error, such as: maintaining the probe temperature as close as possible to the surface temperature, placing lead wires as close as possible to the target

surface, and choosing small size thermocouples and low thermal conductivity thermocouple wire.

Contact Thermal Resistance Error

Renken **[24]** positioned a thermocouple adjacent the inner perimeter of a cavity and traversed the length of the cavity of the substrate, thereby enhancing the heat transfer efficiency from the substrate to the thermocouple.

Leath **[25]** recorded and controlled the temperature of a heater wire by pressing the thermocouple elements on the wire with a spring. They believed the thermal contact was improved in this way.

Shaukatullah and Claassen **[23]** concluded that using tapes and non-thermally conductive epoxy to attach thermocouples results in larger errors.

Anon **[26]** investigated thermocouple attachment methods in semiconductor manufacturing and chose cementing the thermocouple bead in a tapered hole in the wafer with improved reliability.

Sobolik *et al.* **[27]** used Unsteady Surface Element (USE) methods to model a thermocouple wire attached to a thin disk. They also assessed the effect of errors and thermal factors with mathematical techniques.

Dunstan *et al.* **[28]** measured temperature variations in NiTiNOL working elements during cycling using a copper constantan thermocouple made from stripped 0.33 *mm* diameter wires spot-welded onto one of the elements. They found the effectiveness of the operation of the engine was strongly dependent upon the diameter of the NiTiNOL working elements and the performance was excellent with 1.23 *mm* diameter. By

embedding a thermocouple in a hole spark-machined through 0.75 *mm* of the wire diameter at the point of maximum curvature and comparing the centre and corresponding surface temperature profiles, they also suggested that the surface temperatures, which are easier to measure, are adequate for analyses of engine characteristics.

Thermally conductive epoxy can be used in our experiment; presses can also be applied on the sensors against the target surface to make sure they are closely contacted. Spot welding methods have higher thermal conduction than other methods if ignoring the influence of current on thermocouple readings. Though some results or conclusions may not be used in this study, all of these experiments provided valuable information on how to improve thermal contact between the thermocouples and the target surfaces.

Influence of Current on Thermocouple Readings

Volkov **[29]** proposed that thermocouple readings can be affected by current in such a way as to add an effective voltage ΔV to the thermo electro-motive force (EMF) of the thermocouple if it has direct contact with the current carrying surface. He studied this influence in an experiment in which 10 thermocouples were attached to a 0.7 *mm* diameter 650 *mm* long steel wire with three different attachment methods: direct attachment of the thermocouple by spot welding, indirect attachment using a Teflon tube or a film of mica. He concluded that the influence of current on thermocouple readings was a function of the voltage gradient along the current carrying surface. Without properly handling this error, it is impossible to obtain a true temperature of the SMA wire.

System Errors of Thermocouple Thermometry

Zanstra **[30]** developed a junction welding technique that enabled the thermocouples to present a very uniform time response. If rapidly fluctuating temperatures are to be compared, sensors should have small and identical time responses. Thermocouples offer the advantage of minute size, small heat capacity and negligible heat flow to or from the measuring spot. However, characteristics of soldered and welded thermocouple junctions vary considerably. A technique is described for welding uniformly-sized, fine thermocouples, which are producible even by unskilled workers.

Wang *et al.* **[31]** presented a computerized calibration laboratory with automatic data acquisition capabilities and software for thermocouples and RTDs. With this system, for J- type thermocouples on three consecutive lengths, the reproducibility was ± 0.1 ^{0}F up to 500 ^{0}F and ± 0.7 ^{0}F at 1000 ^{0}F. For 100 *ohm* RTDs the reproducibility was 0.01 *ohm* (± 0.025 ^{0}C) at 0 ^{0}C and ± 0.04 *ohm* (± 0.1 ^{0}C) at 200 ^{0}C.

Maeno *et al*. **[32]** developed a simple differential thermometer using a thermocouple with a SQUID (superconducting quantum interference device) detector, which demonstrated a response time of 15 *ms* at 1 *K* and a temperature sensitivity of 10^{-7} *K* with a 10 *Hz* filter.

Sawada and Nishiwaki **[33]** conducted research on the accuracy and response of a thermocouple to transient temperature changes in an attached metal and demonstrated that the accuracy of temperature measurement can be estimated using a Fourier number

and can be improved by selecting suitable combinations of the two kinds of thermocouple wire and their diameters.

Suyama *et al*. **[34]** evaluated the calibration accuracy of R-type thermocouples through comparison with a platinum resistance thermometer. The mean deviation of each thermocouple is found to be about $-0.15\ ^{0}C \sim +0.10\ ^{0}C$ with a standard deviation of less than $\pm 0.05\ ^{0}C$ in the temperature range of $50\ ^{0}C \sim 950\ ^{0}C$.

Ancsin **[35]** studied the stability, reproducibility and accuracy of thermocouples and found that noble metal thermocouples can yield a thermoelectric temperature scale accurate within $\pm 0.1\ ^{0}C$ from room temperature to $962\ ^{0}C$ if they are calibrated after they have been heat treated into a reasonably stable thermoelectric state.

Cengel *et al.* **[36]** increased accuracy and resolution of thermocouples by using operational amplifiers to amplify the voltage signal before sending them to the computer.

The collection of technical papers cited above related to time response, stability, reproducibility and accuracy of thermocouples provide good suggestions on using thermocouples and eliminating systematic errors.

Another research worthy of mentioning is Rego *et al.* **[37]**, where he conducted in-situ temperature measurements of optical fibers subjected to electric arc discharges. In this work, temperature profiles in capillary and optical fibers were estimated by solving the classical heat transfer equations subject to data obtained from thermocouple measurements from fibers of various diameters. The coupling of empirical and analytical data provides an effective mechanism for predicting temperature distribution in fibers and wires of small diameter.

2.1.1.3 Resistance Temperature Detectors

RTDs (Resistance Temperature Detectors) have an advantage of high accuracy and good repeatability; however their relatively large size restricts their use in temperature measurement of wires and ribbons. The achievable uncertainty for a commercially available PRT (Platinum Resistance Thermometer) is generally of order of ± 0.01 ^{0}C to ± 0.2 ^{0}C over the range of 0 ^{0}C to 300 ^{0}C **[38]**. But in order to avoid the instability caused by mechanical shock and strain due to thermal expansion, the PRTs are inevitably constructed too bulky to be used for spot temperature measurement **[39]**.

2.1.1.4 Thermistors

Thermistors have very high sensitivities with values of the order of 50 $mV/^{0}C$, which is more than one hundred times that of PRTs and one thousand times that of thermocouples.

Thermistors can have either a negative temperature coefficient (NTC), where the resistance reduces with temperature, or a positive temperature coefficient (PTC) depending on the type of materials used. NTC thermistors are the most common and can operate at temperatures between – 200 ^{0}C and 1000 ^{0}C. PTC thermistors are not normally used in temperature measurement.

Commercial NTC thermistors can be broadly classified into two groups depending on how the leads are connected to the thermistor body: bead thermistors and metalized surface contacts. Types of bead thermistors include bare beads, glass coated beads, glass probes, glass rods and bead-in-glass enclosures. Metalized surfaced contact thermistor consists of a metalized body fired onto a ceramic thermistor material. A wide range of

metalized surface contact thermistors are available including disks, chips or wafers, surface mounts, flakes, rods, and washers.

The high sensitivity and fast response of thermistors make them ideally suited to precision temperature measurement where resolutions better than 5 μK can be obtained**[40]**. A thermistor could be the preferred choice over other thermometers for measuring temperatures of SMA wires and ribbons as long as sufficiently small bead thermistors can be found. Quality Thermistor Inc. can supply MINI BEAD 0.038" MAX OD thermistor with a tolerance ± 0.2 ^{0}C (0 ^{0}C to 70 ^{0}C) **[41]**. Honeywell can supply small thermistors with bead diameters of 0.014" **[42]**. Some specifications of products need to be verified and efforts should be made to assess the availability of smaller thermistors.

2.1.2 Semi-Invasive Methods

Semi-invasive temperature measurement techniques are classified here as those involving some form of treatment of the surface of interest such as the application of a temperature-sensitive paint and remote observation of the temperature dependent properties of the surface application.

A range of techniques have been developed including thermo-chromic liquid crystals, heat-sensitive crystalline solids and paints, thermographic phosphors and pyrometric cones.

2.1.2.1 Heat-Sensitive Crystalline Solids and Paints

Most temperature sensitive crystalline solids and paints melt on reaching a certain temperature and are used in the form of labels or pellets to indicate whether a particular process temperature has been attained. On heating these products above some critical temperature the indicator material melts, fuses or changes composition providing that a process temperature has been reached or exceeded.

2.1.2.2 Pyrometric Cones

Pyrometric cones and bars have been developed for the ceramics and glass industries to provide an indication of both firing time and temperature.

Heat-sensitive crystalline solids and paints and pyrometric cones cannot be used to measure the temperature of SMA wires or ribbons because they are developed to indicate a specific temperature and the evidential transformation in cones and paints is not reversible. In addition, pyrometric cones are too bulky to be considered in wire or ribbon applications.

2.1.2.3 Temperature Phosphors and Temperature-Sensitive Paints

Temperature phosphors and temperature-sensitive paints are materials that can be excited by the absorption of energy and subsequently emit light in a fashion inversely proportional to their temperature.

The thermographic phosphor thermometry technique can offer sensitivities of 0.05 ^{0}C and an uncertainty of 0.1 % – 5 % of the Celsius temperature reading **[43]**. Applications have included temperature measurements of flat plates in supersonic flows **[44]**, wind

tunnel models **[45]**, **[46]**, turbine blades and components **[47]**, **[48],** curved surfaces **[49]**, surface temperature fields **[50]**, color TV screens **[51]**, and textiles during microwave drying **[52]**.

2.1.2.4 Thermochromic Liquid Crystals

Thermochromic liquid crystals exhibit brilliant changes in color over discrete temperature bands. With a change in temperature, thermochromic liquid crystal mixtures will turn from colorless, black against a black background, to red at a particular temperature and then pass through the visible spectrum (red to orange to yellow to green to blue to violet) before turning colorless again.

Thermochromic liquid crystals have been widely used in the characterization of heat transfer on applications such as: turbine blades **[53]**, jet engine nozzles and vehicle interiors **[54]**. Simonich and Moffat **[55]** report a calibration uncertainty of ± 0.25 ^{0}C using mercury vapor lamp illumination. Ireland and Jones **[56]** demonstrated that liquid crystal formulations typically have a response time constant of 0.003 *s*.

Temperature phosphors and temperature-sensitive paints and thermochromic liquid crystals present high sensitivities and low uncertainties. They can be tried in our work to measure the temperature of SMA wires and ribbons, although the effect of illumination conditions and the process of calibrating the acquired image to temperature will be important to understand.

2.1.3 Non-Invasive Methods

Non-invasive techniques are those where the medium of interest is observed remotely. Infrared thermometry is the most widely used form of non-invasive temperature measurement. A number of other non-invasive measurement techniques have also been developed in addition to the infrared methods which are particularly useful for monitoring gas or plasma temperatures. These non-invasive techniques are based on observing the variation of refractive index, absorption or emission spectroscopy, scattering, fluorescence and acoustics.

Infrared thermometers can be broadly classified into the following categories **[57]**:

- spectral band thermometers
- total radiation thermometers
- ratio thermometers
- multi-waveband thermometers
- special-purpose thermometers and methods
- thermal imagers

Spectral band thermometers are the most common form of infrared temperature measurement. They measure radiant energy across a relatively narrow band of wavelengths somewhere within the range 0.5 μm to 25 μm. In this spectral region, short wavelengths have the advantage that the rate of change of radiant energy with temperature is high (up to 2 % – 3 % ^{0}C) and they are highly sensitive.

Total radiation thermometers measure the total radiance of a surface. As a broadband of wavelengths will contain a large amount of energy at any temperature these are normally used for general purpose or low-temperature application temperature measurements where the energy emitted is relatively low.

Ratio thermometers, which are also known as dual-wavelength or two-color thermometers, measure the radiance at two wavelengths and determine the ratio. The advantage of ratio thermometers is that it is not necessary to know the emissivity of the target. However they are less sensitive than spectral band thermometers.

Multi-waveband thermometers allow measurement of surface temperature when the emissivity is not constant at different wavelengths. Special-purpose infrared thermometers and methods include auxiliary reflector methods, hot surface methods, polar radiometer methods, reflectance methods, temperature-invariant methods and fiber-optic thermometers. These techniques have been mostly developed in an attempt to provide a measurement of temperature that is independent of emissivity.

Thermal imagers can be used to measure the temperature distribution over a target area. The use of a thermal image to provide quantitative information for the temperature distribution, particularly of a surface comprising different material, has to be carefully managed. Without correction for local emissivity values, the thermal imager will assume a default value and apply this to the whole image.

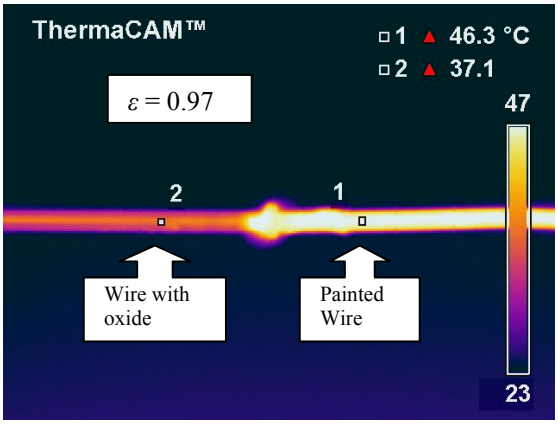

Figure 2-1 Infrared Thermal Imaging of SMA Wire by FLIR ThermaCam S60

In **Figure 2-1**, the emissivity setting on the IR camera is set to 0.97 and the temperatures at point 1 and point 2 are 46.3 ^{0}C and 37.1 ^{0}C. As you will read in **Section 3.3.1**, point 1 and point 2 should have the same temperature, but with different emissivity. So when they are checked by an IR camera with a fixed ε = 0.97, the temperature difference can be 9.2 ^{0}C.

Generally, if a good contact thermometer can be used for the application it is certainly capable of higher accuracy than a radiation thermometer in the same situation **[58]**. When choosing a radiation thermometer, the specifications need also to be considered include: temperature range, accuracy, operating wavelength, field of view, response time, mode of readout, application/manufacturer and calibration, besides emissivity.

The FLIR ThermaCAM S60 equipped with a zoom lens provides all the necessary features for measuring surface temperatures of SMA wires and ribbons, as required in our application. This thermal camera has a 320 x 240 detector, standard temperature range 0 − 500 ^{0}C and an accuracy of 2 % (typically 2 ^{0}C) **[59]**. When equipped with a FLIR 50

Micron Macro Lens, which has a close focus of 14.3 x 10.8 *mm*, **[60]** the FLIR ThermaCAM S60 has a resolution of 0.045 *mm*/*pixel*.

Other research initiatives on radiation thermometry discussing the measurement of temperature of small-scale objects are also reviewed.

The Exergen Company **[61]** used an infrared thermocouple, which emulates a K-type thermocouple, to measure the temperature of a bare cable in preparation for subsequent treatment of the cable with a plastic coating. The problem with this method is the relatively large spot size of the sensor compared with our wire diameter.

Borca-Tascius and Chen **[62]** employed photo-thermal radiometry to measure the temperature of fine wires with an accuracy of 1 % to 2 %, which is of the same order of magnitude as the accuracy of contact methods.

Moron *et al*. **[63]** obtained local temperature values by measuring the intensity of infrared emission of the sample. It is a good reference for constructing a relation between temperatures and other parameters such as current, power, etc.

Shimizu *et al.* **[64]** combined thermo reflectance and RTDs in their work to measure the temperature of micro-scale metal thin films. This method has a 0.2 ^{0}C temperature resolution and a 1 μm spatial resolution at a visibility of 100 %.

Iadicola *et al.* **[65][66][67]** combined an infrared imaging camera and K-type thermocouples to monitor the change of temperature along an SMA wire (using a small quantity of a thermally conductive paste). In order to ensure accuracy, the thermocouples were calibrated to ASTM certified thermometers at two calibration temperatures. The thermal imaging camera calibrates the emissivity of the specimen by comparing to the

thermocouple readings. In this way, they believed the infrared images provide an accurate measurement to within ± 1 ^{0}C in absolute temperature and within about ± 0.2 ^{0}C in differential temperature.

2.2 Review of the Existing Heat Transfer Correlations

Numerous works have been performed to investigate natural convection heat transfer from slender cylinders in different orientations including: horizontal, vertical and various angles in between, as shown in **Figure 2-2**. Many empirical correlation equations have been developed based on experimental data, theoretical deduction or numerical calculation. Studying and understanding these correlations is necessary in this work. Some of these correlations can be used to model heat transfer from current carrying SMA wire; while others that may not be directly applicable to SMA wire can be used as reference material in the development of new correlations.

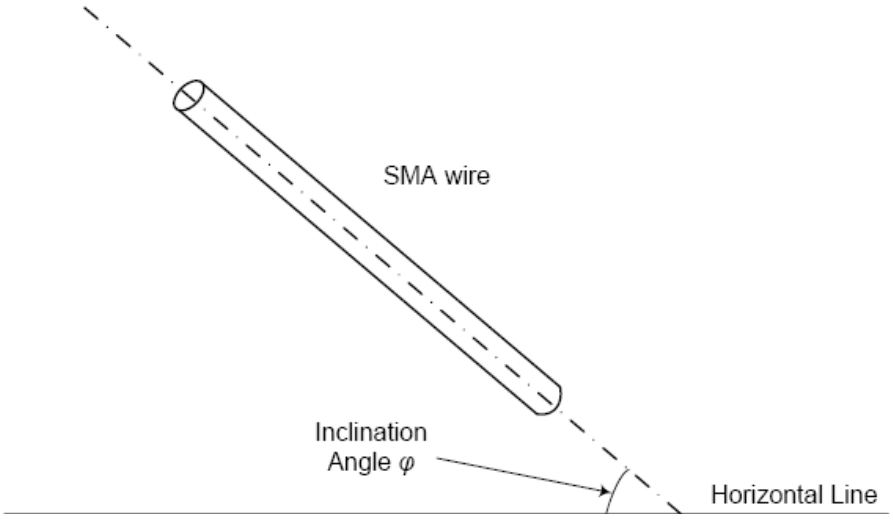

Figure 2-2 Inclination Angle φ

2.2.1 Horizontal

Jaluria **[68]** derived the average Nusselt number Nu_D by using an integral method, which can be applied to a range: $10^{-10} < Ra_D < 10^7$, in **Equation 2-1**.

$$Nu_D = \frac{2}{\pi}\int_0^{\pi/2} Nu_D\left(\frac{x}{D}\right)d\left(\frac{x}{D}\right) = F(\mathrm{Pr})(Ra_D)^{1/4} \tag{2-1}$$

where: $F(Pr) = F(0.7) = 0.436$.

Tsubouchi and Masuda **[69]** developed a correlation of Nu_D - Ra_D ($10^{-6} < Ra_D < 10$) as shown in **Equation 2-2**, based on experiments, in which oil was used as the fluid and the cylinder diameter range was $0.015 - 0.063$ *mm*.

$$Nu_D = 0.36 + 0.56Ra_D^{0.25} \tag{2-2}$$

As a result of the survey of a large number of experimental investigations, Morgan **[70]** suggested a set of correlations for calculating heat transfer from long horizontal cylinders as in **Equation 2-3**.

$$Nu_D = 0.675Ra_D^{0.058}, Ra_D = 10^{-10} - 10^{-2}$$

$$Nu_D = 1.02Ra_D^{0.148}, Ra_D = 10^{-2} - 10^{2} \tag{2-3}$$

$$Nu_D = 0.85Ra_D^{0.188}, Ra_D = 10^{2} - 10^{4}$$

Churchill and Chu **[71]** used a theoretical deduction method and gave a correlation for $Ra_D > 10^{-6}$, as in **Equation 2-4**, which can be used for both laminar and turbulent flow regimes: But they didn't specify the applicable range of cylinder diameter.

$$Nu_D = \left\{ 0.6 + \frac{0.387 Ra_D^{1/6}}{\left[1 + \left(\frac{0.559}{\mathrm{Pr}} \right)^{9/16} \right]^{8/27}} \right\}^2 \tag{2-4}$$

Raithby and Hollands **[72]** performed analysis on the thin-layer of laminar and turbulent flows at a constant temperature of the surface of the cylinder and obtained the following correlation in the Rayleigh number range $10^{-2} < Ra_D < 10^{12}$:

$$Nu_D^{3.337} = [2/\ln(1 + \pi/1.294^{3/4} C_l Ra_D^{1/4})]^{3.337} + (0.72 C_t Ra_D^{1/3})^{3.337} \tag{2-5}$$

where, $C_l = 0.50[1 + (0.49/\mathrm{Pr})^{9/16}]^{-4/9}$, $C_t = [0.14\,\mathrm{Pr}^{0.084}, 0.15]^*$

The operator "[,]*" means that [A, B]* = B if A ≤ B and [A, B]* = A if A > B. Here Pr = 0.7, so $C_t = [0.14 \cdot 0.7^{0.084}, 0.15]^* = [0.1359, 0.15] = 0.15$.

A graphical representation of these correlations is shown in **Figure 2-3** when. *Pr* = 0.7. Due to the different methods used and also due to the different situations in each case, the correlations are not exactly the same.

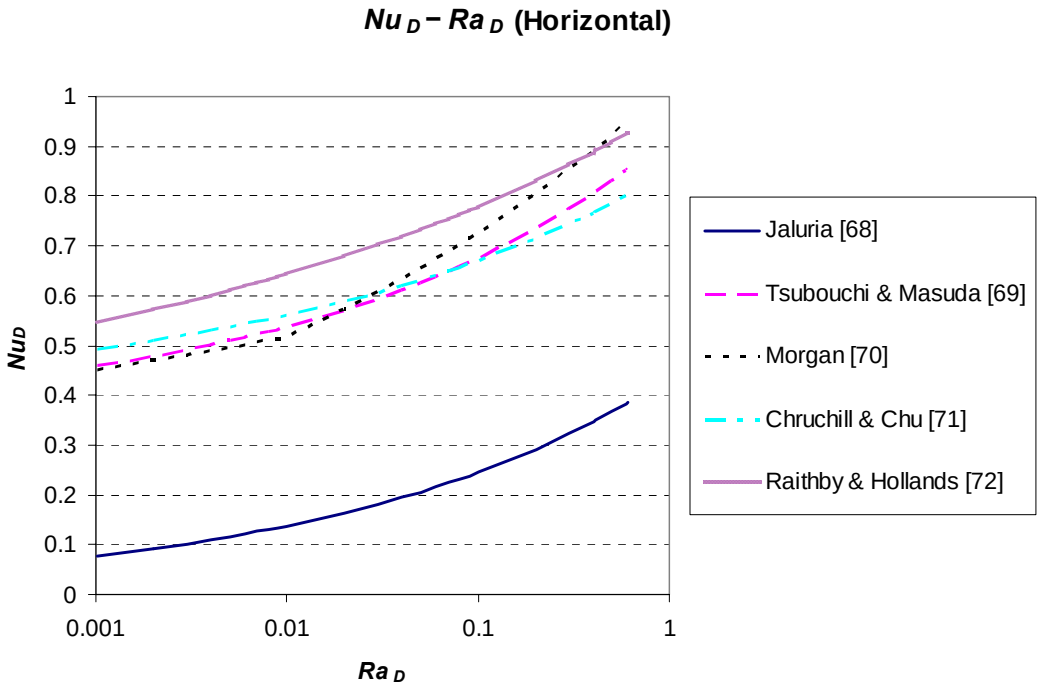

Figure 2-3 Correlations of Nu_D vs Ra_D for Horizontal Slender Cylinders

2.2.2 Vertical

In the vertical orientation, Elenbass **[73]** started with the correlation for a horizontal cylinder, he derived a theoretical equation, as in **Equation 2-6**, for average laminar natural convection from a vertical cylinder by analogizing a vertical cylinder to a vertical plate, without specifying the applicable Rayleigh number range.

$$Nu_D \exp\left(-\frac{2}{Nu_D}\right) = 0.6\left(Ra_D \frac{D}{L}\right)^{0.25} \tag{2-6}$$

Yang **[74]** suggested a general empirical equation with constant wall temperature that applies to all Prandtl numbers and Rayleigh numbers. But in the laminar region, it has big

differences when compared to the experimental data. The length / diameter ratios (L / D) of test cylinders in the experiments are also smaller than the SMA wire in this work.

$$Nu_D = 0.36 + \frac{0.670\left(Ra_D \frac{D}{L}\right)^{0.25}}{\left[1+\left(\frac{0.492}{\mathrm{Pr}}\right)^{9/16}\right]^{4/9}} \tag{2-7}$$

Koch **[75]** proposed a correlation based on experimental data for diameters from 14 *mm* to 100 *mm*, the length / diameter ratio from 20 – 152, and Ra_D (L / D) from 10^9 to 10^{11}.

$$Nu_D = 0.00562\left(Ra_D \frac{L}{D}\right)^{0.312} \tag{2-8}$$

Mueller **[76]** also gave a similar formula but for lower Ra_D ranging from 10^{-6} to 10^{-2}.

$$Nu_D = 1.0(Ra_D)^{0.11} \tag{2-9}$$

Zitsev *et al.* **[77]** investigated the heat transfer in a gas of a very thin vertical wire (D = 10 – 100 μm, Ra_D (D /L) = 10^{-11} – $10^{-4.5}$) through which an electric current flows and obtained the **Equation 2-10** with accuracy within 2 %:

$$\frac{2}{Nu_D} = \ln\left[1+\frac{4.47}{\left(Ra_D \frac{D}{L}\right)^{0.26}}\right] \tag{2-10}$$

Equation 2-6 to **Equation 2-10** are plotted when D = 0.5 *mm*, L = 250 *mm*, Pr = 0.7 as shown in **Figure 2-4**.

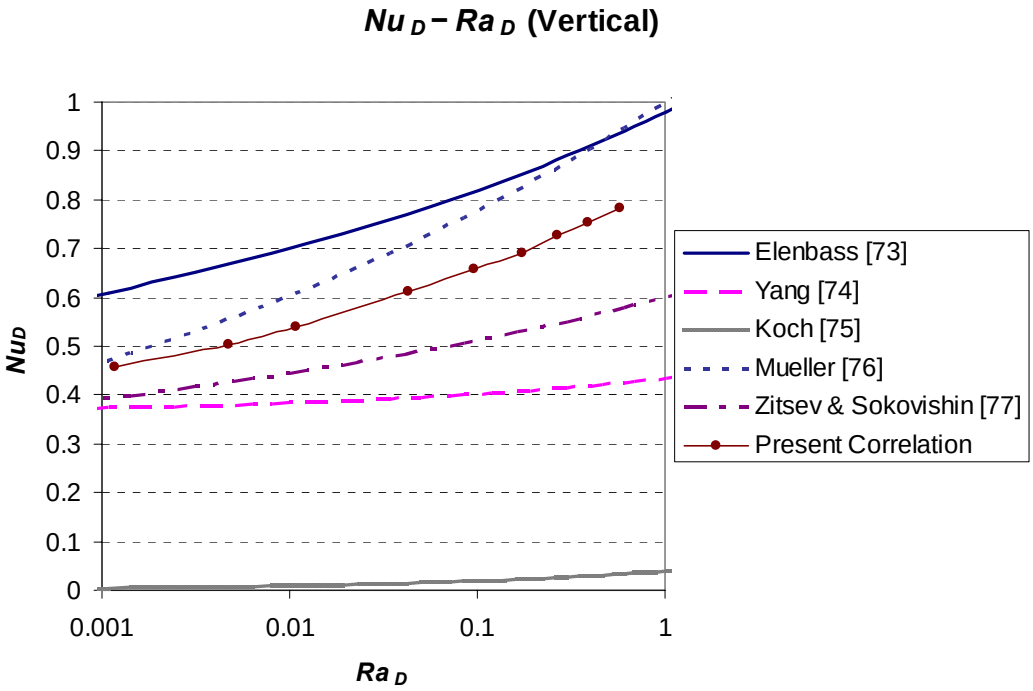

Figure 2-4 Correlations of Nu_D vs Ra_D for Vertical Slender Cylinders

Generally, **Figure 2-3** and **Figure 2-4** have the same trend when Ra_D increases, but Nu_D is higher when the wire is horizontal compared to a vertical orientation. This also leads to another conclusion where Nu_D changes when the wire is inclined at an angle from horizontal.

2.2.3 Inclined Wire

Oosthuizen **[78]** studied flow over an inclined circular cylinder of lengths between 152.4 and 304.8 *mm* and outside diameter between 19.1 and 25.4 *mm*. The results showed that the heat transfer coefficient decreases with increasing angle of inclination φ (wire and horizontal).

In Oosthuizen's result, the Grashof number for an inclined cylinder is determined by the **Equation 2-11**:

$$Gr_D = \frac{g\beta(T_s - T_\infty)D^3 \cos\varphi}{\nu^2} \tag{2-11}$$

In air when $Pr = 0.7$ the following dimensionless dependence can be used to describe the correlation of Nu_D and Ra_D:

$$\frac{Nu_D}{\left(\frac{Ra_D}{0.7}\cos\varphi\right)^{1/4}} = 0.42 \qquad \text{when } L^* > 10 \tag{2-12}$$

$$\frac{Nu_D}{\left(\frac{Ra_D}{0.7}\cos\varphi\right)^{1/4}} = 0.55, \qquad \text{when } L^* < 1 \tag{2-13}$$

$$\frac{Nu_D}{\left(\frac{Ra_D}{0.7}\cos\varphi\right)^{1/4}} = 0.42\left[1+\left(\frac{1.31}{L^{*0.25}}\right)^8\right]^{0.125} \qquad \text{when } 1 < L^* < 10 \tag{2-14}$$

where, $L^* = \frac{L}{D \cdot tg(\varphi)}$, and the Ra_D is from 2.8×10^4 to 6.3×10^4.

In this case, as $L = 250\ mm$, $D = 0.5\ mm$ and $Pr = 0.7$, $L^* > 10$ when $0 < \varphi < 88.9^0$. So it is reasonable to assume that **Equation 2-12** applies to any angle φ. **Equation 2-12** is plotted in **Figure 2-5**.

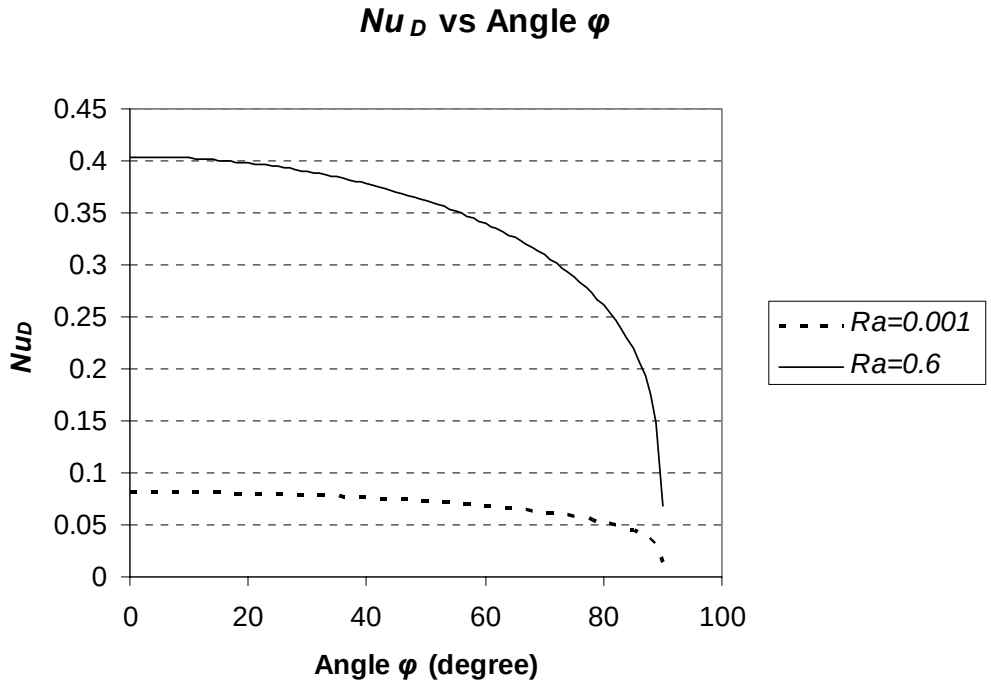

Figure 2-5 The Effect of Inclination on Nu_D for a Slender Cylinder

2.3 Summary of Literature Review

The Temperature Measurement

Thermocouples are more suitable in this work than other invasive methods such as: thermometers, thermistors or RTDs. A thermometer is large in size and is not capable of providing a recordable readout. A RTD is more accurate than a thermocouple, but it is usually much larger than a thermocouple and can not give an accurate temperature reading of a thin SMA wire or ribbon. A thermistor is also more accurate than a thermocouple, but the smallest available commercial thermistor is still five times bigger in diameter than the bead of a thermocouple. Though not as accurate as a RTD or a

thermistor, a thermocouple has an accuracy of 1 ^{0}C with an internal CJC (or an accuracy of 0.1 ^{0}C with ice point CJC and annual calibration). In addition, thermocouples are cheap, easy to fabricate in the lab and can be spot welded onto the SMA wire directly. The main drawback of a thermocouple is the temperature distortion that may be involved.

Infrared thermal imaging can not be the primary method to measure the temperature of the SMA wire in this work due to its low accuracy of 2 ^{0}C and the inability to provide a recordable readout for modeling. (by the current FLIR ThermaCAM S60). But infrared thermal imaging can be a good supplement to thermocouples because it does not need to contact object to give a temperature reading. This can be of great help when monitoring if there is any temperature distortions on the SMA wire, or any carrying current's influence on temperature readings.

The Existing Heat Transfer Correlations

There are very few correlations in the current literature that account for how the Nusselt number changes with the Rayleigh number when a wire (or a slender cylinder) is inclined from the horizontal. In order to predict the temperature of SMA wire and to characterize SMA wire, it is required to develop a new natural convection heat transfer correlation which comprises an inclination angle φ from the horizontal. Some correlations in the horizontal and vertical orientations were developed through different methods such as: theoretical deduction and numerical analysis, or based on the experimental data that are quite different from this work, but they can be good references to verify the new developed correlation as they are applicable over a similar Rayleigh number range with the new correlation.

Chapter 3

Infrared Thermometry in SMA Wire Application

3.1 Principles of Infrared Thermometry

Infrared thermometry is the most widely used form of non-invasive temperature measurement. Heat transfer can occur by means of three fundamental mechanisms: conduction, convection and radiation. The last form can be stated more fully as the transfer of heat energy by means of electromagnetic radiation, which is known as thermal radiation. The emission of energy in the form of electromagnetic radiation can be exploited to undertake a measurement of temperature. A typical infrared measurement system might comprise the source, the medium through which the radiant energy is transmitted, an optical system to gather the electromagnetic radiation, a transducer to convert the radiation into a signal related to temperature and amplification and interface circuitry to control, display and record the measurement.

3.1.1 Fundamentals of Thermal Radiation

Electromagnetic radiation consists of interacting self-sustaining electric and magnetic fields that propagate through vacuum at a speed of 299,792,458 *m/s*. It does not necessarily need a medium for transmission and can travel through vacuum or through a body of fluid.

The known electromagnetic spectrum comprises electromagnetic waves with wavelengths as illustrated in **Figure 3-1 [79]** The classifications are for convenience and the band between 0.1 μm and 100 μm is known as thermal radiation and that between 0.78 μm and 1000 μm as infrared radiation.

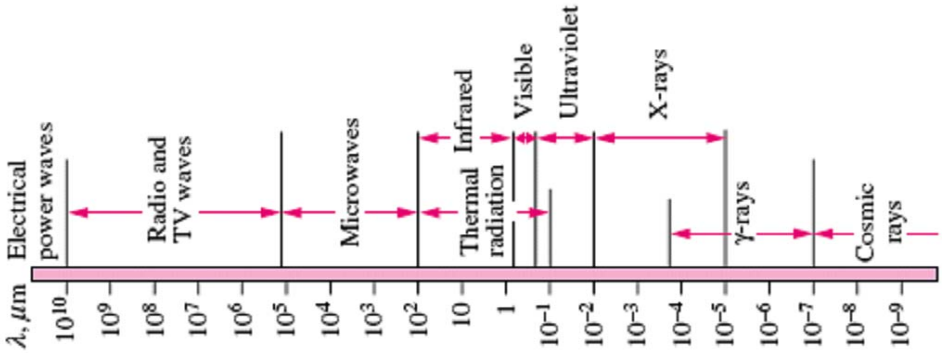

Figure 3-1 Electromagnetic Radiation Covers a Wide Range of Wavelengths

3.1.2 Lambert's Cosine Law

Lambert's Cosine Law can be expressed as:

$$e_{\lambda b}(\lambda,\theta,\varphi) = i_{\lambda b}(\lambda)\cos\theta = e_{\lambda b}(\lambda,\theta) \tag{3-1}$$

where: $e_{\lambda b}(\lambda,\theta,\varphi)$ is the energy emitted by a black surface per unit time within a unit small wavelength interval centred around the wavelength λ, per unit elemental surface area, and into a unit elemental solid angle centred around the direction (θ, φ).

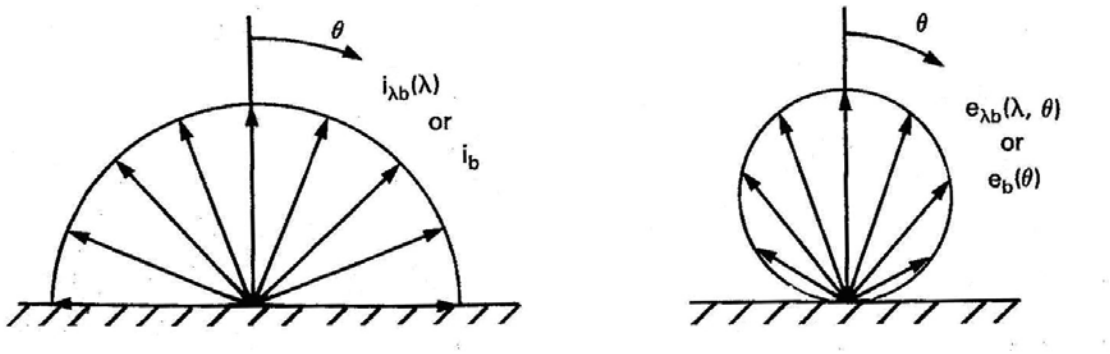

Figure 3-2 The Angular Distribution of Blackbody Intensity and Emissive Power

As shown in **Figure 3-2 [80]** Lambert's cosine law says that the total radiant power observed from a "Lambertian" surface is directly proportional to the cosine of the angle θ between the observer's line of sight and the surface normal. The law is also known as the cosine emission law or Lambert's emission law. Flat diffusing surfaces are said to be ideal diffusers or Lambertian if the geometrical distribution of radiation from the surfaces obeys Lambert's Law. Lambert's Law has important consequences in the measurement of radiation. The cosine factor needs to be considered when making meaningful measurements of radiation with angular distribution.

3.1.3 Planck's Law

Any object will emit energy due to its temperature. The term "thermal radiation" is used to describe the energy that is emitted in the form of electromagnetic radiation at the surface of a body that has been thermally excited.

The thermal radiation emitted by a surface is not equally distributed over all wavelengths. The wavelength dependency of any radiative quantity or surface property is referred to as spectral dependency.

For a blackbody the spectral distribution of hemispherical emissive power and radiant intensity in vacuum are given as a function of wavelength and the blackbody's absolute temperature:

$$e_{\lambda b}(\lambda,T) = \pi \cdot i'_{\lambda b}(\lambda,T) = \frac{2\pi \cdot C_1}{\lambda^5 (e^{C_2/\lambda T} - 1)} \tag{3-2}$$

This is known as Planck's spectral distribution of emissive power. C_1 and C_2 are constants. As shown in **Figure 3-3**, **[81]** the hemispherical spectral emissive power is given as a function of wavelength for several different values of the absolute temperature. It is evident that the energy emitted for all wavelengths increases as the temperature increases. The curves show that this is also true for the energy at each individual wavelength. Another characteristic is that the peak spectral emissive power shifts toward a smaller wavelength as the temperature is increased.

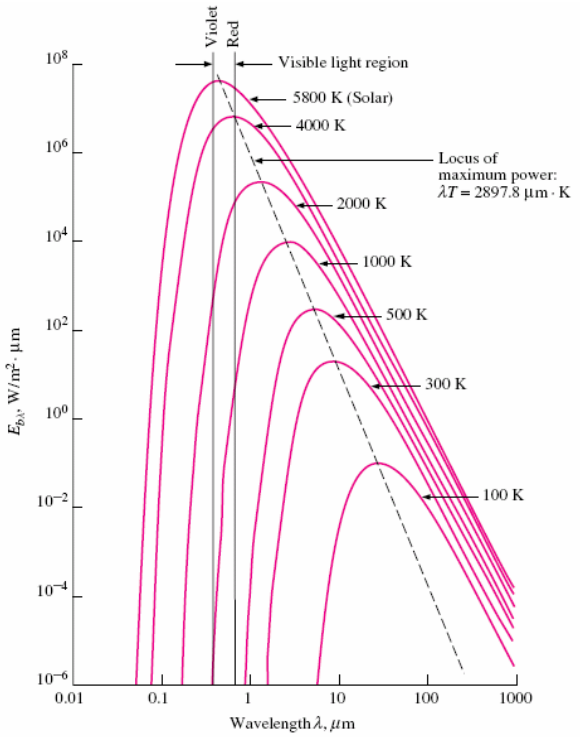

Figure 3-3 The Spectral Emissive Power of Blackbody With Wavelength

3.1.4 Stefan-Boltzmann's Law

The hemispherical total emissive power of a blackbody radiating into a vacuum can be expressed as:

$$e_b = \int_0^\infty e_{\lambda b}(\lambda)d\lambda = \int_0^\infty \pi \cdot i'_{\lambda b}(\lambda)d\lambda = \sigma \cdot T^4 \tag{3-3}$$

This is the Stefan-Boltzmann's law, and σ is the Stefan-Boltzmann's constant. This equation enables a calculation to be made to determine the amount of radiation emitted in all directions over all wavelengths simply from knowledge of the temperature.

3.1.5 Emissivity

The magnitude of radiation from a real surface is a function of both the temperature of the surface and the surface properties. The surface property limiting the quantity of radiation is called emissivity, ε. Emissivity is defined on a scale from 0 to 1 and is the ratio of the electromagnetic flux that is emitted from a surface to the flux that would be emitted from an ideal blackbody at the same temperature.

The hemispherical total emissivity is defined by the ratio of the total emissive power of a grey body to that of a blackbody at the same temperature:

$$\varepsilon(T) = \frac{e(T)}{e_b(T)} \tag{3-4}$$

where: $\varepsilon(T)$ is the total emissivity, $e(T)$ is the emissive power for a grey body (W/m^2).

The emissive power of a grey body at a given temperature can be readily calculated by a modification to the Stefan-Boltzmann's law:

$$e = \varepsilon \int_0^\infty e_{\lambda b}(\lambda) d\lambda = \varepsilon \int_0^\infty \pi \cdot i'_{\lambda b}(\lambda) d\lambda = \varepsilon \cdot \sigma \cdot T^4 \tag{3-5}$$

3.2 Design Element

IR thermometers come in a wide variety of configurations pertaining to optics, electronics, technology, size, and protective enclosures. All, however, have a common chain of IR energy in and an electronic signal out. This basic chain consists of collecting optics, lenses, and/or fiber optics, spectral filtering, and a detector as the front end.

3.2.1 Detectors

An essential component of an infrared thermometer is the transducer used to convert the absorbed electromagnetic radiation into a signal that can be measured. These devices are called detectors or thermal detectors and function by converting the absorbed radiation into heat energy causing the detector temperature to rise accompanied by the output.

Thermal detectors are widely used in infrared thermometry. They convert the absorbed electromagnetic radiation into heat energy causing the detector temperature to rise. This can be sensed by its effects on certain physical properties, such as: electrical resistance used by a bolometer; thermo electro-motive force (EMF) used by thermocouple and thermopile detectors.

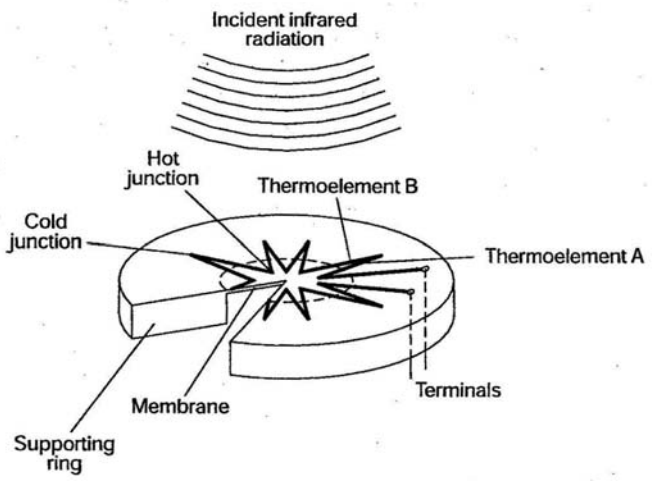

Figure 3-4 Thermopile Sensor in Infrared Camera

As shown in **Figure 3-4 [82]**, a differential temperature between the hot and cold junctions is generated by using a geometry which conducts heat from the hot and cold junction at different rates or by using materials with different thermal conductivity.

3.2.2 Thermal Imaging Scanner

Thermal imaging involves determining the spatial distribution of thermal energy emitted from the surface of an object. This information can be manipulated to provide qualitative and quantitative data of the distribution of temperature on a surface. In their usual form they comprise an optical system, a detector, processing electronics and a display.

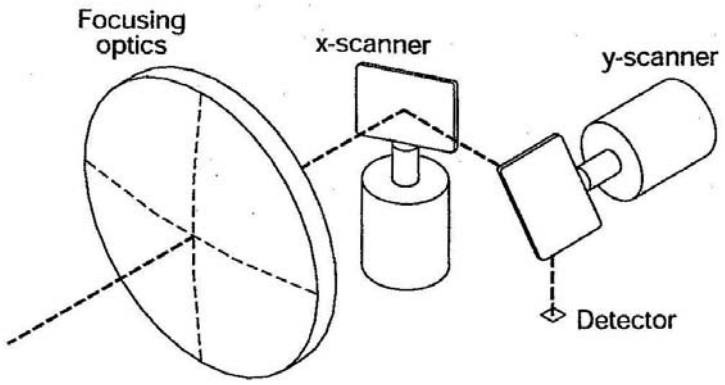

Figure 3-5 Two-Dimensional Scanning for a Small Detector Array

As shown in **Figure 3-5 [83]**, a single detector with some form of scanner can be used to transmit the radiation signal from specific regions of the optical system to enable a two-dimensional image of the temperature distribution to be built up.

3.3 SMA Temperature Determinations Through Thermo Imaging

As mentioned before, there are errors in temperature measurement of SMA wires when using contact methods such as: thermocouples and RTDs. One of these errors is aroused by the current that passes through the SMA wire. The other error is caused by the temperature local distortion when the sensor is introduced. With these errors, it is difficult to know the real temperature readings of SMA wire, and also it is hard to model the electric-thermo characteristic of SMA wire.

Infrared temperature measurement is a non-contact, non-obtrusive method used to obtain temperature readings, thereby eliminating many of the problems associated with methods such as thermocouples, thermistors and RTDs

3.3.1 Emissivity of SMA Wire

In order to obtain an accurate measure of temperature using infrared techniques, it is imperative to obtain an accurate measure of the surface emissivity of the SMA wire. A typical method to obtain emissivity is to compare the infrared reading to the thermocouple reading. Through adjusting the emissivity setting on the IR camera, the infrared reading can be brought into agreement with the thermocouple reading. Then the emissivity setting on IR camera is the emissivity of the object. But in this application, the thermocouple readings contain large errors and this is why the infrared method is introduced. So other ways must be found to obtain the emissivity of SMA wire.

The emissivity of an object can be measured using a Gier Dunkle DB100 Infrared Reflectometer. (**Figure 3-6)** Due to: $\varepsilon(T) + \rho(T) = 1$ (for diffuse-gray surface), so the

reflectometer measures the reflectivity of the object and the emissivity of the object can be calculated. In this way, the emissivity of SMA (Flexinol, dia = 500 μm, spool# = 2-3185B, A_s= 90 ^0C) is obtained as: ε = 0.37. Given the curvature of the SMA wire, it can be very difficult to obtain consistent readings over the perimeter of a wire due to reflection and angle of incidence effects.

wavelength range: 4 – 40 μm
sample size: dia 20 mm min (flat)
accuracy: ± 0.02

Figure 3-6 Gier Dunkle Db100 Infrared Reflectometer

As shown in **Figure 3-7**, another method used in this work is to paint a section of SMA wire with black paint that has a uniform emissivity of 0.97. The emissivity of a SMA wire can be determined by using an indirect method as follows:

- take IR images of painted and non-painted sections of the SMA wire with the emissivity of the camera set to 0.97 (the known value of the painted section)
- record the temperature of the painted section of the SMA wire

- adjust the emissivity setting of the camera until the temperature of the unpainted section is equivalent to the previously recorded temperature for the painted section

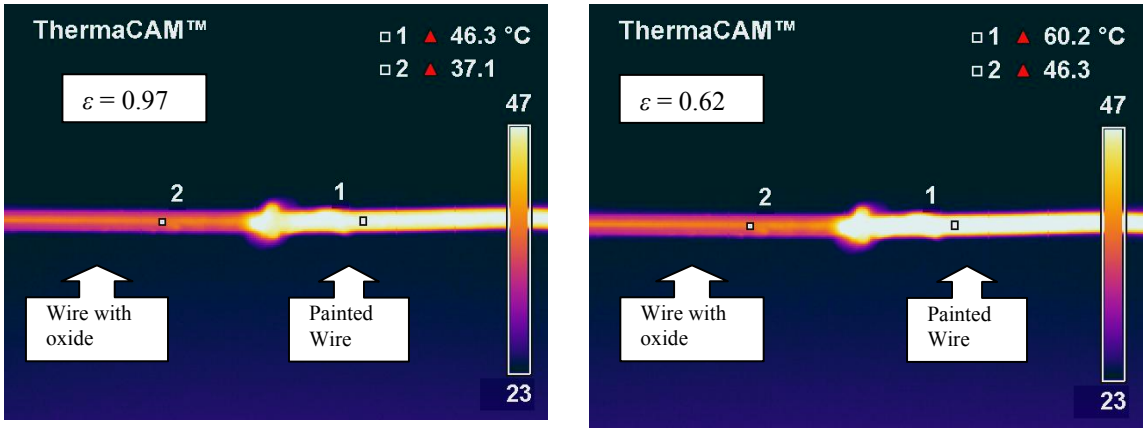

Painted wire vs wire with oxide,

Front view, $I = 0.75A$

Painted wire vs wire with oxide,

Front view, $I = 0.75A$

Figure 3-7 Obtain Emissivity of SMA Wire Through Painting

The last emissivity setting is the SMA wire's emissivity. The distance between point 1 and point 2 in **Figure 3-7** is 4.5 *mm*. When at steady state condition, point 1 and point 2 have the same temperature. Due to the difference of the emissivity, the two points give different temperatures when the emissivity on the IR camera is set to a fixed value. The temperature of the SMA wire can be determined through the known emissivity of the paint and the emissivity of the oxidized wire can then be found through the temperature of the SMA wire.

3.3.2 Determining Temperature of SMA Wire

The infrared temperature readings are dependant on the location of the points that are chosen for analysis. This can be easily understood through the Lambert Cosine Law. (**Figure 3-2**) Lambert's Cosine Law says that the total radiant power $e_{\lambda b}(\lambda,\theta,\varphi)$ observed from a "Lambertian" (or diffusing) surface is directly proportional to the cosine of the angle θ between the observer's line of sight and the surface normal. As shown in **Figure 3-8**, the surface normal of the top point **A** overlaps the line from the detector to the point **A**, so the total radiant power received by the detector is $e_{\lambda b}(\lambda,\theta,\varphi)$. For the point **B**, due to an angle θ between its surface normal and the line from the detector to the point **B**, the total radiant power received by the detector is $e_{\lambda b}(\lambda,\theta,\varphi)\cdot\cos\theta$. The detector receives a higher radiant power from the top point **A** than point **B** and gives a different temperature reading: $T_A > T_B$.

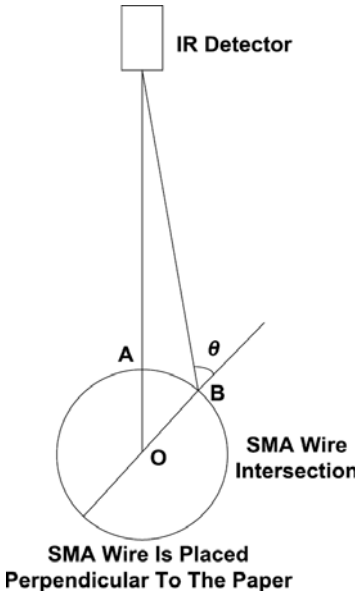

Figure 3-8 Different Points on SMA Wire Observed by a Detector

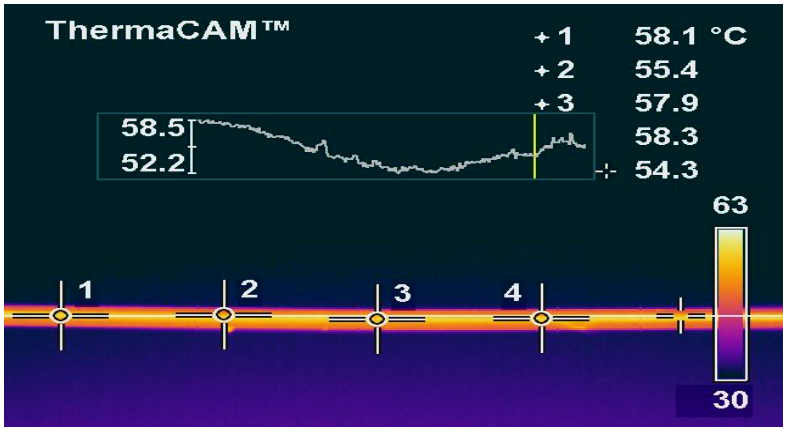

Figure 3-9 Temperature Bias on a Line Analysis Along the Wire

This location error can be seen in **Figure 3-9**. In this figure, a SMA wire is placed horizontally. A line analysis is conducted along the wire and centred on the wire. It is assumed that the temperature along this line should be constant due to the thermal equilibrium established in the SMA wire. But the IR camera readings indicate a temperature difference of 6 ^{0}C between points on the line. The possible reason for this is that the SMA wire is not straight itself. So when a line analysis is conducted along the wire, some points are at different elevations in relation to the centre line. This causes a temperature difference among the measured values.

A practical solution to this error is conducting a line analysis across the SMA wire rather than along the wire. Each cross section is scanned for temperature from top to bottom, with the maximum temperature over the cross section representing the centre line temperature. When heat equilibrium is reached, each top point temperature should be the same as shown in **Figure 3-10**. Another example is shown in **Figure 3-11**, in which, a thermistor is laid on the SMA wire. It clearly shows that the introduced thermistor

disturbs the temperature distribution on the SMA wire and causes a local temperature distortion on SMA wire.

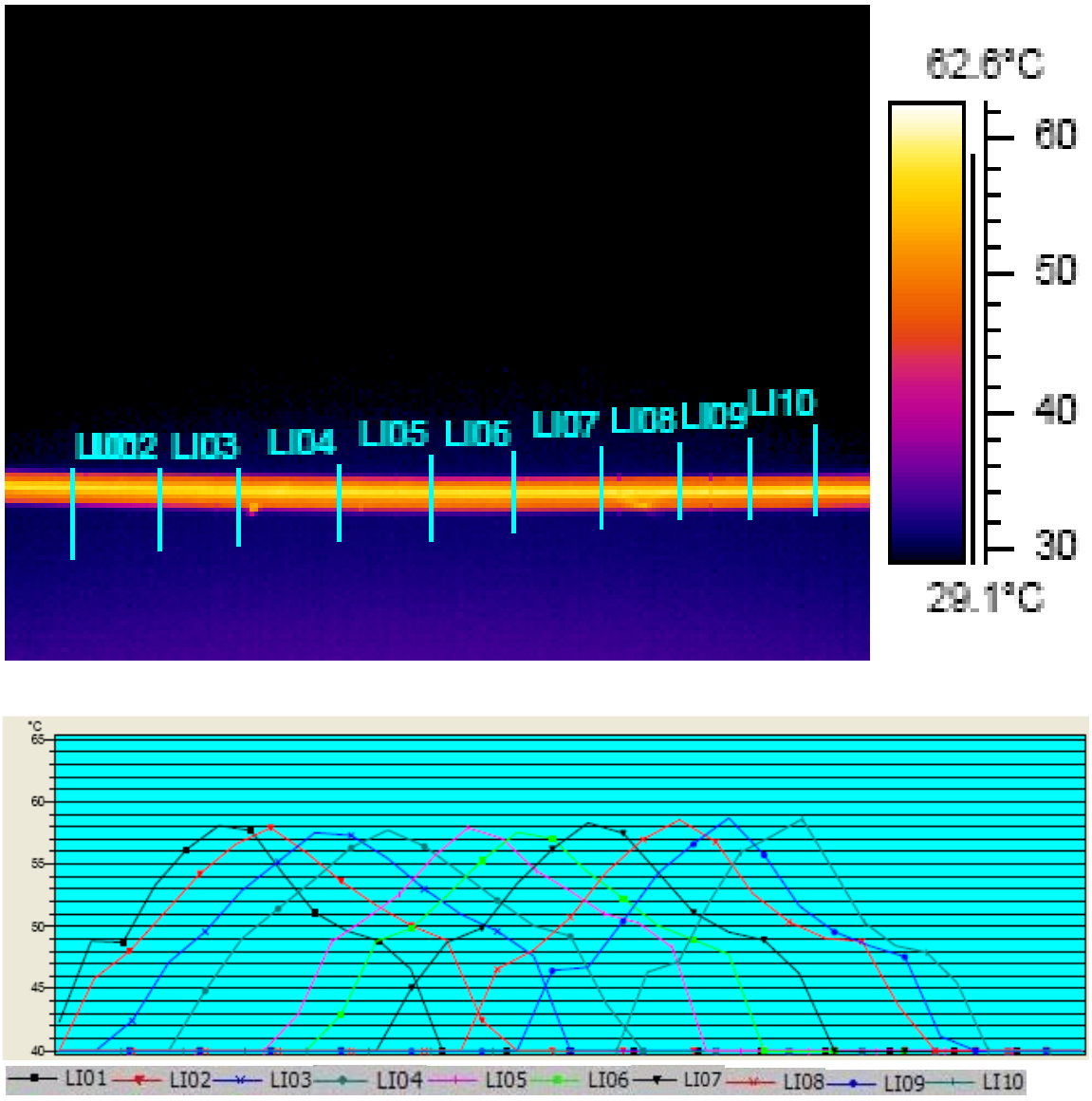

Each temperature distribution line with a different color in the lower picture corresponds to a line across the SMA wire in the top picture

Figure 3-10 Line Analysis Performed Across the Wire

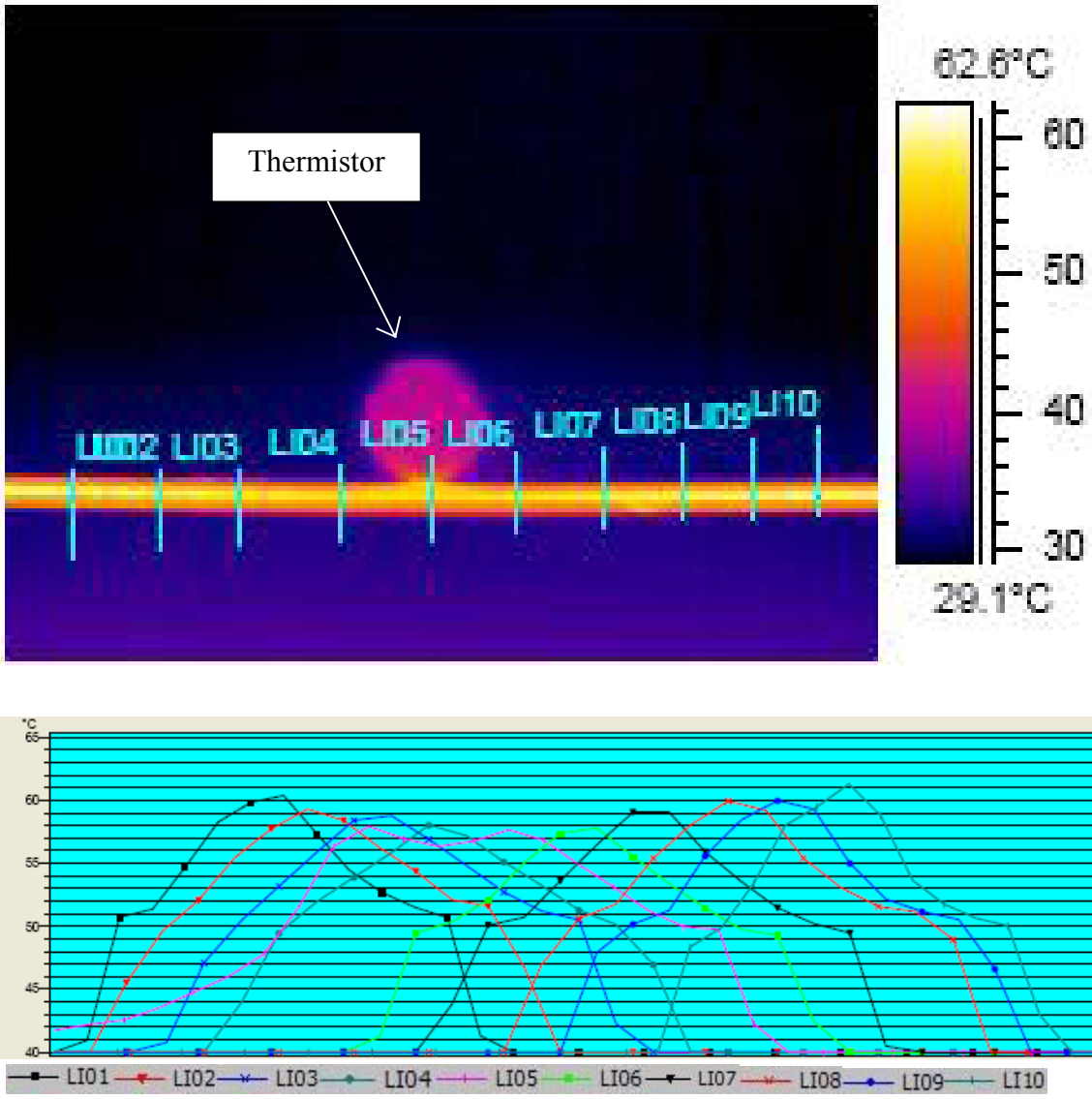

Each temperature distribution line with a different color in the lower picture corresponds to a line across the SMA wire in the top picture

Figure 3-11 A Thermistor is in Contact With the SMA Wire

3.3.3 Verifying of IR Camera

Calibration of the IR camera is an important step to insure the accuracy of IR temperature readings. Several samples (at least two samples) with different emissivity should be used to calibrate the IR camera. Typically, a thermocouple is attached to the sample and the IR camera is then used to measure the point where the TC is attached. When the temperature of that point on the sample is known, the emissivity setting of the camera can be adjusted until a temperature match is achieved. If the IR temperature equals the known temperature, the IR camera can be verified. Otherwise, the IR camera needs to be calibrated.

There can be a problem with low emissivity, shiny metal surfaces. As mentioned above: the Gier Dunkle DB100 Infrared Reflectometer can be used to measure the emissivity of object. It has an emissivity sample which has a gold-plated side with a standard emissivity of 0.04 and a black side with a standard emissivity of 0.90. At room temperature, the sample's temperature should equal the room temperature. When both sides of the sample are photographed by the IR camera with the emissivity setting equal to their standard emissivity values respectively, as shown in **Figure 3-12**, if the IR temperature readings equal room temperature, the IR camera can be verified. The black side is less affected by surrounding objects with higher temperature (e.g. IR camera itself) and calibration can be done perfectly, due to its high emissivity and low reflectivity. The radiant energy that the detector receives from the black side is mainly its emissive power. But when measuring the gold-plated side, IR temperature reading is around 30 ^{0}C, much higher than room temperature as shown in **Figure 3-13**.

Gier Dunkle Calibrated Standard

	Reflectivity	Emissivity
Gold	0.96	0.04
Black	0.10	0.90

Figure 3-12 Gier Dunkel Emissivity Sample is Tested by IR Camera Imaging

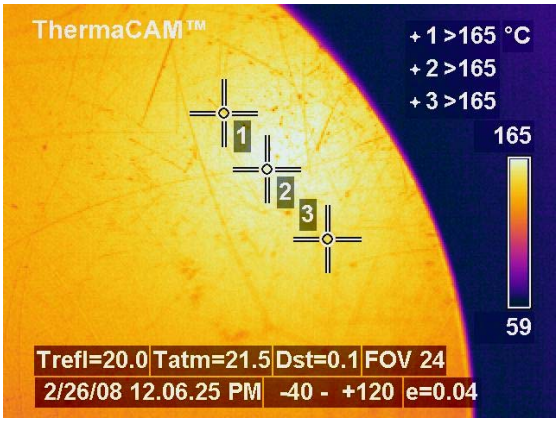

Gold side $\varepsilon = 0.04$, $T_{amb} = 21.5\ ^{0}C$

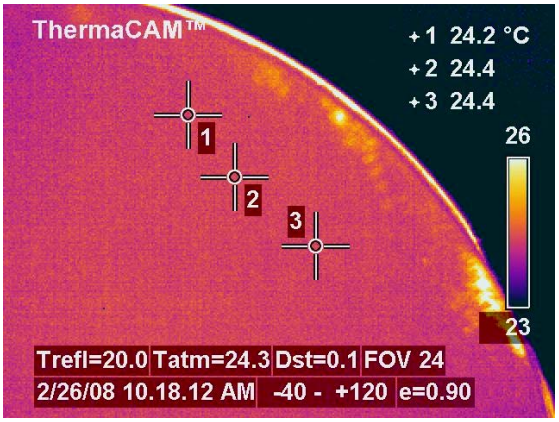

Black side $\varepsilon = 0.90$, $T_{amb} = 24.3\ ^{0}C$

Figure 3-13 IR Temperature Reading is Much Higher Than Room Temperature

This can be explained by radiosity in radiation heat transfer. The term radiosity is defined as: the rate at which radiation energy leaves a surface by combined emission and reflection of radiation.

$$q_o = \varepsilon \cdot \sigma \cdot T^4 + \rho \cdot q_i = \varepsilon \cdot \sigma \cdot T^4 + (1-\varepsilon) \cdot q_i \tag{3-6}$$

where q_o is radiosity of the surface. q_i is the incident heat flux that arrives at the surface.

Surfaces emit radiation as well as reflecting it, and thus the radiation leaving a surface consists of emitted and reflected components. The IR camera detects the total radiation energy streaming away from the gold plated surface, with no regard for its origin. The gold surface has a very small emissivity of 0.04 and a large reflectivity 0.96. At room temperature, the energy it reflects to the IR camera is much greater than that it emits. Because it faces the IR camera normal, it reflects the radiation of the camera back to the camera itself. So the IR temperature reading represents the temperature of camera. This agrees with the fact that IR camera's working temperature is around 30 – 35 ^0C.

In order to verify the IR camera, another sample with an emissivity that is lower than 0.9 should be used, besides the black side of the emissivity sample. A thermistor can be a perfect choice because the thermistor has good accuracy ± 0.2 ^0C (0 ^0C to 70 ^0C) **[41]** and the size of the thermistor bead is big enough for an IR camera to read temperature on a thermal picture. So a thermistor senses the temperature through its bead and the temperature can be read by a data logger (such as a Keithley 2700). The temperature of its bead can also be measured through the IR camera in the same time. Adjust the emissivity setting of the camera until the IR temperature reading equals the reading from the data logger and the emissivity of the thermistor bead is obtained. Keep this emissivity

setting on the IR camera and heat the thermistor bead with a heat gun. When the temperature readings from the data logger and the IR camera agree over a range of temperatures, it shows that the IR camera can give correct temperature readings when given the new emissivity of the thermistor. Thus the IR camera can be verified because it is correct at two different emissivity samples: the black side of the emissivity sample and the thermistor. As shown in **Figure 3-14**, a TPC thermistor (NI24MA0502G) was used in the experiment. The temperature readings from the two sources agree at all temperature, so the IR camera can be verified.

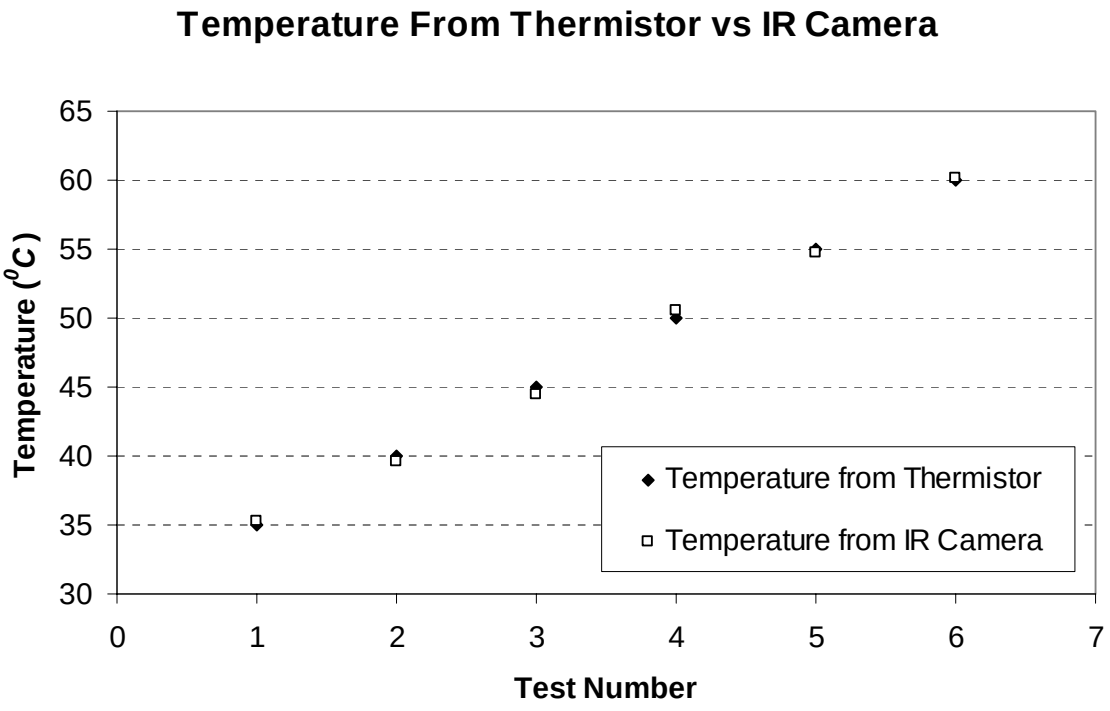

Figure 3-14 IR Camera Verified, Thermistor Bead Temperature from Two Sources

3.4 Summary of Infrared Thermal Imaging in SMA Wire Application

Infrared thermal imaging is useful in this work, but it can not be used independently. It has a relatively poor accuracy of 2 ^{0}C and the readout can not be easily recorded for modeling heat transfer (given the existing equipment: FLIR ThermaCAM S60).

Infrared thermal imaging belongs in the category of non-invasive temperature measurement methods. When the surface emissivity is known, an IR camera can give the temperature of the SMA wire through the analysis software without touching the SMA wire. This provides advantages over the invasive temperature measurement methods such as: thermocouples, thermistors, etc. As described in **Section 2.1.1**, an invasive probe senses the temperature of an object through direct contact with the object; thereby transferring heat between the object and the probe. Once the sensor establishes thermal equilibrium with the object, the temperature of the probe accurately reflects the temperature of the target object. Given the heat transfer between the object and the probe, the temperature of the object will be affected by the measurement probe. So there is a temperature distortion on the target object when a probe is introduced and this distortion can be significant at times. Infrared thermal imaging, on the other hand, provides the temperature of an object through detecting the radiant power from the object and interpreting this power strength to corresponding temperature value. An IR camera doesn't need to contact an object to give its temperature, so it can be used to monitor temperature distortion when attaching a thermocouple or a thermistor to the SMA wire.

Chapter 4

Improved Spot Welded Thermocouples in SMA Wire Application

Thermocouples are a common choice for temperature measurement because of their self-energization, low cost, robust nature and wide temperature range. With minor calibration corrections, thermocouples can have accuracies of $0.25 – 0.5\ ^{0}C$. Michalski *et al*. **[19]** conducted research on measuring the temperature of solid bodies with a thermocouple and pointed out that temperature measurement of a solid surface has possible errors including: *temperature distortion error* of the solid surface when introducing a thermocouple, and *contact thermal resistance error* between the solid surface and the thermocouple.

Volkov **[29]** observed that thermocouple readings can be affected by current in such a way as to add a "spurious voltage" ΔV to the thermo electro-motive force (EMF) of the thermocouple if it has direct contact with the current carrying surface. He concluded that the influence of current on thermocouple readings was a function of the voltage gradient along the current carrying surface. In **Figure 4-1**, when the pre-formed thermocouple bead is spot welded on the SMA wire, the thermocouple legs contact the SMA wire directly and there is a spatial offset ΔX between two legs along the axial direction of the SMA wire. When a current passes the SMA wire, there is a voltage $\Delta V = I * R$ between two legs, which is proportional to ΔX. R is the resistance between two thermocouple legs. Furthermore, both Dutton **[84]** and Mulford **[85]** propose a method using two thermocouple junctions of opposing polarity, affixed next to each other on a current-carrying conductor, to measure and compensate for the current-induced error.

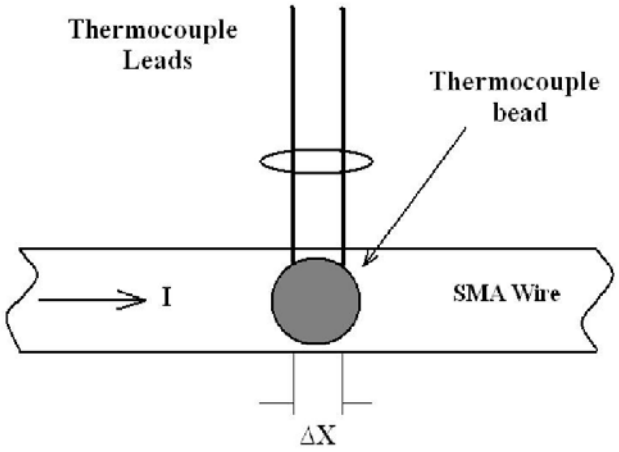

Figure 4-1 Thermocouple Reading is Affected by Spatial Offset Across TC Leads

Kuribayashi **[86]** used a thermocouple twist junction attached in close proximity to the SMA wire to avoid measurement errors due to the current going through the SMA wire. He also used isolation transformers to electrically separate the sensor circuit from the SMA wire heating circuit.

There is little further evidence of consideration of this problem in the literature, perhaps due to the particular nature of the SMA wire. For temperature measurement of larger-diameter conductors, electrically-insulated thermocouples are recommended**[29]**. However, the insulation increases the volume of the bead relative to the thin wire under test, introducing further uncertainty in the measurement.

As described in **Section 2.3**, thermocouple is better over other methods to measure the temperature of SMA wire. In this chapter, experiments are performed to investigate how to eliminate the carrying current's influence when using thermocouples to measure the temperature of SMA wire. This includes: different methods to attach thermocouples to SMA wire; improving the spot welding attachment; analysis and calculation of the

"spurious voltage" ΔV, etc. The errors are also investigated according to the theory of temperature measurement of a solid surface with a thermocouple in this chapter and solutions are proposed to minimize these errors.

4.1 Current's Influence on Spot Welded Thermocouple

In an early experiment comparing thermocouple attachment methods, two 500 *mm* long samples of 500 μm diameter SMA wire (Flexinol, from Dynalloy) were prepared by affixing seven T-type 36 AWG thermocouples along the wire length at regular 50*mm* separations between 100 *mm* and 400*mm* along the wire. 36 AWG copper and constantan wires are used to make the thermocouples. Thermocouple beads are prepared using a Therm-X Model 258B welder. On one wire, the pre-formed thermocouple beads were spot-welded using a capacity welder after first removing the oxide layer from the SMA using an abrasive paper, the power setting on the capacity welder was 1 *W*. While on the other wire, they were affixed with adhesive gel (QuickTite, from Loctite) and cured in room temperature for 1 hour. Examples are shown in **Figure 4-2**.

A current of 250 *mA* was applied to each of the wires, first in one direction then in the opposite, and the steady-state readings from all thermocouples recorded. The results are shown in **Figure 4-4**. For the glued thermocouples, there are measurement differences (less than 0.9 ^0C, the biggest one is between TC6 and TC7) along the length of the wire which can be easily ascribed to thermocouple accuracy and variability in the gluing process as evidenced by comparing **Figure 4-3 (a)** and **Figure 4-3 (b)**. The difference in readings when current is reversed is 0.2 ^0C. The spot-welded thermocouples, on the other hand, show wider variability between thermocouples. TC4 is 28.2 ^0C, TC5 is 22.8 ^0C, and

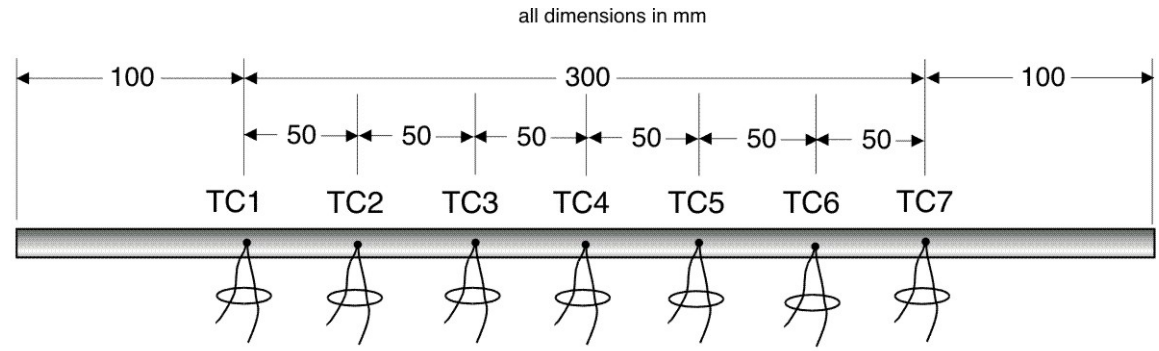

Figure 4-2 SMA Wire with Thermocouple Attachment Points

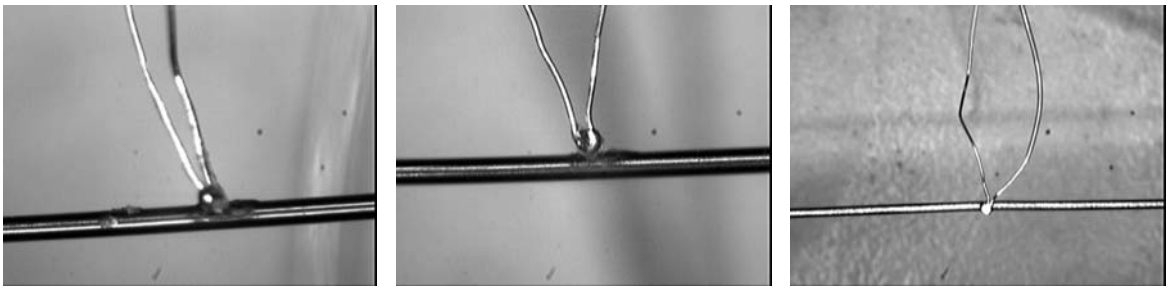

(a), TC 2 glue spot **(b),** TC 4 glue spot **(c),** TC 7 spot welded

Figure 4-3 Comparison of Glue Spot TC and Spot Welded TC

TC4 is 5.4 ^{0}C higher than TC5. In addition, the current direction has a large influence on readings, producing mirror-image curves which appear symmetric about approximately 26 ^{0}C. As shown in **Figure 4-4,** when the current is reversed, TC4 becomes 23.6 ^{0}C, TC5 is 29.1 ^{0}C, and TC4 is 5.5 ^{0}C higher than TC5. The average reading from the glued thermocouples is also about one degree lower than the average from the spot-welded

thermocouples, which is not unexpected given the greater thermal resistance of the adhesive.

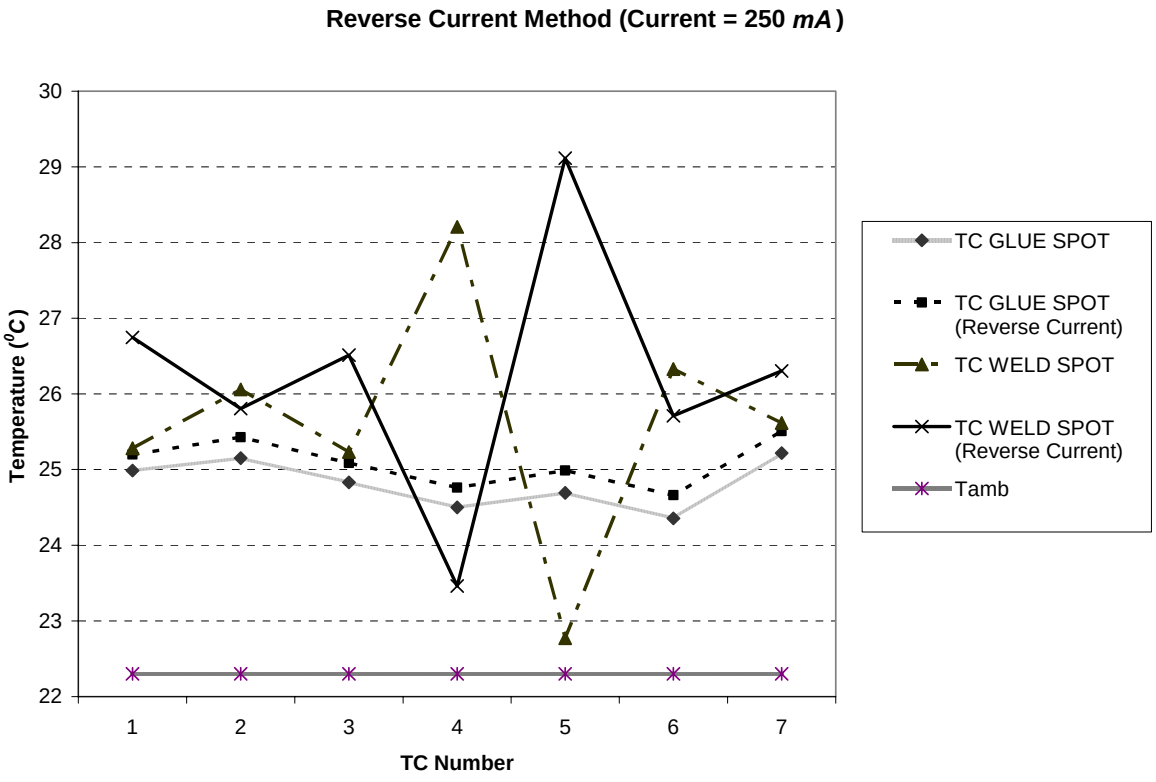

Figure 4-4 Temperature Measurement of Spot Welded TC and Glue Spot TC

Looking closely at the spot-welded thermocouples in **Figure 4-3(c)**, **Figure 4-5 (a)**, **(b)**, and **(c)**, (the close up pictures at the top left corners) it can be seen that the spatial offsets between each of the thermocouple leads on the SMA wire are not exactly the same. In the absence of current in the SMA wire, and assuming a constant wire temperature, this offset should have no influence on the thermocouple thermo electro-motive force (EMF). However, we hypothesize that the wire current induces an ohmic drop proportional to the lateral separation of the leads. This additional voltage corrupts the thermoelectric voltage generated by the thermal field, leading to an erroneous reading

which deviates from the average reading of 26 ^{0}C. The fact that the error-induced offset reverses its sign when the current is reversed supports this hypothesis.

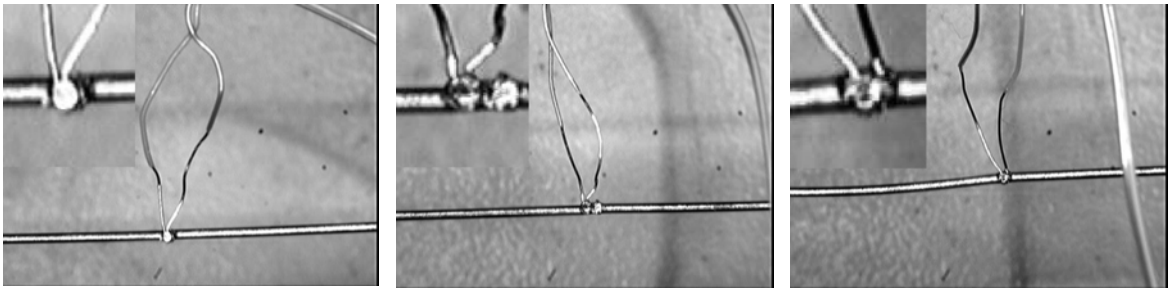

(a), TC 1 spot welded **(b),** TC 3 spot welded **(c),** TC 4 spot welded

Figure 4-5 Spot Welded TC

To further verify this idea, we can calculate the lateral offset suggested by the observed errors, by comparing the measured thermocouple voltages with the expected thermo electro-motive force (EMF) for a T-type thermocouple at 26 ^{0}C. The equation is

$$V_{26C} - V_{measured} = I \cdot \rho \cdot \Delta x \tag{4-1}$$

Where V is the T-type thermocouple thermo electro-motive force (EMF), I is the wire current (250 mA), ρ is the linear resistance of the wire (6.3 Ω/m **[87]**), and ΔX is the thermocouple lead separation. T-type thermocouple thermo electro-motive force (EMF) for TC 1 readings from **Figure 4-4** were computed from thermocouple coefficients in the NIST ITS-90 database **[88]**, and are given in **Table 4-1**.

The lateral offset between the leads in TC1 can then be estimated using **Equation 4-1**, giving a separation of 21 μm. Similarly, the offsets of TC3, TC4 and TC7 can be estimated at 17 μm, 61 μm and 9 μm respectively. It can be seen from this experiment and analysis that even very small offsets can introduce significant measurement error,

particularly at relatively high currents and temperatures close to room temperature. Since currents of 250 *mA* or higher, and room temperature operation are very normal conditions for an SMA actuator, it is important to develop a method to account for these current-induced measurement errors.

Table 4-1 Temperature Readings and Corresponding Voltages for TC1

Temp (^0C)	V (mV)	Comment
26.0	1.033	average reading
26.8	1.066	reverse current
25.2	1.000	forward current

4.2 Current Reversal and Averaging Method

Since the error component of the measured thermocouple voltage is due to an ohmic drop, its sign is dependent on the direction of current flow, as seen in **Figure 4-4**. One approach to compensate for this effect which has been previously proposed is to use a "compensated thermocouple" comprised of three thermocouple leads **[85]**. Two leads of a similar metal are affixed to the surface under measurement, and the third lead, of a dissimilar metal, is affixed in the centre. This creates two thermocouple junctions which will have opposite current-induced errors, and the average voltage can be read to get the "true" temperature. This approach still relies on the precise relative positioning of the leads on the surface, but residual errors due to lateral spacing differences would be smaller than the original current-induced errors.

Often, the amplitude or pulse-width modulation (PWM) duty cycle of the current in an SMA wire is controlled by a computer or embedded microcontroller, in order to control temperature and hence actuator motion. The greater the amplitude or duty cycle, the more power is delivered to the wire and the faster the heating. In this case, another approach using a single traditional thermocouple can be used to reduce or eliminate current-induced measurement errors. Since current *direction* does not affect heating, the control electronics can be used to alternate current direction while achieving the same overall desired control. If temperature measurements are synchronized with the current reversals, the average thermocouple thermo electro-motive force (EMF) can be used to eliminate the effects of the ohmic drop on the temperature reading.

4.3 Pulse Shut-Off Measurement Method

The pulse shut-off method takes advantage of the fact that the electrical time constant is much smaller than the thermal time constant of the system: the problematic ohmic drop disappears as soon as the current is removed, while the wire takes longer to cool. This is illustrated in **Figure 4-6**, which shows the response of a K-type 40 AWG thermocouple spot-welded to a 500 μm diameter Flexinol wire. Thermocouple readings were recorded during two trials, in which 750 mA was run through the wire, in opposite directions in each trial. At steady state with current flowing, the measured thermocouple temperatures are - 4 ^0C with current in one direction, and 78 ^0C after the polarity is switched. When the current is shut off, the thermocouple reading in both cases jumps almost immediately to 37 ^0C, the average of the two. The jump is followed by an identical slow decrease in measured temperature as the wire cools to ambient temperature.

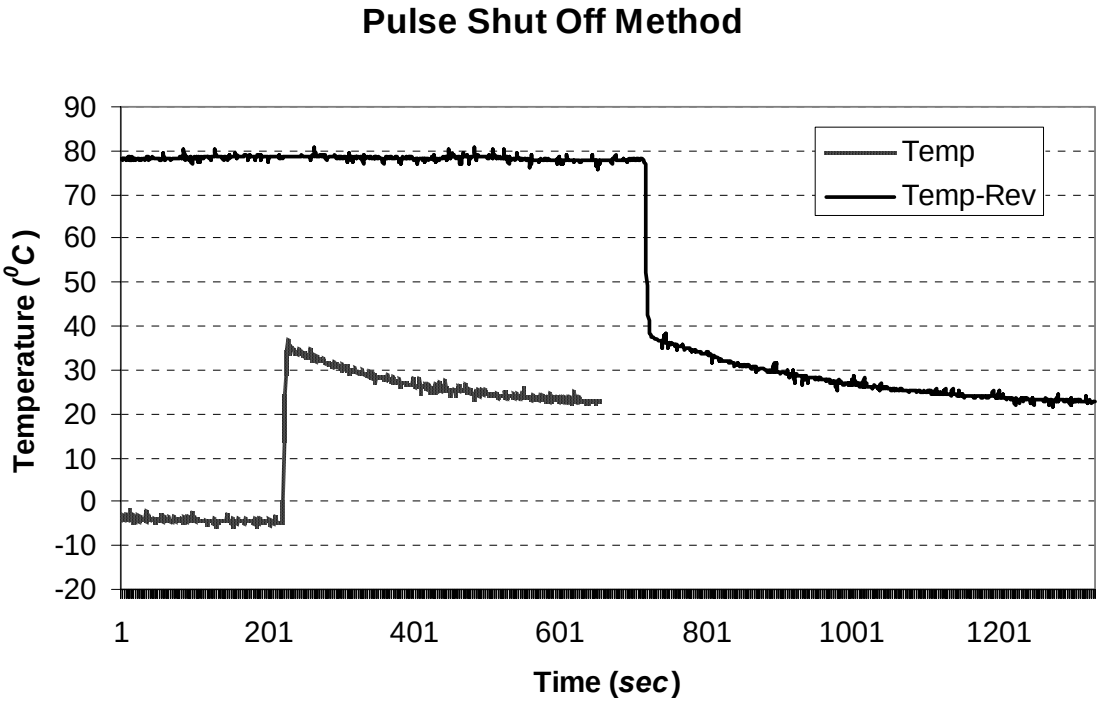

Figure 4-6 Pulse Shut-Off Method

By synchronizing the temperature measurement with the removal of the current in the wire, a single spot-welded thermocouple can be used to get an accurate reading, avoiding errors induced due to ohmic drop. This is particularly suited to SMA actuator applications where heating is controlled using a PWM current signal, as the measurement can be synchronized with the off-cycle of the control signal.

To further confirm the validity of the averaged and pulse shut-off measurements, we can use a first-order heating model accounting for Joule-heating and convection, to approximate the expected steady-state temperature of the wire in our experiments**[89]**:

$$T_{ss} = T_{\infty} + \frac{\rho}{h \cdot \pi \cdot d} I^2 \tag{4-2}$$

where T_{ss} is the steady-state temperature, T_∞ is the ambient temperature, I is the wire current (250 mA), ρ is the linear resistance of the wire (6.3 Ω/m, **[87]**), d is the wire diameter (500 μm), and h is the convection coefficient (75 $W/m^2 \cdot K$, **[89]**). **(4-2** confirms that at a measured ambient temperature of 23 ^0C, the steady state temperatures for our wire at 250 mA and 750 mA are approximately 25 ^0C and 38 ^0C respectively. Within thermocouple measurement error, these are the two average temperatures observed in **Figure 4-4** and **Figure 4-6**.

4.4 Two-Step Spot Welded Thermocouple

Different from the two methods above, the zero-offset spot weld method focuses on the joint point where the thermocouple is attached on the SMA wire and eliminates the ohmic drop through improved spot welding techniques. The conventional way to attach a thermocouple on an SMA wire is to make the thermocouple bead first and then spot weld the bead on the SMA wire. Experimental results show that the readings of a regular spot welded thermocouple contain current effects that make temperature readings higher or lower than real temperatures. The picture of a regular spot welded thermocouple (**Figure 4-5**) shows that two thermocouple leads contact the SMA wire at two distinct points despite the formation of a single thermocouple bead prior to spot welding. Inevitably, there is voltage drop across the thermocouple bead at this kind of junction when a current passes through the SMA wire. Another potential method of attachment is to spot weld the two thermocouple leads directly onto the SMA wire. However, experiments show that two distinct points of contact result even when using this method. In addition, the

problem with using this procedure is the control and placement of the very thin thermocouple leads under the microscope during the spot welding process.

A two-step spot weld thermocouple provides a good solution to ensure that the two thermocouple leads are attached to the SMA wire at a single point in a small junction. **Figure 4-7** shows the procedure for the two-step spot welding of thermocouples. The goal of this procedure is to ensure that the two thermocouple wires can be welded exactly at the same point on the SMA wire, which negates the current effect and provides good thermal contact. The attachment procedure is performed under a 3*X* microscope. The bead that is formed from one thermocouple wire is welded onto the SMA wire prior to the attachment of the second thermocouple wire, providing minimal separation of the wires thus minimizing current effects.

The two-step spot welding of thermocouples needs to be investigated using the average reverse current method or the pulse shut off method to see if there is any influence of the passing on the temperature readout. The verification procedure involves applying a current on the SMA wire and reading the temperature $T_{1,}$ then reversing the polarity of the same current and reading another temperature T_2. If $T_1 = T_2$, this verifies a good spot welded thermocouple. If $T_1 \neq T_2$, this indicates a poor spot welded thermocouple. Then the two step welding procedure needs to be repeated until $T_1 = T_2$. If $T_1 \neq T_2$, the average of T_1 and T_2 represents the real temperature of SMA wire.

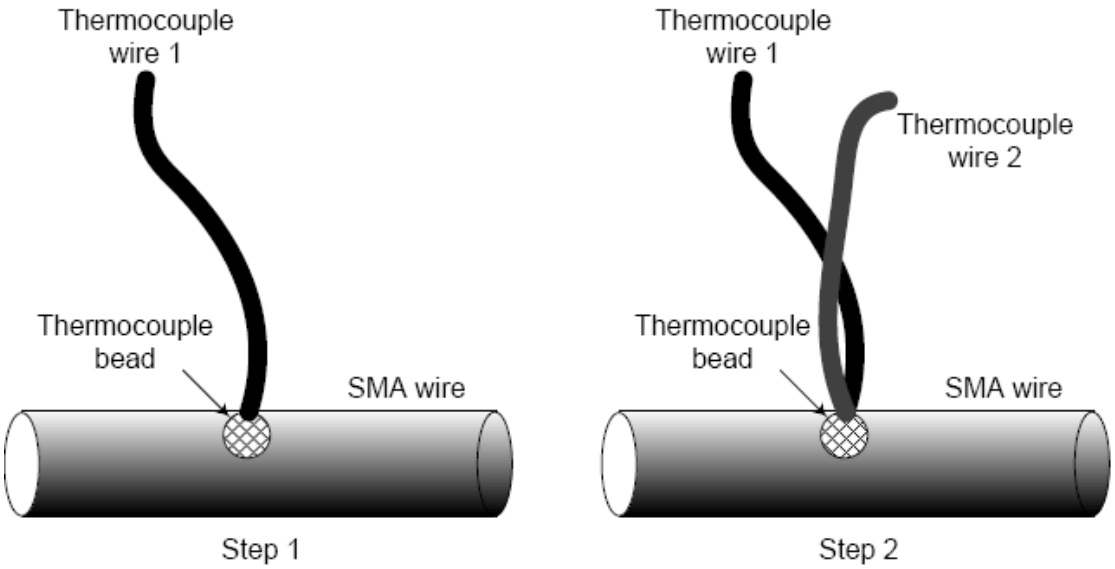

Make a bead from one thermocouple wire first; spot weld the bead on the SMA wire. Attach the other thermocouple wire on the bead; the current influence can be eliminated

Figure 4-7 Two-Step Spot Welded Thermocouple

4.5 Temperature Distribution Along SMA Wire

Examining the temperature distribution along an SMA wire is an important step in modeling the heat transfer and characterization of the thermal properties of this material. According to thermodynamic theory, when a current passes through the SMA wire and reaches a thermal equilibrium, the temperature along the SMA wire should be the same. This assumption is verified in the experimental heat transfer coefficient measurement, as shown in **Figure 4-8**.

In **Figure 4-8**, a 50 *cm* long, 0.5*mm* diameter SMA wire was supported on a fixture. Two ring terminals were crimped onto the SMA wire at points 12.5 *cm* away from each end. The two ring terminals were then tied and suspended onto the fixture. Five E-type 40

AWG thermocouples were attached on the centre section of the SMA wire with an offset of 5 *cm* from one another using the two-step spot welding method.

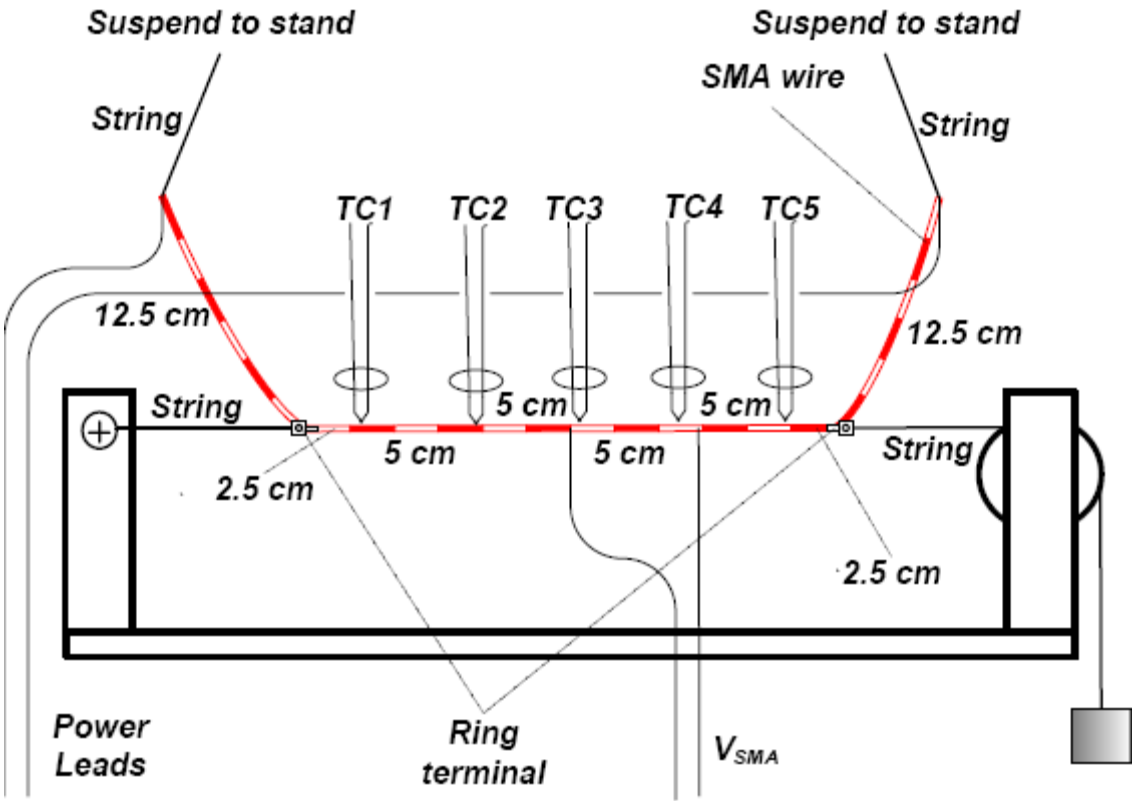

Figure 4-8 Five Thermocouples, Voltage Measurement Leads and Power Leads Layout

When each thermocouple was welded onto the SMA wire, a pulse shut off method was used to examine the influence of current influence on the thermocouples. Their temperature and time profiles are shown in **Figure 4-9**. It could be noted that all the thermocouples attached on the SMA wire showed no current influence on their readouts.

The complete setup together with all thermocouples was placed in the vacuum of 10^{-8} *torr*. Different currents were fed to the SMA wire and the temperature of the 5 thermocouples were recorded and plotted as in **Figure 4-10**

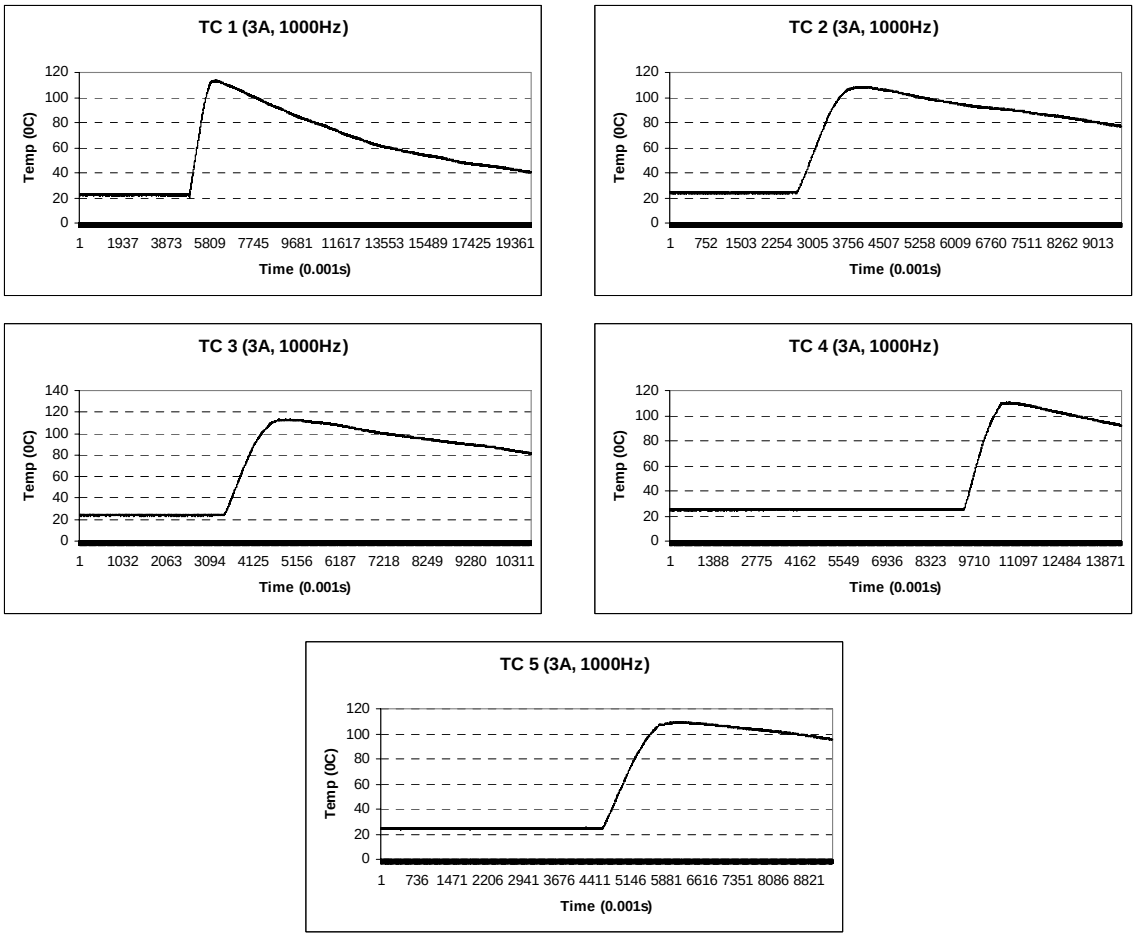

Figure 4-9 No Current Influence on Two-Step Spot Welded Thermocouple Reading

In **Figure 4-10**, when the current increased, the temperature readings of the 5 points also increased. When the current was reversed during the experiment, the temperature values didn't change. This further proved evidence that there was no current effect on thermocouple readings. TC2, 3 and 4 agreed at all current levels, TC5 was a little lower than TC2, 3 and 4. TC1 was the lowest value and TC1 became much lower than others at larger currents.

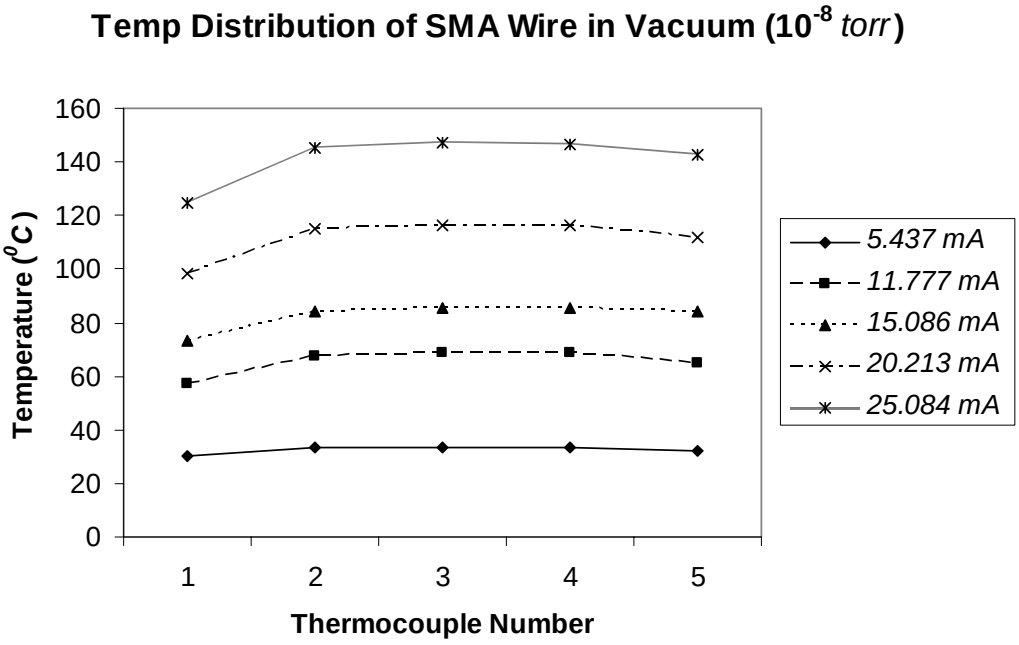

Figure 4-10 The Temperature Reading From TC1 is Much Lower Than Other TCs

The two-step spot welding method was used to attach thermocouples onto the SMA wire, the pulse shut off method and the average reverse current method were both used to verify thermocouples before and during the experiment to show that there was no current influence on the temperature readouts. There were systematic errors in the thermocouple circuit, such as: cold reference junction, low accuracy of measurement meter, but none of these errors were significant enough to produce the temperature differences observed between TC5 and the other TCs. A possible reason is that TC1 has a poorer spot weld than other TCs. If the spot weld is poor, the thermal resistance between the thermocouple and the SMA wire will be higher, so it will give a lower temperature reading at the same condition. This can be verified by checking temperature profiles in **Figure 4-9**. It can be seen that TC1 cools at a higher rate than other TCs when the power is turned off.

4.6 Summary of Improved Two-Step Spot Welded Thermocouple

It can be concluded that a two step spot weld thermocouple is the best practice in this work to measure the temperature of SMA wire.

A glue-spot attachment is not suitable to measure the fine SMA wire due to its higher thermal contact resistance than metal. Glue-spot attachment also means an extra material will have to be introduced and more power will be consumed when heat equilibrium is reached between the thermocouple bead and the SMA wire. This results in a higher temperature distortion on the SMA wire and a bigger error in measurement. In addition, glue has a lower melt point, which makes the thermocouple bead detach from the SMA wire when temperature increases to a degree.

A pre-formed thermocouple bead is not an ideal option, either. At first, due to the technical constraint, the bead can not be made small enough. The smallest bead that can be made with the current equipment is a diameter of 0.25 *mm*. Similar to the glue spot procedure, spot welding a bead on an SMA wire also introduces extra material to the attachment and brings a higher error to the measurement. Another vital drawback with the pre-formed bead-spot welding is that this method makes it hard to control where two thermocouple legs contact the SMA wire. Improper arrangement of two thermocouple legs on the SMA wire results in the spatial offset between the two legs, which leads to errors in temperature measurement.

The two-step spot welding procedure successfully controls the placement of the two thermocouple legs. Two legs can be precisely spot welded onto an SMA wire one after another, so the spatial offset will not exist and the spurious voltage will not occur.

Because the two legs are spot welded onto the SMA wire one by one during the spot welding, there is no bead and the error related to temperature distortion is minimized.

Chapter 5

Experimental Methods

A series of experiments were performed to collect the data necessary to model convective heat transfer of a heated SMA wire. As described in the literature review, no existing heat transfer correlations can be directly applied to SMA wires with confidence since these correlations were developed under different conditions. The primary goal of the experiment conducted in this work is to obtain data that can be used to produce a natural convective heat transfer model that relates Nusselt number to Rayleigh number for SMA wires of sub millimeter diameter.

5.1 Background

An accurate heat transfer model is of great importance when modeling SMA actuator dynamics. SMA wires are ideal as actuators in automobile applications because of the unique temperature dependent phase transformations. They can be deformed in the low temperature martensite (M) phase, but return to their original un-deformed configuration when heated to a higher temperature austenite (A) phase. This phase transformation is accompanied by a large force during the re-arrangement of crystalline structure and the two phases have very different thermal, mechanical and electrical properties. The SMA constitutive and phase kinetic behaviors are directly controlled by the heat transfer rate to and from the wires and as a result a detailed heat transfer model is needed to monitor and predict the thermophysical behavior of SMA wires.

The SMA wire actuator is usually driven by a current. When a current is passed through a SMA wire, the SMA wire is heated via the Joule effect. The input energy is then dissipated to the environment through convective, radiative and conductive heat transfer. The convective heat transfer is a complicated mechanism which is dependent on a series of conditions, such as: the geometry, orientation and the fluid properties. The convective heat transfer coefficient *h* can be nondimensionlized with the Nusselt number (*Nu*) and the parameters that reflect these conditions are expressed as: Rayleigh number (*Ra*).

The Nusselt number (Nu) is the ratio of the convective heat transfer associated with movement of the surrounding fluid through a thin boundary layer to the conductive heat transfer through the same fluid layer when the fluid is motionless ($Nu = Q_{conv} / Q_{cond}$). The Nusselt number (*Nu*) is a measure of the heat transfer enhancement associated with convection as compared to conduction in the fluid. The Rayleigh number is also a dimensionless number associated with the transition from laminar to turbulent flow for natural convection heat transfer within a fluid. The Rayleigh number is defined as the product of the Grashof number (*Gr*), which describes the relationship between buoyancy and viscosity within a fluid, and the Prandtl number (*Pr*), which describes the relationship between momentum diffusivity and thermal diffusivity. A simple empirical correlation for the average Nusselt number (*Nu*) in natural convection can be expressed as: $Nu = C \cdot Ra^n$. The constant C and n depend on the geometry of the surface and the flow regime, which is characterized by the Rayleigh number (*Ra*).

A correlation can be determined based on prescribed experimental conditions, where test conditions such as wire temperature, geometry and ambient properties can be used to

obtain a range of Rayleigh numbers. A 500 μm diameter SMA wire is used as a sample to model convective heat transfer. The convective heat transfer coefficient can not be measured directly; it can only be calculated by the parameters that will be collected in the experiment. This section describes the pressure variation method and the type of data that is necessary to compute *Nu* and *Ra* for heat transfer modeling.

5.1.1 Pressure Variation Method

The goal of this experiment was to accurately measure the natural convective heat transfer coefficient from a heated SMA wire over a wide range of Rayleigh numbers (*Ra*). The Rayleigh number is the product of the Grashof number (Gr_L) and the Prandtl number (*Pr*) and can be written as:

$$Ra_L = Gr_L \cdot \Pr = \frac{g\beta(T_s - T_\infty)L_c^3}{\nu^2}\Pr \quad \textbf{[90]} \tag{5-1}$$

where:

Ra_L is the Rayleigh number

Pr is the Prandtl number

g is the gravitational acceleration (m/s^2)

β is the coefficient of volume expansion ($1/K$)

T_s is the temperature of the surface (K)

T_∞ is the temperature of the fluid sufficiently far from the surface ($1/K$)

L_c is the characteristic length of the geometry (m)

v is the kinematic viscosity of the fluid (m^2/s)

g is a constant. Pr is independent of pressure and changes in a very small range from 0.6935 to 0.7539 for air temperature changes from -150 ^0C to 2000 ^0C, so it can be treated as constant as well. Assuming that the air in the test environment is an ideal gas,

$$\beta = \frac{1}{T_\infty} \tag{5-2}$$

T_∞ is usually 296 K (23 ^0C), so β can also be treated as a constant. The Rayleigh number (Ra_L) can thereby be expressed as a function of T_s, L_c and v.

$$Ra_L = f(T_s, L_c, v) \tag{5-3}$$

In this case, the temperature of the surface T_s is T_{SMA}; the characteristic length L_c is the diameter of SMA wire D; v is the kinematic viscosity of air.

Changing T_{SMA} can vary Ra_L, but T_{SMA} can only change Ra_L over a small range. If T_∞= 296 K, air pressure is 1 atm, (β = 1/296 $1/K$; Pr=0.7282; v=1.562 × 10^{-5} m^2/s), for a 0.5 mm diameter SMA wire, a change in T_{SMA} from room temperature 296 K (23 ^0C) to 673 K (400 ^0C) results in a change in Ra_L from 0.3 to 6.97. Since the temperature of the SMA wire should not be higher than 200 ^0C, using temperature to obtain a range of Rayleigh number is very limiting.

Changing the diameter of SMA wire is not effective either to adjust Ra_L because there are limited diameters of SMA wire to choose from. The diameter of SMA wire varies from 0.025 mm to 0.5 mm and when the diameter is small it becomes very difficult to measure the temperature of the SMA wire.

However, varying the ambient fluid properties can be a very effective method for obtaining a wide range of Rayleigh number. The kinematic viscosity is given:

$$\nu = \frac{\mu}{\rho} \tag{5-4}$$

where:

μ is the dynamic viscosity of air ($kg/(m.s)$)

ρ is the density of air (kg/m^3)

μ is independent of air pressure and alters only in a small range from 1.849×10^{-5} to 2.181×10^{-5} $kg/(m.s)$ when T_m changes from 296 K (23 ^0C) to 373 K (100 ^0C), so it can be treated as a constant. ρ varies significantly from 1.184 kg/m^3 to 1.72×10^{-3} kg/m^3 when the air pressure varies from 1 *atm* to a near vacuum when air pressure is 1 *torr*. When T_{SMA} = 373 K (100 ^0C), T_∞= 296 K (23 ^0C), (β = 1/296 $1/K$; Pr = 0.7202; μ =2.008×10^{-5} $kg/(m.s)$), for a 0.5 *mm* diameter SMA wire, if ρ varies from 1.184 kg/m^3 to 1.72×10^{-3} kg/m^3 , Ra_L varies from 6.4 to 7.86×10^{-6} according to **Equation 5-1**.

The air in the test environment is assumed to be an ideal gas, so:

$$\rho = \frac{P}{RT_m Z} \tag{5-5}$$

where;

P is the pressure of air (Pa);

R is the gas constant of air ($kJ/(kg.K)$);

T_m is the average temperature of air and SMA wire (K) ($T_m = (T_{SMA} + T_\infty) / 2$),

Z is the compressibility factor of air.

If T_m, R and Z are assumed to be constant, **Equation 5-5** clearly shows a direct relationship between density and pressure, therefore an experiment in which the ambient pressure is reduced will result in a lowing of air density. P is easy to control with a vacuum station using a bell jar and a mechanical / diffusion vacuum pump to evacuate the air pressure from 1 *atm* to 0.001 *torr*. The pressure variation method is an ideal choice in this experiment to alter Ra_L over a wider range.

5.1.2 Data Collection

The following section provides detailed descriptions on collecting data that are necessary to determine an empirical correlation of Nusselt number versus Rayleigh number for natural convection heat transfer from a heated SMA wire.

5.1.2.1 The Rayleigh Number (*Ra*)

A modified version of the Rayleigh number can be obtained by substituting **Equations 5-2, 5-4** and **5-5** into **Equation 5-1**, where the characteristic length L_c and the temperature of the surface T_s are replaced by the diameter of the SMA wire D and T_{SMA}.

$$Ra_D = \frac{g(T_{SMA} - T_\infty)D^3P^2}{\mu^2 T_\infty R^2 Z^2 T_m^2}\Pr \tag{5-6}$$

g, Pr, μ, R, Z are constants. g = 9.8 m/s^2, R = 0.287 *kJ/(kg·K)*. Z is the compressibility factor of air, where air is assumed to be ideal gas and Z = 1. Pr and μ can be obtained from standard air property tables when the mean temperature T_m is determined. T_m is the average of the ambient temperature and the temperature of the SMA wire: $T_m = (T_{SMA} +$

T_∞) / 2 (K). The remaining parameters $T_{SMA,}$ $T_{\infty,}$ P and D need to be measured in the experiment to calculate Ra_D.

5.1.2.2 The Nusselt Number (*Nu*)

The Nusselt number (Nu) is the non-dimensional convective heat transfer coefficient which can be expressed as:

$$Nu_L = \frac{hL_c}{k} \tag{5-7}$$

where:

h is convection heat transfer coefficient ($W/(m^2\ K)$)

L_c is the characteristic length (m)

k is the thermal conductivity of the fluid ($W/(m\ K)$)

The convective heat transfer coefficient h can be defined as: the rate of heat transfer between a solid surface and a fluid per unit surface area per unit temperature difference. The convective heat transfer coefficient is then expressed as:

$$h = \frac{Q_{conv}}{A_s \cdot (T_s - T_\infty)} \tag{5-8}$$

where:

h is the convective heat transfer coefficient ($W/m^2 \cdot K$)

Q_{conv} is the convective heat transfer rate (W),

A_s is the convective heat transfer surface area (m^2)

T_s is the temperature of the surface *(K)*

T_∞ is the temperature of the fluid sufficiently far away from the surface *(K)*

In this case, the characteristic length L_c is the diameter of the SMA wire D. Substituting **Equation 5-8** into **5-7**, the Nusselt number becomes:

$$Nu_D = \frac{hD}{k} = \frac{Q_{conv}D}{kA_s(T_s - T_\infty)} \tag{5-9}$$

k is constant which can be obtained from standard air property tables. D and l can be measured, therefore A_s can be calculated, $A_s = \pi \cdot D \cdot l$ (mm^2).

The convective heat transfer rate Q_{conv} can be determined by performing a heat balance on the test section of SMA wire when at a thermal equilibrium, as shown in **Figure 5-1**. Usually the SMA wire is heated by passing a current through the wire. When the temperature of the SMA wire increases, heat transfer occurs between the SMA wire and the environment through conduction, convection and radiation due to the temperature difference between the SMA wire and the environment. At a steady state, the power input to the SMA wire should equal the heat dissipation from the SMA wire via conduction, convection and radiation as shown in **Figure 5-1**, where $VI = Q_{conv} + Q_{cond} + Q_{rad}$. If VI, Q_{cond} and Q_{rad} are known, Q_{conv} can be easily determined.

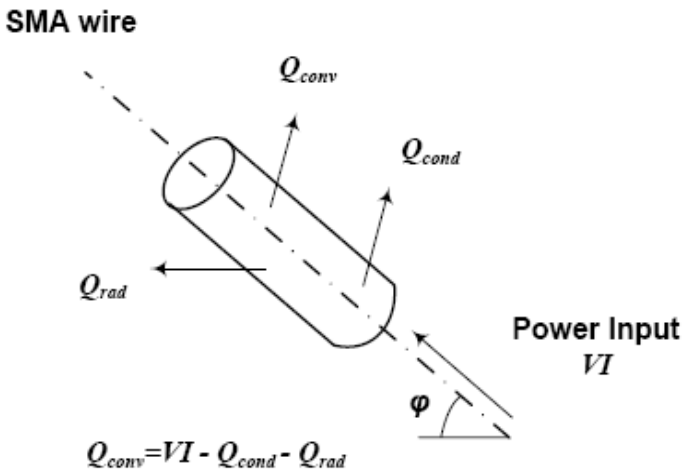

Figure 5-1 Thermal Analysis on the SMA Wire Test Section at Steady-State

Q_{cond} is the heat dissipation from the SMA wire through the attached thermocouple leads, the voltage measurement leads, the power leads, the string and the ring terminals. As described in the **Appendix A** and **C**, the conduction losses through above paths can be minimized and neglected when the SMA wire is properly setup on the fixture.

Q_{rad} is the heat exchange between the SMA wire and the environment through electromagnetic waves as a result of the temperature difference between T_{SMA} and the surrounding environment at T_{∞}.

$$Q_{rad} = \varepsilon \cdot \sigma \cdot A_s \cdot (T_{SMA}^4 - T_{\infty}^4) \tag{5-10}$$

where:

ε is the emissivity of the SMA wire;

σ is the Stefan-Boltzmann's constant ($\sigma = 5.67\times10^{-8}\ W/(m^2 \cdot K^4)$)

A_s is the surface area of the test section of SMA wire (m^2)

T_{SMA}, is the temperature of the SMA wire (K)

T_∞ is the temperature of the surrounds (K)

Since radiative heat transfer is independent of the transfer medium, Q_{rad} for the SMA will be the same in a vacuum as in ambient air at 1 *atm* if T_∞ is preserved. At thermal equilibrium in a vacuum, the power input to the SMA wire equals Q_{rad} only. For the same section of SMA wire, Q_{rad} at a prescribed temperature and air pressure is equivalent to the power input at the same temperature in a vacuum:

$$Q_{rad} = VI_{vacuum} \tag{5-11}$$

With the power input VI and the radiation Q_{rad} determined, and the conduction losses considered negligible, the convection can be calculated as: $Q_{conv} = VI - Q_{rad}$, or

$$Q_{conv} = VI - VI_{vacuum} \tag{5-12}$$

5.1.2.3 The Inclination Angle

When an SMA wire is inclined at an angle φ, as shown in **Figure 5-8**, the convective heat transfer is affected as a result of an axial component of air flow which decreases the convection. To develop a correlation that contains the inclination angle φ, the SMA wire was inclined from the horizontal at angles: 15^0, 30^0, 45^0, 60^0, 75^0, and 90^0 (vertical) by elevating one side of the test fixture as described in the **Section 5.4.1**.

5.2 SMA Wire Test Fixture

As described previously, a sample SMA wire was used to collect empirical data necessary to model natural convection heat transfer. The sample SMA wire was heated by an electric current; its temperature and power input were then measured.

5.2.1 Level Temperature Distribution on the SMA Wire

The test section of the SMA wire should be maintained at a uniform temperature during the test procedure; otherwise there can be large errors when calculating the Nusselt number (*Nu*) and the Rayleigh number (*Ra*). First, to collect data and to heat up the SMA wire, thermocouples, voltage measurement leads and power leads have to be attached to the SMA wire. These extraneous connections can lead to temperature distortions in the test section of SMA wire, and introduce errors in the results. Similarly, when the ring terminals are crimped onto the sample SMA wire to suspend the SMA wire to the fixture, they also introduce temperature distortion to the SMA wire due to their larger surface area which results in enhanced convection to the air.

The expected uniform temperature distribution over the test section of the SMA wire is shown in **Figure 5-2.** The factors that distort the uniform temperature distribution on the SMA wire are: the size of the SMA wire; the attached thermocouple, voltage measurement leads, power leads and ring terminals, as described in the next **Sections 5.2.2**. Choosing a larger diameter sample SMA wire and properly arranging the locations of the thermocouple, voltage measurement leads, power leads and ring terminals on the sample SMA wire can minimize the conduction heat losses and keep a uniform temperature distribution on the sample SMA wire.

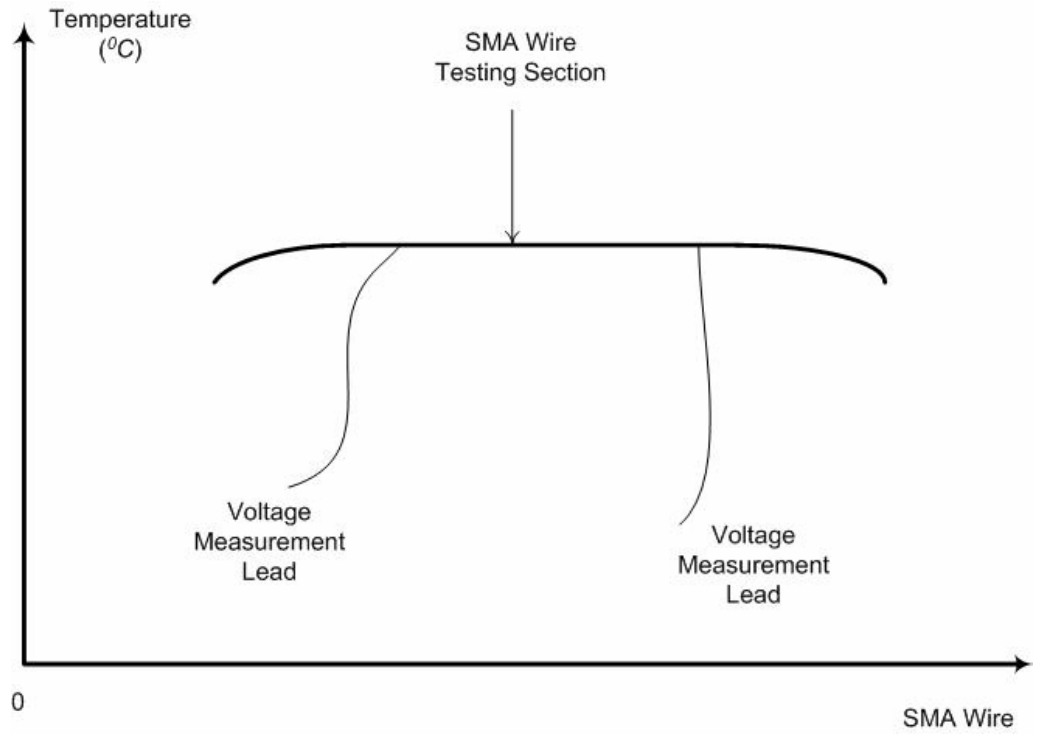

Figure 5-2 Expected Uniform Temperature Distribution on the SMA Wire

5.2.2 Sample SMA Wire

The SMA wire is a commercial product from DYNALLOY, INC: FLEXINOL Actuator Wire. It is a new roll of SMA wire with a total length of 20 meters. The specifications of the SMA wire are: diameter: 500 μm (0.020"), A_s Temp: 90 ^0C, Spool #: 9CF9513K. The selection of the specific diameter, length, preparation method and setup is based on experimental constraints, the temperature distortion on the sample SMA wire and the attachment accessories.

5.2.2.1 Diameter of the Sample SMA Wire

There are several diameters of SMA wire that can be chosen: 500 μm, 380 μm and 250 μm, etc., but only 500 μm is used in this experiment due to the need to spot weld thermocouples to the SMA wire. As described in the previous chapter, the temperature measurement of the SMA wire is performed using a thermocouple which is spot welded onto a section of SMA wire using a two-step spot welding procedure. At present, the two-step spot welding method works well only on a 500 μm diameter SMA wire. Another reason to use 500 μm diameter SMA wires is that it helps to decrease the temperature distortion over the SMA wire.

5.2.2.2 Length of the Sample SMA Wire

The maximum length of the SMA wire that can be used is 25 *cm* given the need to work within the bell jar of the vacuum chamber. The experiment is operated within a vacuum chamber with a 18" diameter (45.7 *cm*) Pyrex bell jar to allow the pressure variation method to be employed. As discussed in the following sections, the sample SMA wire is suspended on a supporting fixture which is placed on a metallic stand inside the bell jar. There should be a distance of 10 *cm* between the bell jar and the fixture to allow the bell jar to move down freely to cover the baseplate; therefore the length of the sample SMA wire must be less than 25 *cm*.

5.2.2.3 Oxide of the Sample SMA Wire

The SMA oxide should be removed before attaching thermocouples, voltage measurement leads and power leads so that good electrical contact can be achieved. Paper

sheet (3M Wetordry431Q, in 180 ^{0}C weight) was used to remove the oxide as described in **Section 5.5**.

5.2.2.4 Ring Terminal

(a) Before crimping (b) After crimping

Figure 5-3 Ring Terminal (DYNALLOY, INC)

Ring terminals from Dynalloy, Inc are attached to the SMA wire to provide a means to connect to the fixture. The detailed specifications can be downloaded from the website (http://www.dynalloy.com/CrimpPdfs/6983.pdf). The ring terminals provide a good method to hold the sample SMA wire tightly when they are properly crimped onto the sample SMA wire. A crimping tool is required to obtain a good connection with the SMA wire. In this work, a crimping tool SPC CCT-8424-01 is used to crimp the ring terminals onto the sample SMA wire. Before crimping, a piece of metal is curved to form a groove on the lower part of the ring terminal, where the end of the SMA wire can be placed, as in **Figure 5-3 (a)**. When the sample SMA wire end is in the groove, the crimping tool applies a force on the groove and the two pieces of metal attach firmly onto the SMA wire, as in **Figure 5-3 (b)**. The ring terminal can bear up to 4.5 kg of force.

5.2.3 SMA Wire Setup on the Fixture

As described previously, it is very important to keep a uniform temperature distribution on the SMA wire during the experiment, so the SMA wire should be as big in diameter as possible, while the thermocouple leads, voltage measurement leads; power leads should be as thin as possible to minimize conduction losses. The placement of the thermocouples, the voltage measurement leads, the power leads and the ring terminals should also be properly arranged to keep a uniform temperature distribution on the SMA wire. The SMA wire setup on the test fixture is given in **Figure 5-4.**

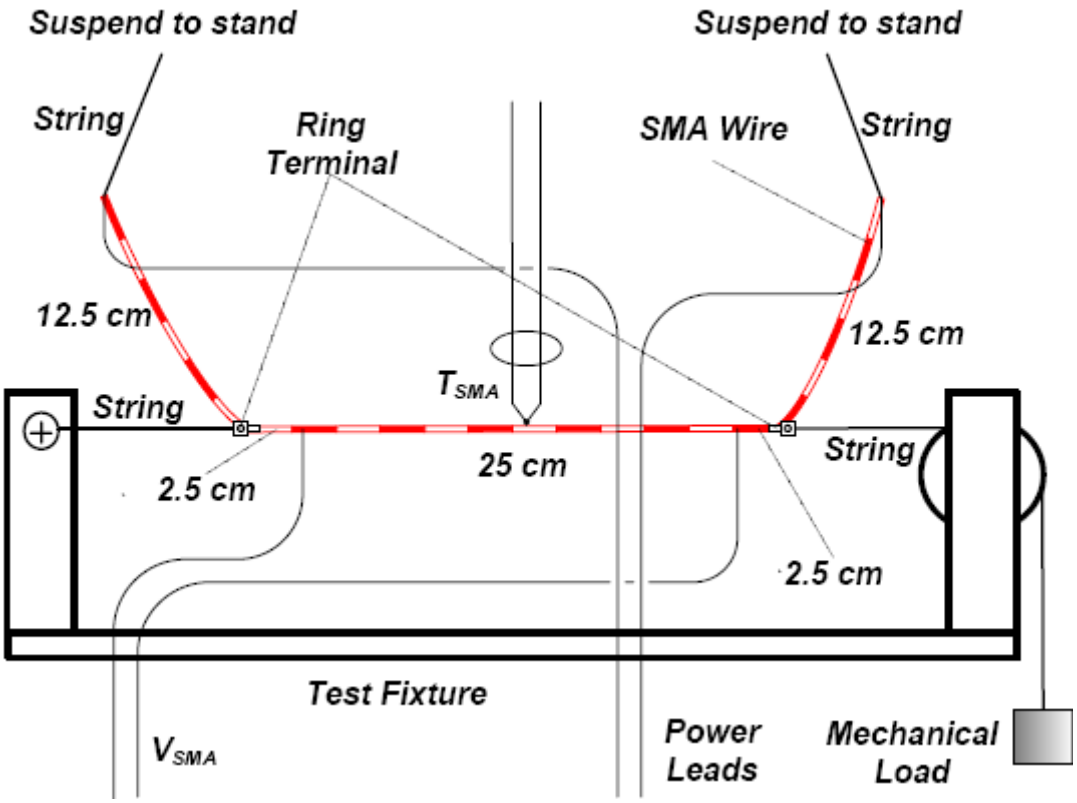

Figure 5-4 Sample SMA Wire Setup on the Fixture

In **Figure 5-4**, the test section of the SMA wire is 50 *cm* in length. Two ring terminals are crimped onto the SMA wire 12.5 *cm* from each end. One ring terminal is suspended to the left side of the fixture on the screw by a piece of string while the other ring terminal is connected to a mechanical load with another piece of string across a pulley. An E-type 40 AWG thermocouple is attached to the centre of the 50 *cm* sample SMA wire using a two-step spot welding procedure which is described in the **Section 4.4**. Two constantan 40 AWG thermocouple wires are spot welded on the SMA wire 2.5 *cm* closer to the centre of the sample SMA wire. Two 30 AWG copper wires are connected to the two ends of the SMA wire using two alligator clips. The two ends of the SMA wire are then suspended in a horizontal orientation above the fixture.

5.2.3.1 E-type 40 AWG Thermocouple

When thermocouples are attached to an SMA wire, it can lead to conductive heat transfer along the thermocouple wire, thus making the temperature of the SMA wire lower at the attachment point than other locations. In order to minimize the temperature drop of the SMA wire at the attachment point, thermocouples should be as thin in diameter as possible and its thermal conductivity should be as low as possible in order to minimize the temperature distortion that the thermocouple may bring to the SMA wire.

40 AWG thermocouple wire is one of the thinnest thermocouples available. E-type thermocouples contain constantan and chromel thermocouple wires. Constantan's thermal conductivity is 21.8 *W/(m·K)*, chromel's thermal conductivity is 19.2 *W/(m·K),* which are much lower than copper's thermal conductivity: 391 *W/(m·K)* that is found in T-type thermocouples.

A E-type 40 AWG thermocouple was attached to the centre of the SMA wire test section. It is assumed that the temperature reading at this point represents the temperature along the entire test section of the SMA wire. The thermocouple was spot welded onto the SMA wire using the two-step spot welding method in order to obtain a joint that provides good thermal contact and eliminates the influence of the current that passes through the SMA wire.

5.2.3.2 Voltage Measurement Leads

Similar to the selection of the thermocouples, two 40 AWG, constantan wires were used as voltage measurement leads in the experiment due to their small diameter and low thermal conductivity. The voltage measurement leads were spot welded onto the SMA wire to provide good electrical connections. The location of the voltage measurement leads is discussed in **Section 5.2.3.4**.

5.2.3.3 Power Leads

Power leads also contribute to temperature distortion in the SMA wire; therefore power leads can not be too thick in diameter. On the other hand, power leads should be large enough to carry the required current up to 2 A. As a balance of these two factors, 30 AWG copper wires were used as power leads in the experiment. Copper has high thermal conductivity (391 $W/(m \cdot K)$), and acts as a very good conductor. The power leads were connected to the two ends of the SMA wire using two alligator clips. The placement of power lead is discussed in the following section.

5.2.3.4 Placement of TCs, Volt Measurement Leads, Power Leads and Ring Terminal

In order to keep a uniform temperature over the test section of the SMA wire, the locations of the thermocouple leads, voltage measurement leads and power leads must be given proper consideration.

A 2.5 *cm* distance between the ring terminal and the voltage measurement leads on the SMA wire is necessary to help reduce the temperature drop that the ring terminal brings to the test section of the SMA wire. If the SMA wire test section is too close to the ring terminal, there is large temperature difference over the SMA wire and the SMA wire that is farther away from the ring terminal will have a higher temperature than the SMA wire adjacent to the ring terminal. This will lead to uncertainties when modeling the heat transfer from the SMA wire. The infrared thermal imaging in **Appendix A** shows that when the SMA wire is 1.5 *cm* away from the ring terminal, it is not significantly affected by the ring terminal.

A 12.5 *cm* offset is required to reduce the influence from the power leads for the same reason. The power leads are 30 AWG copper wires, which have a large thermal conductivity (391 *W/(m·K)*). When the power leads are attached too close to the SMA test section, the measured temperature of the SMA wire appears to be lower than expected, as a result of a conduction loss along the highly conductive power leads.

5.2.3.5 String

The strings in **Figure 5-4** are all cotton string, which connect the sample SMA wire to the fixture, the load, and the level stand above the fixture. Cotton string is flexible and it

is easy to tie cotton string onto the ring terminal or the fixture. Cotton string is also strong enough to bear the force when a load is applied to the SMA wire. There is no conduction loss along the cotton string when it connects the sample SMA wire to the fixture.

Two cotton strings are used to tie each end of the SMA wire to the level stand above the fixture so that they do not contact with the metallic fixture. If the SMA wire touches the fixture, a conductive loss occurs which makes the temperature of the SMA wire at these locations lower than other locations on the SMA wire.

5.2.3.6 Fixture

The test fixture was made in the machine shop of the Faculty of Engineering at the University of Waterloo, according to the fixture schematic shown in **Figure 5-5**. On the left side, the SMA wire is suspended to a screw by a piece of cotton string; on the right side, the SMA wire is pulled downward by a mechanical load through another piece of string along a pulley. The pulley is designed to allow the SMA wire to contract when heated and relax when cooled without exerting any unwanted forces.

5.2.3.7 Mechanical Load

The load is a block with a weight of 300 g, which pulls the SMA wire to keep it in tension. Because the SMA wire contracts and extends when turning on /off the power input, it is necessary to use a load to keep the SMA in tension during the experiment, which conform with the assumption of a straight thin circular cylinder for the heat transfer model.

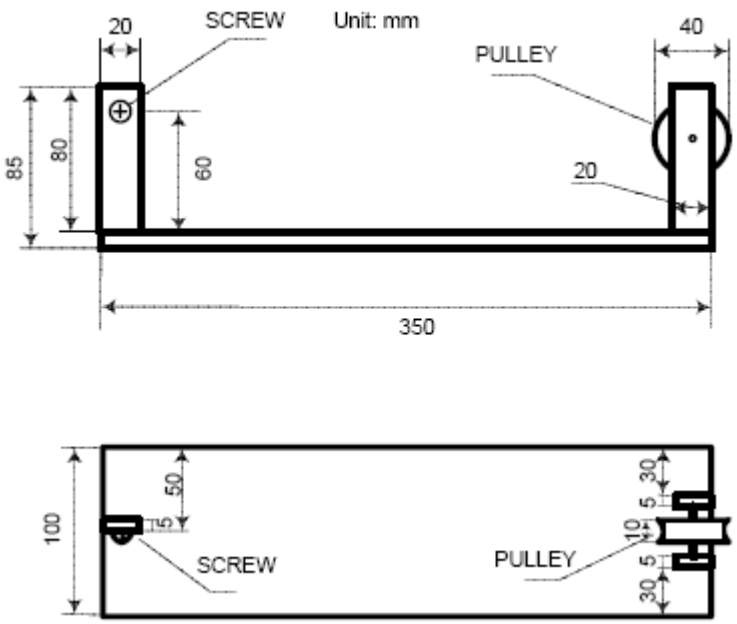

Figure 5-5 Test Fixture

5.3 Experimental Setup Diagrams

The experimental setup diagram is shown in **Figure 5-6**. There are four parts in the experimental setup: the inclination angle control; the pressure control and monitor; the power supply circuit and the data acquisition system. A close up diagram of the bell jar vacuum chamber is shown in **Figure 5-7**, which gives more details on the SMA setup on the fixture in the bell jar.

Inclination Angle Control

As shown in **Figure 5-7**, the inclination angle control is realized by an orientation adjustment string in the bell jar. The orientation adjustment string is tied to the left side of the fixture at the location A, at the other end; it connects to the level stand at the location

B. By adjusting the string length between A and B, the SMA wire is inclined from horizontal at a desired angle, as shown in **Figure 5-8**.

The Pressure Control and Monitor

The pressure control is performed by using an air release valve, the vacuum pump valve, vacuum pump and vacuum gauge that are connected to the platform by metal tubing. A Pyrex bell jar is used to cover the test fixture and establish a controlled ambient environment around the fixture. The air pressure is measured using a Varian CeramiCel vacuum gauge which was installed on the baseplate of the NRC 3117 vacuum station. The Varian CeramiCel vacuum gauge transfers the pressure signals to a Keithley 2700/7700 for recording and analyzing.

The Power Supply Circuit

The power supply circuit consists of the DC power supply, the current shunt and the SMA wire, which are connected in a series arrangement.

The Data Acquisition

As shown in **Figure 5-6**, data acquisition was performed using a Keithley 2700/7700, with measurements for: T_{amb}, T_{SMA}, V_{SMA}, V_{shunt} and $V_{pressure}$. The Keithley 2700/7700 is connected to a computer and is operated under the control of the manufacturer's software: Keithley *ExceLINX*.

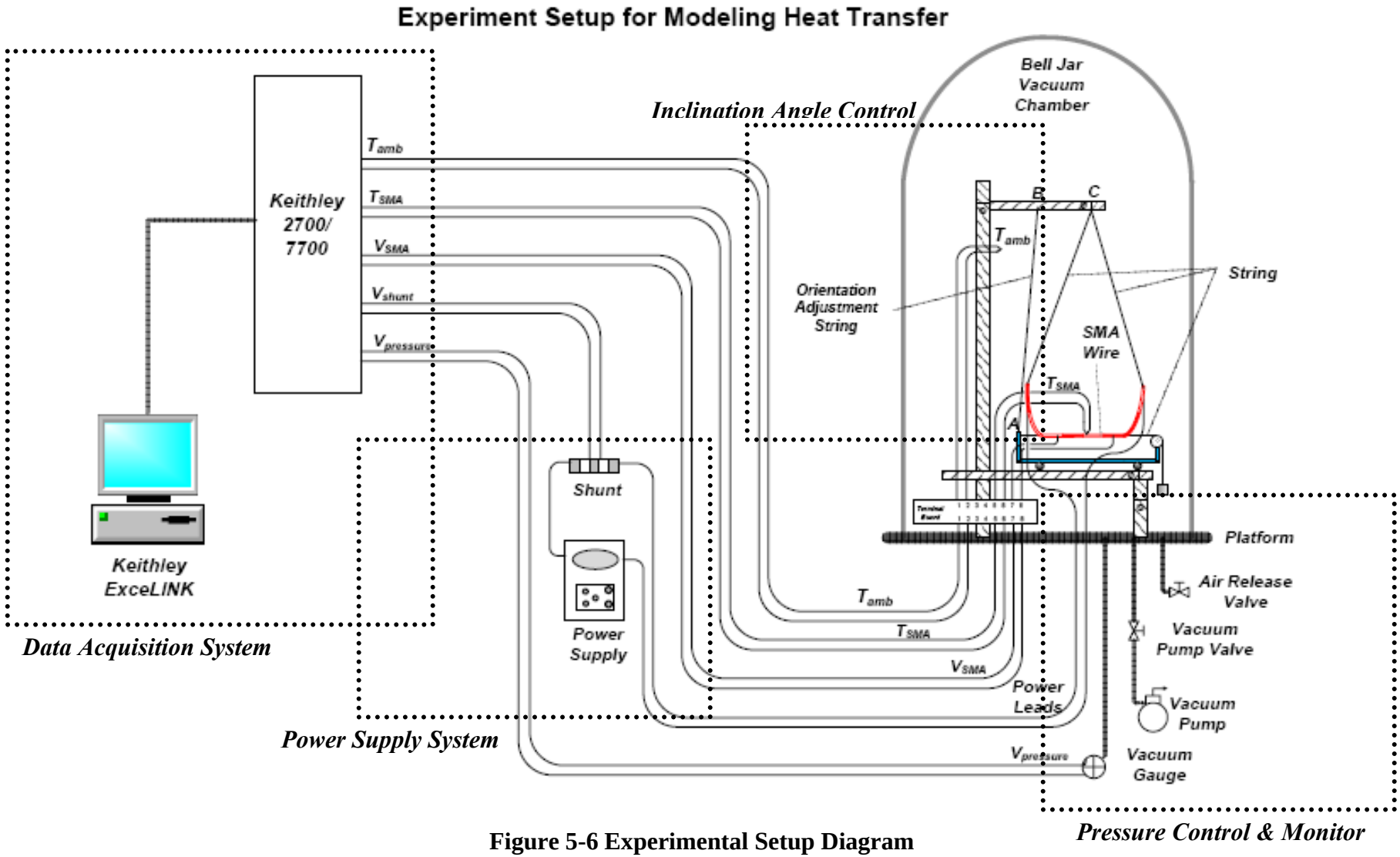

Figure 5-6 Experimental Setup Diagram

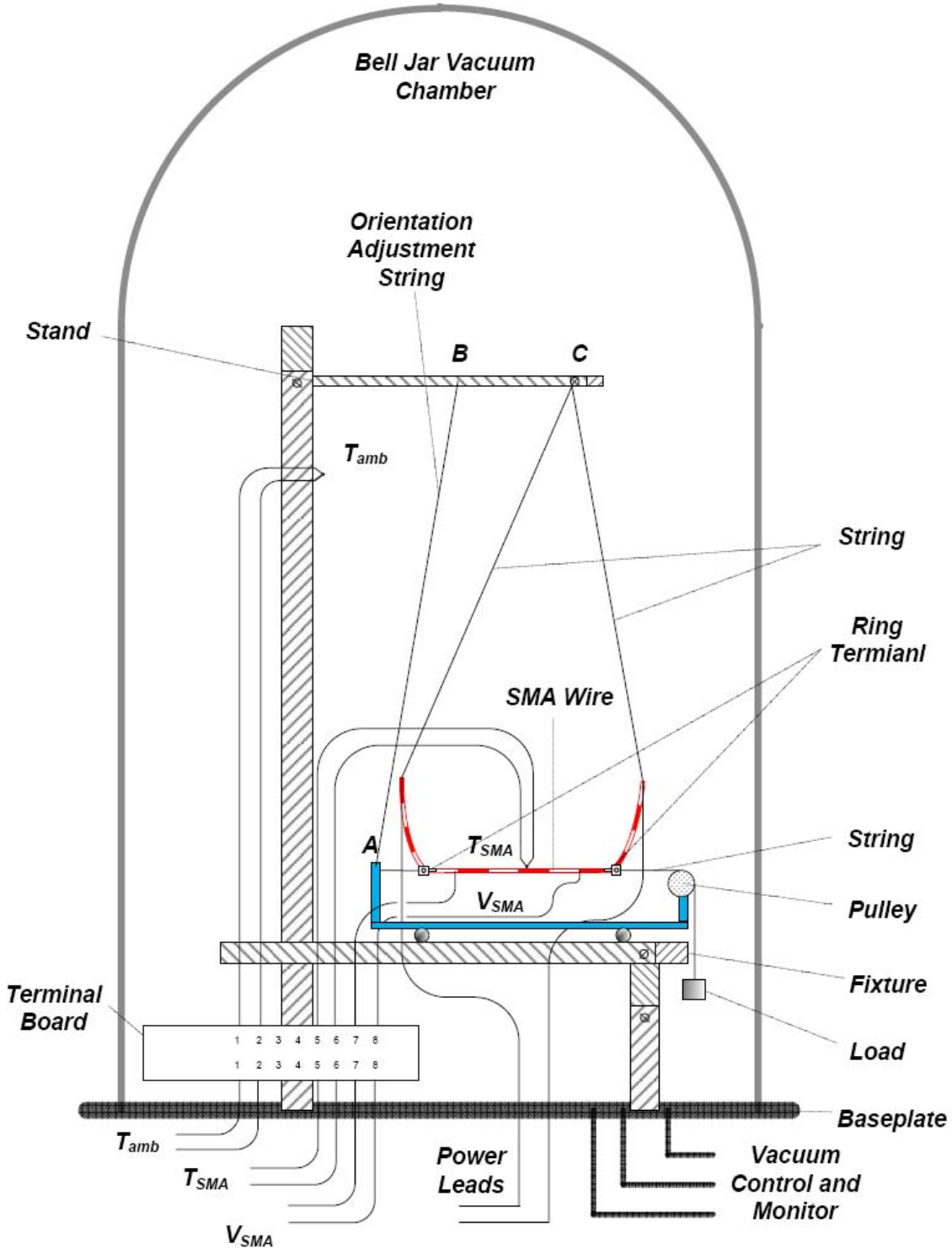

Figure 5-7 Experimental Close Up Diagram of Bell Jar

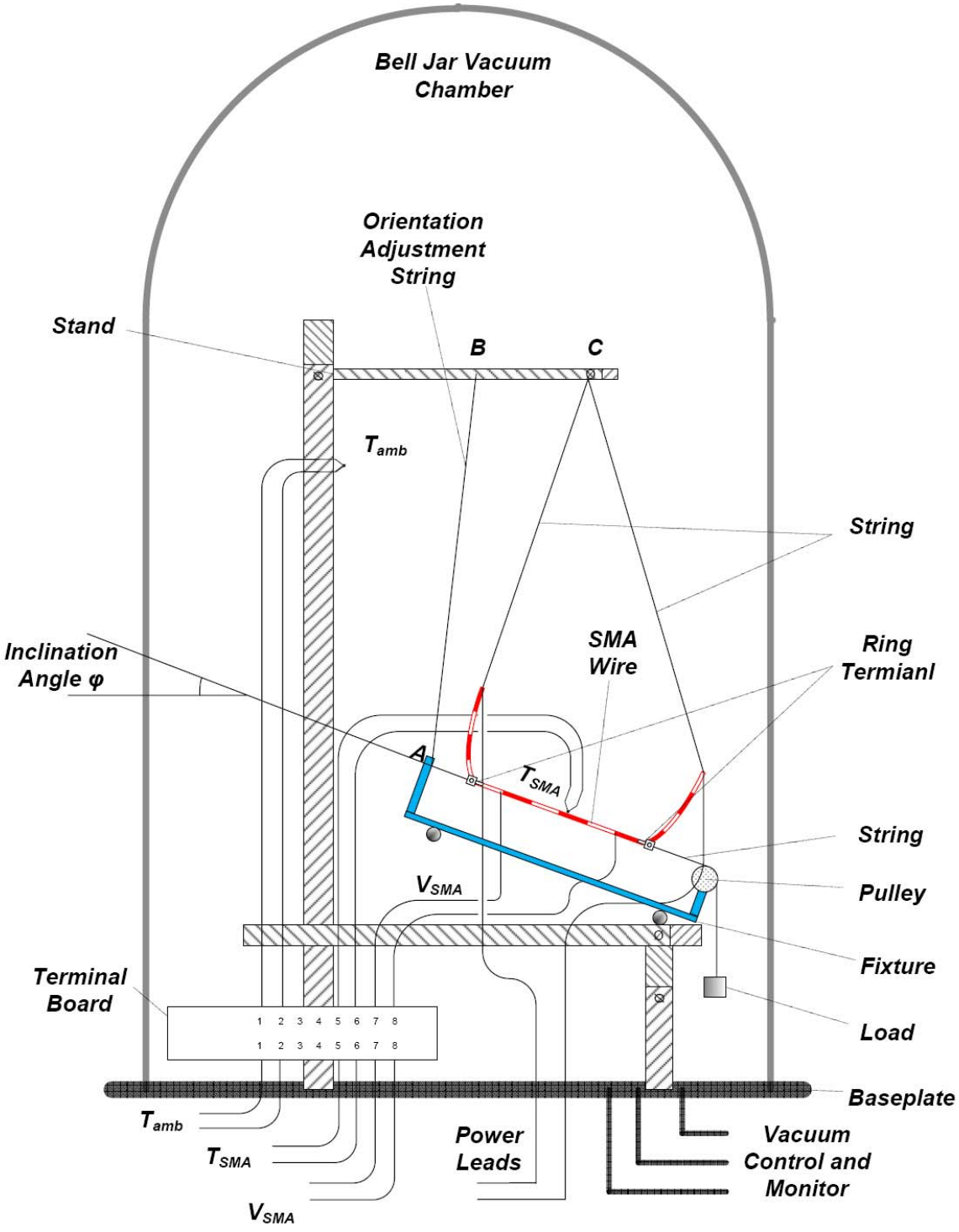

Figure 5-8 SMA Wire Inclined From Horizontal at an Angle φ

5.4 Equipment

5.4.1 Inclination Angle Control

The orientation adjust control consists of a cotton string, which connects the fixture at the location A and the stand at the location B, as shown in **Figure 5-7**. When the SMA wire needs to be inclined from horizontal at an angle φ during the experiment, for example: 15^0, 30^0, 45^0, 60^0, 75^0 and 90^0 (vertical), the fixture can be raised at the left side to make the SMA wire inclined at a prescribed angle. A protractor with $\pm 0.5^0$ accuracy is used to verify that the SMA wire is inclined by the prescribed angle.

5.4.2 Pressure Control and Monitor

5.4.2.1 NRC 3117 Vacuum Station

Pressure variation is controlled using a NRC 3117 vacuum station, which includes a 18" dia x 30" tall Pyrex bell jar with implosion cage on a 20" dia stainless steel baseplate; electromechanical hoists installed on the baseplate; a pumping system that connects the baseplate to a 17 CFM mechanical roughing pump, a NRC VHS 6 diffusion pump rated at 2400 *L / s*, a NRC 316 series LN 2 trap and electropneumatic valves. The fixture and the sample SMA wire are placed on the stand which is covered by the bell jar.

The mechanical roughing pump can achieve a vacuum from 1 *atm* (760 *torr*) to around 0.001 *torr*, which meets the air pressure requirement for modeling natural convective heat transfer. But the diffusion pump can make a higher vacuum from 10^{-7} *torr* to 10^{-3} *torr*,

which is necessary to estimate the conduction heat loss at a prescribed temperature, which is described in the **Appendix A**.

5.4.2.2 CeramiCel VCMT-13 Vacuum Gauge

The air pressure in the bell jar is measured using a CeramiCel / Varian Capacitance Diaphragm Gauge VCMT-13. The CeramiCel VCMT-13 is a highly accurate, compact and temperature-compensated vacuum pressure transducer that can operate at ambient temperature. The CeramiCel VCMT-13 features a ceramic capacitive sensor element which transfers pressure signals of air in the bell jar to direct voltage signals that can be measured and recorded by the Keithley 2700/7700. The CeramiCel VCMT-13 is powered by 24 *VDC* and outputs 0 – 10 *VDC* corresponding to the air pressure in the bell jar from 0 *torr* to 1000 *torr,* allowing *P* to be calculated as

$$P = V_{pressure} \times 100 \times 133.3\ Pa \tag{5-13}$$

The CeramiCel VCMT-13 has a resolution of 0.0015 % at full scale.

5.4.3 Power Supply and Current Shunt

Figure 5-9 Power Supply and Current Shunt

5.4.3.1 Power Supply

A BK PRECISION 1760A was used as the power supply to heat up the sample. The BK PRECISION 1760A has a constant current power supply mode, which is very helpful to monitor the magnitude of power input. The BK PRECISION 1760A can fix the voltage to a value and adjust the current that passes through the circuit, so the magnitude of the current reflects the magnitude of the power input during the experiment. The BK PRECISION 1760A can accurately adjust the current with an increment of 1 mA, this feature is very useful when adjusting power input to bring the SMA wire to a prescribed temperature in vacuum.

5.4.3.2 Current Shunt

The current shunt provides a fixed and stable resistance, so when the voltage across the shunt is measured, the current passing through the shunt can be accurately calculated by the formula: $I = V / R$. The shunt was connected with the SMA wire in a series circuit, so the current passing through the SMA wire could be determined by measuring V_{shunt} and calculating I in the circuit. In this experiment, the shunt has resistance 0.05 Ω, and current can be determined as:

$$I_{SMA} = V_{shunt} / 0.05 \tag{5-14}$$

5.4.4 Data Acquisition

5.4.4.1 Keithley 2700

Figure 5-10 Keithley 2700

The Keithley 2700 as shown in **Figure 5-10** was used in this experiment for it's auto range feature and it's manual operation feature. It can change its range automatically according to the magnitude of the measuring value. This feature provides great convenience when measuring V_{SMA}, V_{shunt} and $V_{pressure}$ because they are quite different in magnitude and require different measurement ranges. Another important feature of the Keithley 2700 is that it can operate manually. If you want to verify an unexpected value, you measure a value without considering any software or system factors.

5.4.4.2 Keithley 7700 Module Card

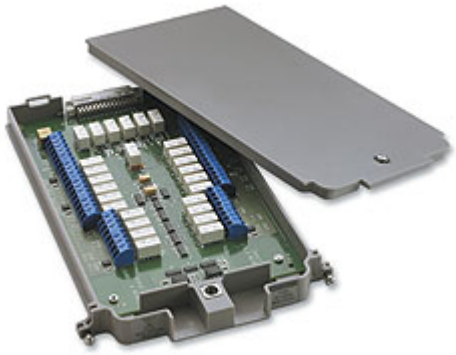

Figure 5-11 Keithley 7700 Module

The Keithley 7700 card is a 20-Channel, Multiplexer Module, as in **Figure 5-11**. Up to 20 channels different signals can be connected to the 7700 Module directly and these signals can be recorded by the computer for further analysis when the Keithley 2700 is operating. The Keithley 7700 module has an on board cold junction compensate feature for temperature measurement.

5.4.4.3 ExceLINX

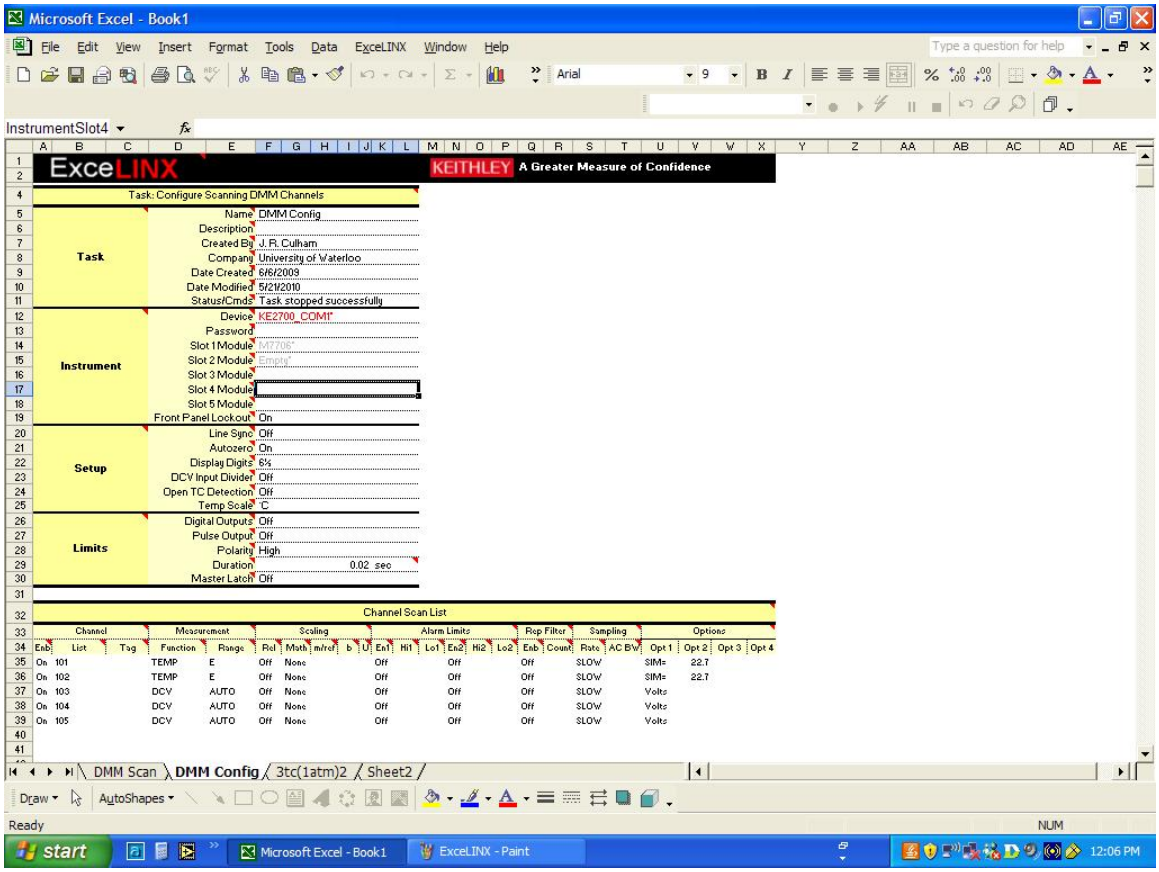

Figure 5-12 *ExceLINX* Channel Confiugration

Figure 5-12 is a screenshot of *ExceLINX*. *ExceLINX* is a Microsoft Excel add-in software. It is flexible and easy-to-use software with no programming required. Channel configuring and scan list setting can be completed in Microsoft Excel. Data are acquired from the Keithley 2700/7700 and are written into Microsoft Excel directly for further analysis.

5.4.5 Welder and Microscope

The two-step spot welding procedure was performed on the capacitor-discharge spot-welder; using a microscope to monitor the operation due to the small size of the thermocouple and the SMA wire.

5.4.5.1 Capacitor-Discharge Spot-Welder

The capacitor-discharge spot-welder consists of a power control unit, an electrode holder and a foot step. **Figure 5-13** shows the power control unit and the electrode holder.

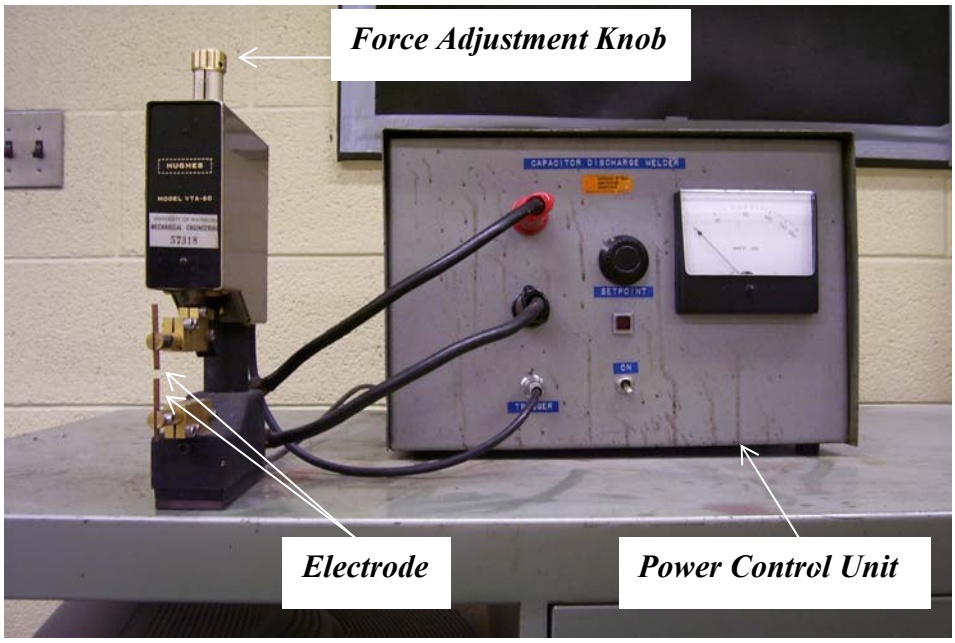

Figure 5-13 Capacitor-Discharge Spot-Welder

The power control unit supplies power to the electrodes, an analog meter that displays power output, an adjust knob to control the power output and a power switch to turn on / off the power unit. The power output needs to be set to 0.85 *W* due to the small size of the

thermocouple wire and the SMA wire. Larger power output can damage the thermocouple wire and the SMA wire instead of joining them together.

The electrode holder holds two electrodes, one is at the top location which can move downward allowing two electrodes to touch, and the other one is fixed at the bottom location. There is a force adjusting knob which controls the magnitude of the force applied on the top electrode when it presses onto the bottom electrode. In this work, the force is set to the minimum, again due to the small size of the thermocouple wire and the SMA wire. Large force settings can damage the wires during the spot welding.

The foot step controls the movement of the top electrode.

5.4.5.2 Microscope

The microscope is a 3X optical microscope. The location of the microscope needs to be properly adjusted so that the object lens focuses on the top of the bottom electrode and the spot welding operation can be monitored clearly through the microscope.

5.4.5.3 Thermocouple Welder

The ambient thermocouple fixed to the stand to measure the air temperature T_{amb} in the bell jar, as shown in **Figure 5-7.** This thermocouple bead can be made on the thermocouple welder: THERM-X (Model 258B). The detailed information about the welder can be downloaded from the website: http://www.therm-x.com/assets/5/258b.pdf . The minimum bead size that can be made on this welder is 0.25 *mm* dia, as shown in **Figure 5-14**. Though the beads are very small in size, they are still big when attaching them onto the SMA wire to measure T_{SMA}. Spot welding these beads onto the SMA wire

can cause a temperature jump/drop when measuring the temperature of a current carrying SMA wire. But for the temperature measurement of air in the bell jar, there is no problem with carrying current, so the thermocouple welder can be used to make these thermocouples.

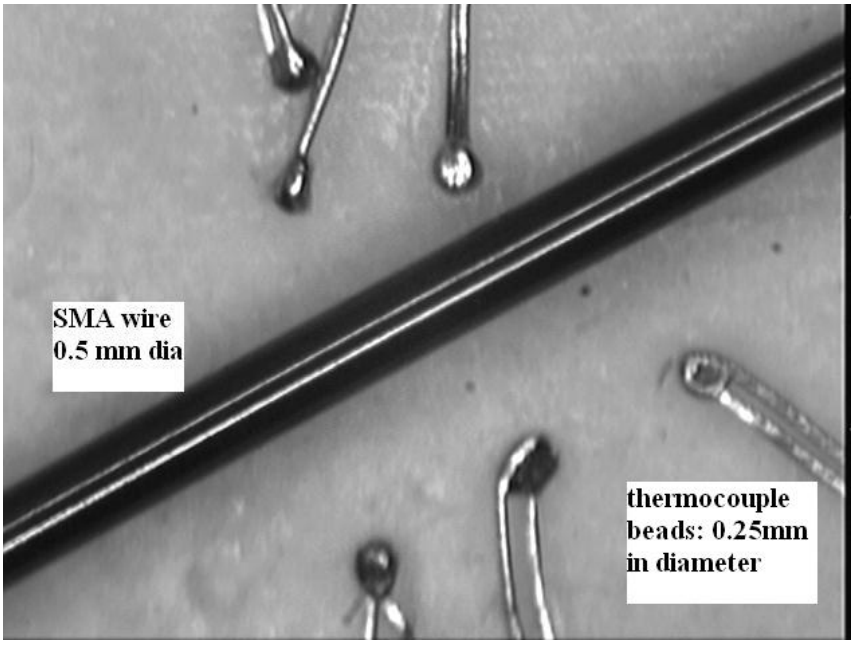

Figure 5-14 The Smallest Thermocouple Bead Made on THERM-X (Model 258B)

5.5 Experimental Procedure

The experiment consisted of three phases: general setup preparation; determination of Q_{rad} and convection heat transfer modeling. In the first phase, a sample SMA wire was prepared and suspended onto the fixture according to **Figure 5-4**; with the equipment wiring shown in **Figure 5-6**. In the second phase, the air pressure was decreased to 10^{-8} *torr* by the mechanical pump and the diffusion pump to determine the Q_{rad} of the test

section of the SMA wire at 100 ^{0}C. In the third phase, the test section of the SMA wire was heated to 100 ^{0}C again to collect data for heat transfer modeling.

The experimental steps are as follow:

General Setup Preparation

1. Cut a piece of Flexinol SMA wire with a diameter 0.5 *mm* (0.02”), length is 50 *cm*. Record its product’s specification including: the spool number, A_s and D.
2. Sand two ends of the SMA wire using Paper Sheet (3M Wetordry431Q, in 180C weight).
3. Crimp two Dynalloy ring terminals using the crimping tool (SPC CTT-8424-01) at the locations that are 12.5 *cm* away from the two ends. Tie the ring terminals onto the fixture with cotton string as shown in **Figure 5-4**.
4. Sand the centre point of the SMA wire as in step 2 for attaching thermocouple.
5. Choose E-type 40 AWG thermocouple 40 *cm*. Strip the ends of the two thermocouple wires and spot weld onto the SMA wire using the two step spot welding technique described in the **Section 4.4**.
6. Test the thermocouple using the pulse shut off method and the reverse current method that are described in the **Section 4.2** and **4.3**, to see if there is current influence on the temperature readout. If there is a current influence, re-weld the thermocouple on SMA wire according to the spot welding procedure in step 5.
7. Choose two constantan 40 AWG thermocouple wires 40 *cm*, strip the ends and spot weld onto the SMA wire at the points 2.5 *cm* away from the ring terminal

toward the centre. These two thermocouple wires are used as the voltage measurement leads.

8. Make an E-type 40 AWG, thermocouple on the thermocouple welder: THERM-X (Model 258B).

9. Place the fixture on the stand and wire the thermocouples, the voltage measurement leads, the power leads as in **Figure 5-6**.

10. Apply Dow Corning high vacuum grease on the edge of the bell jar and cover the bell jar on the baseplate. Check the state of all the valves status on the vacuum station NRC 3117, make sure that the air release valve is opened and the vacuum pump valve is closed.

Determination of Q_{rad}

11. Turn on the mechanical pump. After 5 minutes, when the vacuum pump is running normally, close the air release valve and open the vacuum pump valve

12. Keep evacuating, when the pressure is lower than 0.02 *torr*, proceed to the next step.

13. Turn on the diffusion pump.

14. After half an hour, run *ExceLINX*, which is pre-configured as in **Figure 5-12** at a scan speed of 5 *s*. Observe the temperature readout on *ExceLINX*.

15. Turn on the power supply, set to the constant voltage mode. Adjust the current output slowly to bring the SMA wire temperature to 100 ^{0}C. When the temperature readout on *ExceLINX* repeats 10 times, it shows the temperature is

stable and the sample SMA wire is in steady state. Turn off the power supply and *ExceLINX*.

16. Turn off the diffusion pump.
17. After 1 hour, turn off the mechanical pump. Open the air release valve to bring the pressure to 760 *torr*.
18. Close *ExceLINX*.

Convection Heat Transfer Modeling

19. Run *ExceLINX*, which is pre-configured as in **Figure 5-12** at a scan speed of 5s. Observe the temperature readout on *ExceLINX*
20. Turn on the power supply, set to the constant voltage mode. Adjust the current output slowly to bring the SMA wire temperature to 100 ^{0}C. When the temperature readout on *ExceLINX* repeats 10 times, it shows the temperature is stable and the sample SMA wire is in steady state. Turn off the power, the SMA wire temperature drops to the room temperature.
21. Turn on the mechanical vacuum pump to bring the pressure to 600 *torr*. Turn on the power and adjust the current to bring the SMA wire temperature to $100^{0}C$. When the temperature readout on *ExceLINX* repeats 10 times, turn off the power, the SMA wire temperature drops to the room temperature.
22. Change pressure to 500 *torr*, 400 *torr*, 300 *torr*, 200 *torr*, 100 *torr*, 66 *torr*, 33 *torr* and 1 *torr*, repeat the step 21.
23. Close *ExceLINX*.

24. Open the bell jar, change the inclination angle from 0^0 (horizontal) to 15^0, 30^0, 45^0, 60^0, 75^0, 90^0 (vertical), then repeat above step from 19 to 23.

5.6 Uncertainty Error Analysis

A full uncertainty analysis was carried out to estimate the uncertainty errors of each measurement and calculation results. Analysis detail is presented in **Appendix B**. The uncertainty of Q_{rad} is 0.142 %. The average uncertainties for the Rayleigh numbers (Ra_D) and the Nusselt numbers (Nu_D) are 11.2 % and 4.65 %, respectively. The uncertainties for each individual Ra_D and Nu_D are presented in **Table 6-1** to **6-7**.

5.7 Summary of Experimental Methods

The detailed experimental methods have been discussed step by step: from the background of the experiment to the setup of sample SMA wire on the test fixture; from the experimental setup diagrams to the descriptions of the equipment which are required to collect data. In the end, the experimental procedure and the uncertainty error analysis method were provided. The experiment tests were performed following the descriptions in this chapter and the experimental results are present and discussed in the next chapter.

Chapter 6

Results and Discussions

In the **Section 6.1**, the raw data are processed and presented; the computational results are tabulated and plotted for modeling. A new heat transfer correlation is developed from the results of *Nu* and *Ra* in the **Section 6.2**. The comparisons between the new correlation and the existing correlations are presented and discussed. **Section 6.3** gives three examples of SMA wire in different diameters and inclination angles to explain how to use the new correlation to predict the temperature of the SMA wire when current I is provided.

6.1 Experimental Data Reduction

Following the steps described in the **Section 5.5**, a set of data was collected during the experiment. Using the appropriate equations, the Rayleigh numbers (Ra_D) and the Nusselt numbers (Nu_D) at each inclination angle were calculated. The data and the results are presented in this section.

g, Pr, μ, R, Z are constants. $g = 9.8\ m/s^2$, $R = 0.287\ kJ/(kg{\cdot}K)$. Z is the compressibility factor of air. Since air is assumed to be an ideal gas, $Z = 1$.

The experiment was designed to heat the SMA wire to $T_{SMA} = 373\ K$ ($100\ ^0C$), under which Nu_D and Ra_D were determined and a heat transfer correlation was developed. The ambient temperature $T_\infty = 296\ K$ ($23\ ^0C$), the mean temperature is $T_m = 334\ K$ ($61.5\ ^0C$). The constants can be determined at $T_m = 334\ K$: $\mu = 2.008 \times 10^{-5}\ kg/(m.s)$; $Pr = 0.7202$.

The diameter and the length of the SMA wire test section were measured as: D = 0.49 *mm*; l = 191 *mm*.

Air pressure can be calculated from $V_{pressure}$ using **Equation 5-13**, as described in the **Section 5.4.2.2** ($P = V_{pressure} \times 100 \times 133.3$ *Pa)*.

The current of the SMA wire is calculated using **Equation 5-14** ($I_{SMA} = V_{shunt}$ / 0.05 A), as described in **Section 5.4.3.2**

A preliminary test was performed in vacuum to determine the power input to the SMA wire test section VI_{vacuum} =0.0924 ± 0.00013 *W,* when T_{SMA} = 373 *K*. From **Equation 5-11**, Q_{rad} = 0.0924 ± 0.00013 *W*. Its uncertainty is calculated by **Equation B-19** in **Appendix B**

The Rayleigh number (Ra_D) is calculated using **Equation 5-6**, its uncertainty is calculated by **Equation B-22** in **Appendix B**, the Nusselt number (Nu_D) is calculated by **Equation 5-9**, its uncertainty is calculated by **Equation B-20** in **Appendix B**

The calculation results along with the raw data T_{SMA}, T_∞, V_{shunt}, V_{SMA}, and $V_{pressure}$, are tabulated in **Table 6-1 to 6-7.** Nu_D vs Ra_D is plotted in **Figure 6-1**.

The Nu_D-Ra_D curves in **Figure 6-1** are generally smooth except for two instances in the range $0.4 < Ra_D < 0.6$ when the inclination angles are 15^0 and 60^0. These inconsistencies are a result of instability in the temperature field leading to fluctuations in the natural convection flow, primarily for an ambient air pressure between 600 and 760 *torr*. As a result, the SMA wire temperature must be closely monitored and the power adjusted to maintain a temperature of approximately 100 ^0C. The two instances in **Figure 6-1** are a result of not responding quickly enough to a sudden change in wire temperature.

Experimental data reduction has been performed. The raw data and the computational results of Nu_D and Ra_D, along with the uncertainty of each Nu_D and Ra_D, have been tabulated for each inclination angle. Nu_D vs Ra_D for all inclination angles have been plotted and are ready for development of new heat transfer correlation in the next section.

Table 6-1 Raw Data and the Results Nu_D, Ra_D at Inclination Angle $\varphi = 0^0$

T_{SMA} (K)	T_∞ (K)	V_{shunt} (V)	V_{SMA} (V)	$V_{pressure}$ (V)	Nu_D	Ra_D	$\delta Nu_D/Nu_D$	$\delta Ra_D/Ra_D$
373.64	295.49	0.0719	1.0461	7.6000	1.0703	0.6069	4.784 %	11.531 %
373.05	295.49	0.0699	1.0171	6.2186	1.0166	0.4035	4.784 %	11.531 %
373.02	295.60	0.0684	0.9950	5.2037	0.9724	0.2815	4.765 %	11.483 %
373.22	295.64	0.0666	0.9684	4.1407	0.9162	0.1783	4.757 %	11.465 %
373.16	295.70	0.0643	0.9345	3.1119	0.8505	0.1004	4.745 %	11.434 %
373.10	295.77	0.0613	0.8920	2.0746	0.7705	0.0445	4.733 %	11.405 %
373.15	295.86	0.0570	0.8278	1.0416	0.6552	0.0112	4.717 %	11.363 %
373.26	295.90	0.0548	0.7959	0.6850	0.5997	0.0048	4.711 %	11.349 %
373.12	295.96	0.0518	0.7525	0.3434	0.5303	0.0012	4.700 %	11.321 %

Table 6-2 Raw Data and the Results Nu_D, Ra_D at Inclination Angle $\varphi = 15^0$

T_{SMA} (K)	T_∞ (K)	V_{shunt} (V)	V_{SMA} (V)	$V_{pressure}$ (V)	Nu_D	Ra_D	$\delta Nu_D/Nu_D$	$\delta Ra_D/Ra_D$
373.25	295.64	0.0712	1.0386	7.6000	1.0581	0.6035	4.758 %	11.465 %
372.41	295.60	0.0690	1.0065	6.1761	1.0016	0.3948	4.766 %	11.486 %
373.17	295.70	0.0674	0.9817	5.1369	0.9426	0.2742	4.746 %	11.436 %
373.02	295.73	0.0656	0.9558	4.1146	0.8929	0.1753	4.740 %	11.422 %
373.06	295.77	0.0634	0.9239	3.0854	0.8303	0.0984	4.734 %	11.405 %
373.23	295.84	0.0608	0.8851	2.0561	0.7558	0.0437	4.722 %	11.375 %
372.98	295.94	0.0567	0.8256	1.0279	0.6501	0.0109	4.703 %	11.329 %
372.99	295.97	0.0544	0.7919	0.6796	0.5928	0.0048	4.698 %	11.316 %
372.98	296.00	0.0514	0.7482	0.3398	0.5224	0.0012	4.693 %	11.305 %

Table 6-3 Raw Data and the Results Nu_D, Ra_D at Inclination Angle $\varphi = 30^0$

T_{SMA} (K)	T_∞ (K)	V_{shunt} (V)	V_{SMA} (V)	$V_{pressure}$ (V)	Nu_D	Ra_D	$\delta Nu_D/Nu_D$	$\delta Ra_D/Ra_D$
373.59	296.37	0.0701	1.0202	7.6000	1.0315	0.5919	4.629 %	11.144 %
373.08	296.43	0.0683	0.9939	6.1760	0.9839	0.3879	4.619 %	11.119 %
372.98	296.51	0.0667	0.9711	5.1481	0.9389	0.2685	4.607 %	11.089 %
373.11	296.55	0.0650	0.9468	4.1187	0.8881	0.1719	4.600 %	11.072 %
373.06	296.61	0.0629	0.9154	3.0891	0.8273	0.0965	4.589 %	11.045 %
373.18	296.68	0.0602	0.8755	2.0599	0.7504	0.0429	4.578 %	11.017 %
373.04	296.76	0.0560	0.8149	1.0384	0.6428	0.0109	4.565 %	10.984 %
373.01	296.78	0.0538	0.7833	0.6838	0.5887	0.0047	4.562 %	10.978 %
373.18	296.81	0.0508	0.7394	0.3403	0.5159	0.0012	4.556 %	10.964 %

Table 6-4 Raw Data and the Results Nu_D, Ra_D at Inclination Angle $\varphi = 45^0$

T_{SMA} (K)	T_∞ (K)	V_{shunt} (V)	V_{SMA} (V)	$V_{pressure}$ (V)	Nu_D	Ra_D	$\delta Nu_D/Nu_D$	$\delta Ra_D/Ra_D$
373.24	295.33	0.0697	1.0158	7.6000	0.9609	0.5947	4.674 %	11.256 %
373.45	295.30	0.0681	0.9918	6.1983	0.8891	0.3989	4.671 %	11.249 %
373.08	295.31	0.0662	0.9640	5.1667	0.8689	0.2758	4.671 %	11.249 %
373.38	295.30	0.0647	0.9418	4.1391	0.8195	0.1762	4.660 %	11.223 %
373.01	295.34	0.0625	0.9094	3.0924	0.7778	0.0991	4.654 %	11.208 %
373.18	295.43	0.0599	0.8717	2.0656	0.7099	0.0438	4.645 %	11.184 %
373.19	295.49	0.0558	0.8124	1.0364	0.6089	0.0109	4.636 %	11.161 %
373.15	295.53	0.0536	0.7802	0.6812	0.5549	0.0047	4.626 %	11.136 %
373.07	295.61	0.0502	0.7296	0.3394	0.4846	0.0012	4.614 %	11.107 %

Table 6-5 Raw Data and the Results Nu_D, Ra_D at Inclination Angle $\varphi = 60^0$

T_{SMA} (K)	T_∞ (K)	V_{shunt} (V)	V_{SMA} (V)	$V_{pressure}$ (V)	Nu_D	Ra_D	$\delta Nu_D/Nu_D$	$\delta Ra_D/Ra_D$
372.97	296.11	0.0678	0.9865	7.6000	0.9609	0.5947	4.674 %	11.256 %
373.56	296.12	0.0656	0.9544	6.2100	0.8891	0.3989	4.671 %	11.249 %
373.22	296.12	0.0647	0.9421	5.1758	0.8689	0.2758	4.671 %	11.249 %
373.17	296.19	0.0630	0.9160	4.1419	0.8195	0.1762	4.660 %	11.223 %
373.50	296.22	0.0616	0.8958	3.1038	0.7778	0.0991	4.654 %	11.208 %
373.20	296.28	0.0589	0.8571	2.0682	0.7099	0.0438	4.645 %	11.184 %
373.00	296.33	0.0549	0.7982	1.0359	0.6089	0.0109	4.636 %	11.161 %
372.96	296.39	0.0526	0.7653	0.6830	0.5549	0.0047	4.626 %	11.136 %
373.28	296.46	0.0496	0.7220	0.3425	0.4846	0.0012	4.614 %	11.107 %

Table 6-6 Raw Data and the Results Nu_D, Ra_D at Inclination Angle $\varphi = 75^0$

T_{SMA} (K)	T_∞ (K)	V_{shunt} (V)	V_{SMA} (V)	$V_{pressure}$ (V)	Nu_D	Ra_D	$\delta Nu_D/Nu_D$	$\delta Ra_D/Ra_D$
373.25	296.73	0.0648	0.9444	7.6000	0.8768	0.5900	4.569 %	10.996 %
373.05	296.71	0.0633	0.9213	6.2100	0.8339	0.3929	4.573 %	11.006 %
373.23	296.76	0.0621	0.9036	5.1732	0.7995	0.2723	4.565 %	10.984 %
373.14	296.82	0.0606	0.8822	4.1423	0.7616	0.1738	4.554 %	10.959 %
373.29	296.86	0.0587	0.8538	3.1028	0.7081	0.0975	4.548 %	10.942 %
373.09	296.90	0.0563	0.8186	2.0706	0.6480	0.0433	4.542 %	10.929 %
373.03	296.97	0.0528	0.7680	1.0368	0.5634	0.0108	4.530 %	10.898 %
373.08	297.02	0.0509	0.7403	0.6823	0.5188	0.0047	4.522 %	10.878 %
373.09	297.06	0.0485	0.7054	0.3421	0.4647	0.0012	4.517 %	10.865 %

Table 6-7 Raw Data and the Results Nu_D, Ra_D at Inclination Angle $\varphi = 90^0$

T_{SMA} (K)	T_∞ (K)	V_{shunt} (V)	V_{SMA} (V)	$V_{pressure}$ (V)	Nu_D	Ra_D	$\delta Nu_D/Nu_D$	$\delta Ra_D/Ra_D$
372.94	297.05	0.0612	0.8898	7.6000	0.7814	0.5811	4.518 %	10.868 %
373.06	297.06	0.0603	0.8762	6.2063	0.7547	0.3878	4.516 %	10.863 %
373.34	297.10	0.0593	0.8617	5.1730	0.7255	0.2699	4.508 %	10.844 %
373.23	297.18	0.0579	0.8419	4.1392	0.6910	0.1724	4.497 %	10.817 %
373.03	297.25	0.0565	0.8214	3.1084	0.6573	0.0968	4.486 %	10.789 %
373.27	297.28	0.0548	0.7966	2.0738	0.6126	0.0431	4.481 %	10.777 %
373.32	297.32	0.0519	0.7536	1.0362	0.5407	0.0108	4.475 %	10.762 %
373.14	297.36	0.0502	0.7288	0.6850	0.5026	0.0047	4.469 %	10.747 %
373.21	297.40	0.0481	0.6984	0.3419	0.4556	0.0012	4.462 %	10.729 %

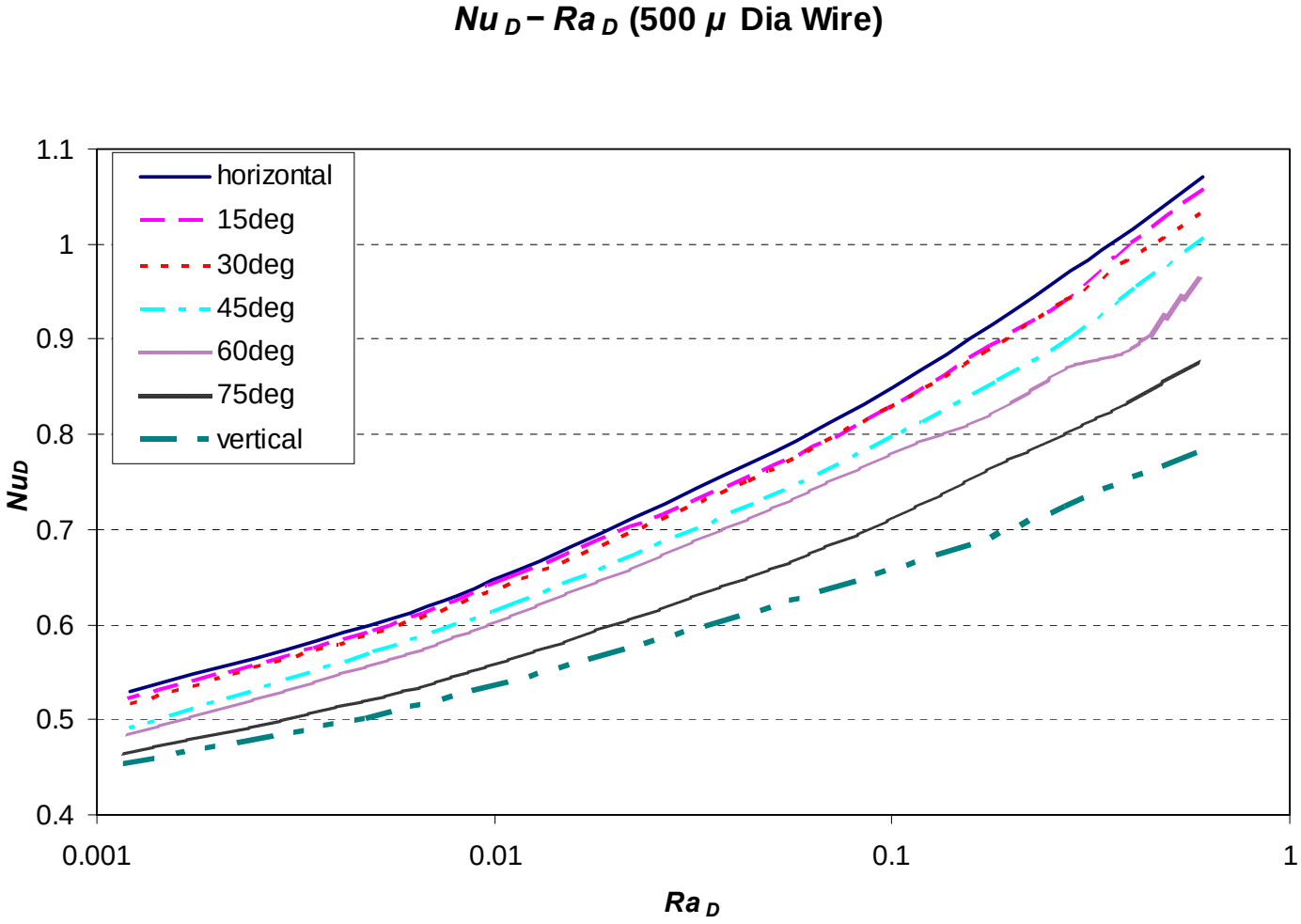

Figure 6-1 Nu_D vs Ra_D at Inclination Angles From 0 To 90^0 (Ra_D = 0.001 – 0.6)

6.2 Convective Heat Transfer Modeling

6.2.1 Development of Convective Heat Transfer Correlation

The Nu_D can be correlated with Ra_D in a power equation form: $Nu_D = CRa_D^n$ by using the "add trend line" feature in MS Excel, at each inclination angle.

Table 6-8 Correlation Nu_D = C Ra_D^n at Each Inclination Angle φ

Inclination Angle (degree)	$Nu_D = CRa_D^n$	*R-squared value*
0	$Nu_D = 1.1194 Ra_D^{0.1153}$	0.9965
15	$Nu_D = 1.0969 Ra_D^{0.1137}$	0.9959
30	$Nu_D = 1.0854 Ra_D^{0.113}$	0.998
45	$Nu_D = 1.049 Ra_D^{0.1144}$	0.9984
60	$Nu_D = 0.9971 Ra_D^{0.1085}$	0.9982
75	$Nu_D = 0.9122 Ra_D^{0.1036}$	0.9961
90	$Nu_D = 0.8128 Ra_D^{0.0882}$	0.9976

From **Table 6-8**, the constant coefficient C at each inclination angle can be further correlated with the inclination angle in a two order polynomial, by using the "add trend line" feature in MS Excel again:

$$C = -0.0033 \cdot \varphi + 1.158 \qquad (6\text{-}1)$$
$$R^2 = 0.8994$$

Similarly, the constant exponent n can be expressed relative to the inclination angle φ as:

$$n = -0.0003 \cdot \varphi + 0.1195 \quad (6\text{-}2)$$
$$R^2 = 0.7124$$

A correlation that comprises the inclination angle φ can be expressed as:

$$Nu_D = (-0.0033 \cdot \varphi + 1.158) \cdot Ra_D^{(-0.0003 \cdot \varphi + 0.1195)} \quad (6\text{-}3)$$

6.2.2 Verification of Convective Heat Transfer Correlation

The verification of the new convective heat transfer correlation is performed by comparing to existing correlations at various angles between horizontal and vertical. Due to very limited data available for inclined orientations and the only reviewed correlation for inclined wires from Oosthuizen **[78]** showing a much lower value compared to the new correlation, the verification focuses on the comparison to existing correlations in horizontal and vertical orientations. The new correlation is plotted in **Figure 6-4** in the horizontal orientation and **Figure 6-5** in the vertical orientation at a Rayleigh number range: $0.001 < Ra_D < 0.6$, with the respective existing correlations as reviewed in the **Section 2.2**.

6.2.2.1 Comparisons in Vertical and Horizontal

Figure 6-5 shows that the new correlation has the same trend as other correlations. However, there are minor differences between the new correlation and the other existing correlations. These discrepancies are the result of the different methods and conditions, or even the errors when the existing correlations were developed. Considering the new

correlation is positioned in the middle among the existing correlations: lower than Elenbass **[73]** and Mueller **[76]**; but higher than Zitsev & Sokovishin **[77]** and Yang **[74],** the new correlation should be acceptable in the vertical orientation.

Figure 6-4 shows that the discrepancies among the existing correlations are relatively smaller than that in **Figure 6-5**, and the trends of the existing correlations are very similar. The new correlation agrees with the existing correlations when the Rayleigh number (Ra_D) is low ($0.001 < Ra_D < 0.05$), but when the Rayleigh number is high, the new correlation is higher than the existing correlations. It is quite unusual that these four existing correlations have very similar trends and small discrepancies: ΔNu_D between maximum and minimum is 0.1 when Ra_D=0.001; ΔNu_D = 0.2 at Ra_D = 0.6, because they were developed for different conditions with completely different methods. Tsubouchi and Masuda **[69]** used oil as the fluid to developed their correlation, Morgan **[70]** suggested his correlation after analyzing numerous of correlations developed from others; though Churchill and Chu **[71]**, Raithby and Hollands **[72]** all developed their correlations using a theoretical method, their respective theoretical methods were completely different. The difference between the current correlation and the existing correlations is insignificant when Rayleigh number is low, but with Rayleigh number increasing, this difference becomes prominent, ΔNu_D between the current correlation and Raithby, Hollands **[72]** is 0.2 at Ra_D=0.6, which is 15.5 % higher than Raithby and Hollands' data. There are many possible reasons for these differences with increasing Rayleigh number including: air pressure, or temperature distortion on the SMA wire which is the result of the thermocouple attachment.

6.2.2.2 Temperature Distortion on SMA Wire

As it has been stated in the **Section 2.1.2**, there can be a temperature distortion error when measuring the temperature of a solid surface using a thermocouple. Before a thermocouple is attached to the SMA wire, the SMA wire is in thermal equilibrium in which the heat generated due to the Joule effect is dissipated to the environment through convection and radiation. There is no conduction along the SMA wire since the temperature of the SMA wire is constant along its length. When a thermocouple is spot welded to the SMA wire, conduction occurs along the thermocouple lead drawing heat away from the SMA wire in addition to convection. As a result, the temperature at the attachment point starts to drop and conduction along the SMA wire occurs in the direction towards to the attachment point due to the temperature gradient that now exists along the SMA wire. When a new thermal equilibrium is reached at the attachment point, its temperature stabilizes at a lower value than the previous temperature on the SMA wire. The difference between the previous temperature and the new balanced temperature at the attachment point is referred to as temperature distortion. The thermocouple measures the temperature at the attachment, but the SMA wire is actually at a higher temperature leading to a higher convection heat transfer rate.

The temperature distortion becomes larger when the air pressure is higher. In vacuum, there is no convection and the thermocouple wires dissipate heat through radiation when the heat flows into the thermocouple wires from the SMA wire at the attachment point. When there is a positive air pressure, the thermocouple wires have higher rates of heat dissipation because of convection in addition to radiation. As a result, the conduction leaving the attachment point increases and the temperature at the attachment point

becomes lower and the temperature distortion becomes larger. The convection increases with the air pressure, so the temperature distortion also increases with the air pressure. This explains that the difference between the new correlation and the existing correlation is larger when the Rayleigh number (Ra_D) is larger.

When the SMA wire is in vertical, the temperature distortion is not as large as that when the SMA wire is horizontal because the air adjacent to the SMA wire in vertical orientation is hotter which makes the attachment point temperature higher. When the SMA wire is placed horizontally, the air adjacent is heated up and becomes lighter. It then rises to form a plume at the top and then leaves the SMA wire. The cooler air fills the position where the heated air leaves as shown in **Figure 6-2 (a) & (b)**. **[91]** When the SMA wire is placed in a vertical orientation, as shown in **Figure 6-2 (c) [92]**, the adjacent air is heated by the SMA wire and rises to leave its original position. But the air that fills in is from below, which has previously been heated up by the SMA wire, therefore is hotter than in the horizontal orientation. The relative hotter air that rises from below can provide extra energy that balances the conduction via the thermocouple wires. The conduction along the SMA wire is not as large as in the horizontal orientation, and the temperature gradient along the SMA wire is not as large as in horizontal SMA wire as well. This is the reason why the temperature distortion in the vertical SMA wire is smaller than in the horizontal SMA wire. This explains why there is not an obvious difference between the new correlation and the existing correlations when the SMA wire is in the vertical orientation.

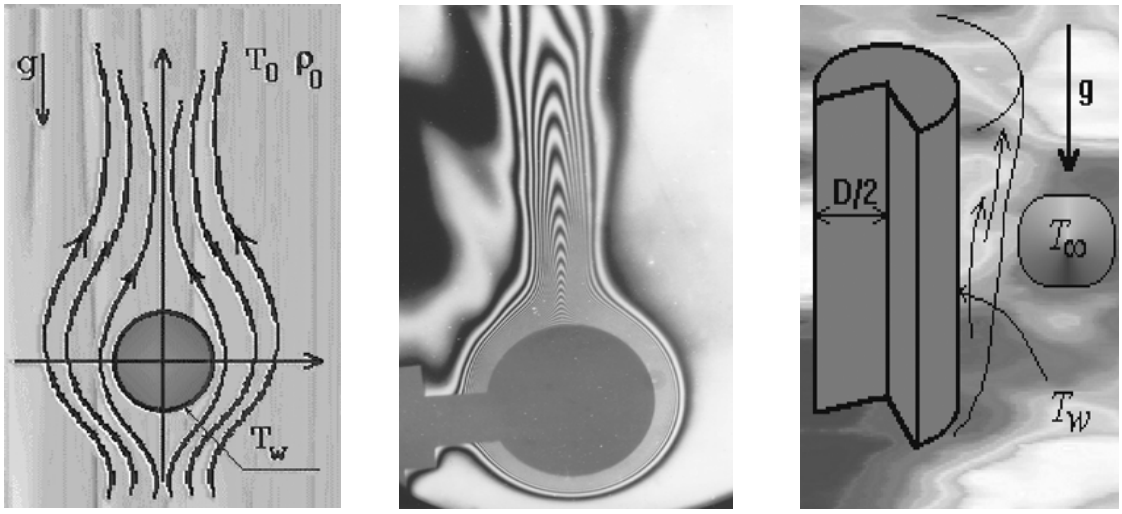

(a) **(b)** **(c)**

Figure 6-2 Natural Convective Flow Near Horizontal Cylinder and Vertical Cylinder

6.2.2.3 IR Picture Verifies the Temperature Distortion on SMA Wire

The temperature distortion error is hard to measure using any contact methods since any contact temperature sensors bring in new distortions. Invasive infrared thermal imaging can easily find the temperature distortion when using a thermocouple to measure the temperature of the SMA wire. The infrared thermal photo in **Figure 6-3** shows that: at the location on the SMA wire where the thermocouple is attached, the color is yellow, while at other locations on the SMA wire, the colors are white. The temperature distribution along the SMA wire below the thermal photo, which is the result of the line analysis on the thermal photo as stated in the **Section 3.3.2**, shows clearly that the temperature where the thermocouple is attached onto the SMA wire is 7 ^{0}C lower than other locations of the SMA wire.

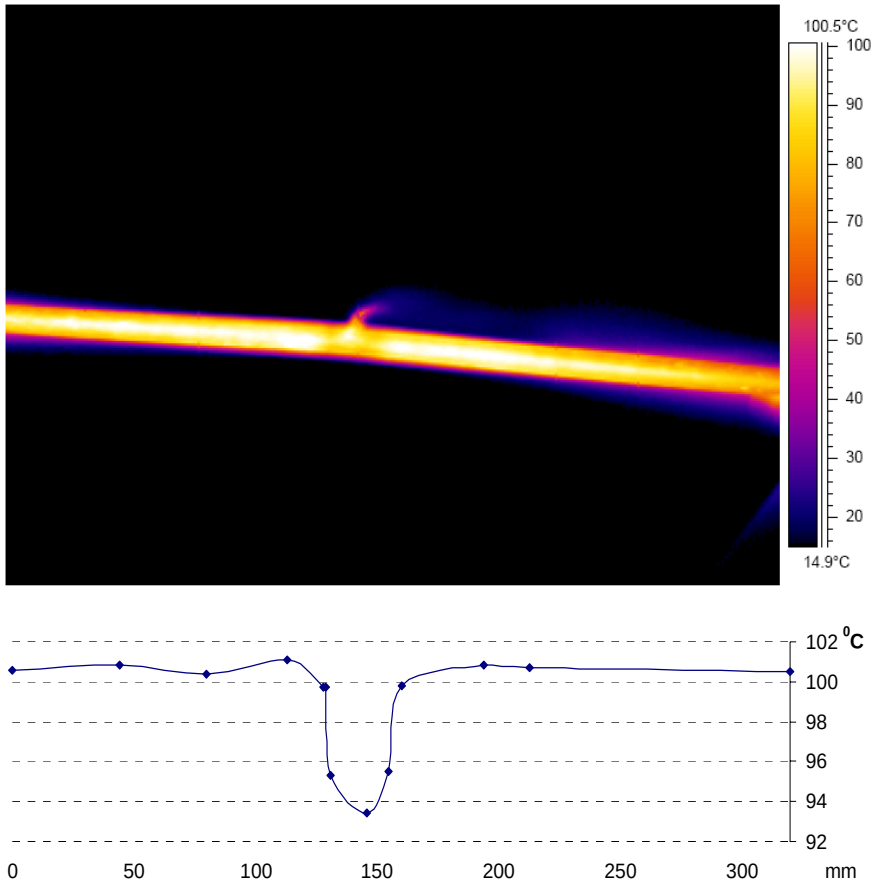

Figure 6-3 IR Picture Shows Temperature Distortion at Thermocouple Attachment

Due to the temperature distortion on the SMA wire, it is plausible to assume the actual temperature of the SMA wire is 110 ^{0}C at 1 *atm* when the thermocouple has a reading 100 ^{0}C. Using **Equations 5-6** and **5-9**, when T_{SMA} = 383K (110 ^{0}C), the recalculated results are: Ra_D = 0.6608; Nu_D = 0.96, which are different from the results in **Table 6-1**. Since the temperature distortion increases with the air pressure, it can be assumed that there is a potential correlation based on the actual SMA wire temperature, as shown in **Figure 6-4**. It is clear that if there is no temperature distortion on the SMA wire, the potential correlation agrees well with the theoretical correlation from Raithby and Hollands **[72]**.

Temperature distortion error is an inherent error when measuring a solid surface using contact temperature sensors, especially a thin wire. Infrared thermal imaging can measure the temperature of a thin wire without contacting it, but there are some constraints when using an infrared camera with close up lens, ie, an infrared camera may not be used in vacuum. An improved thermocouple **[21]** used to measure the temperature of micro chip maybe a good choice to eliminate temperature distortion to measure the temperature of thin wires.

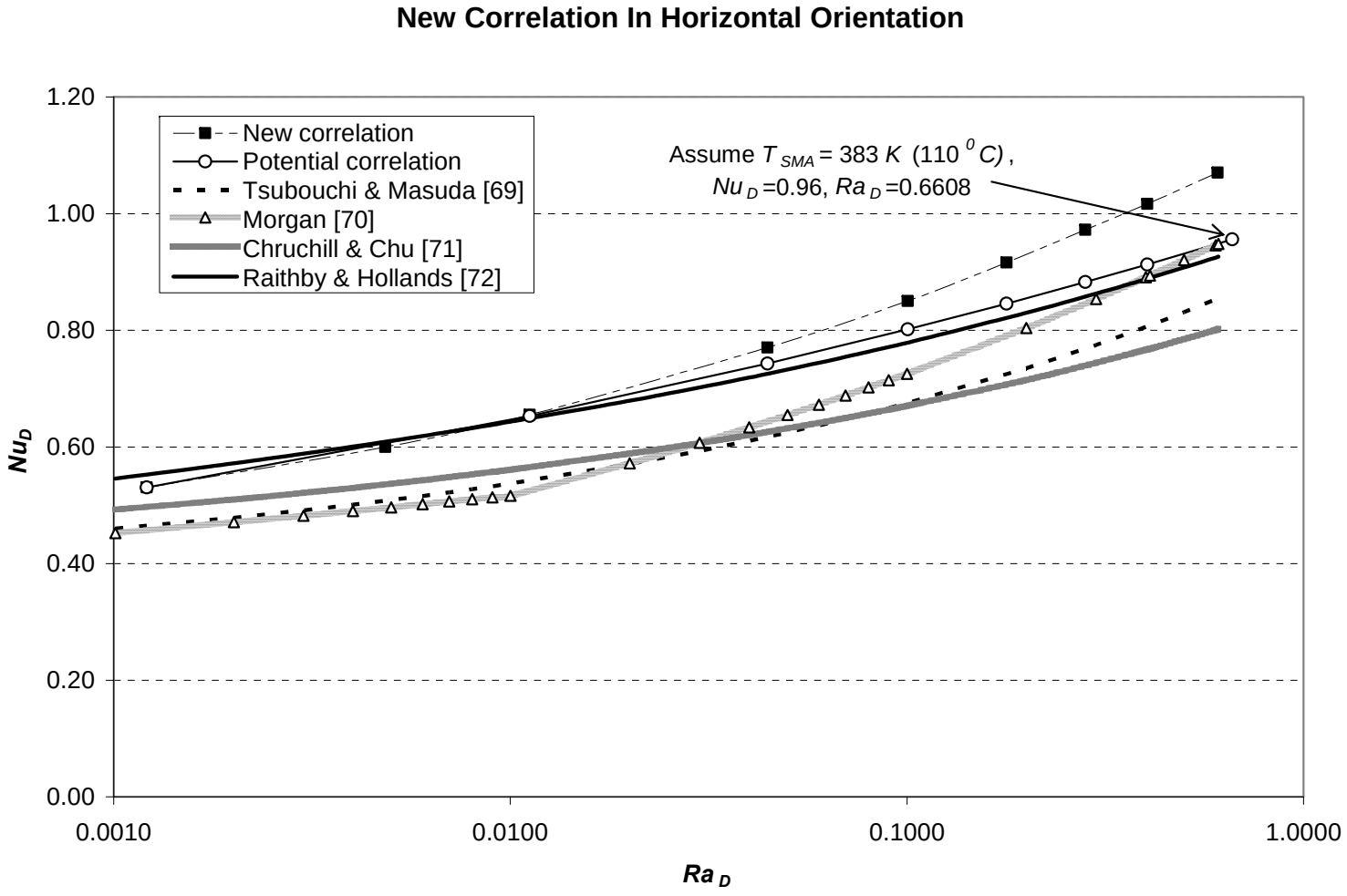

Figure 6-4 Comparison To the Existing Correlations in Horizontal Orientation

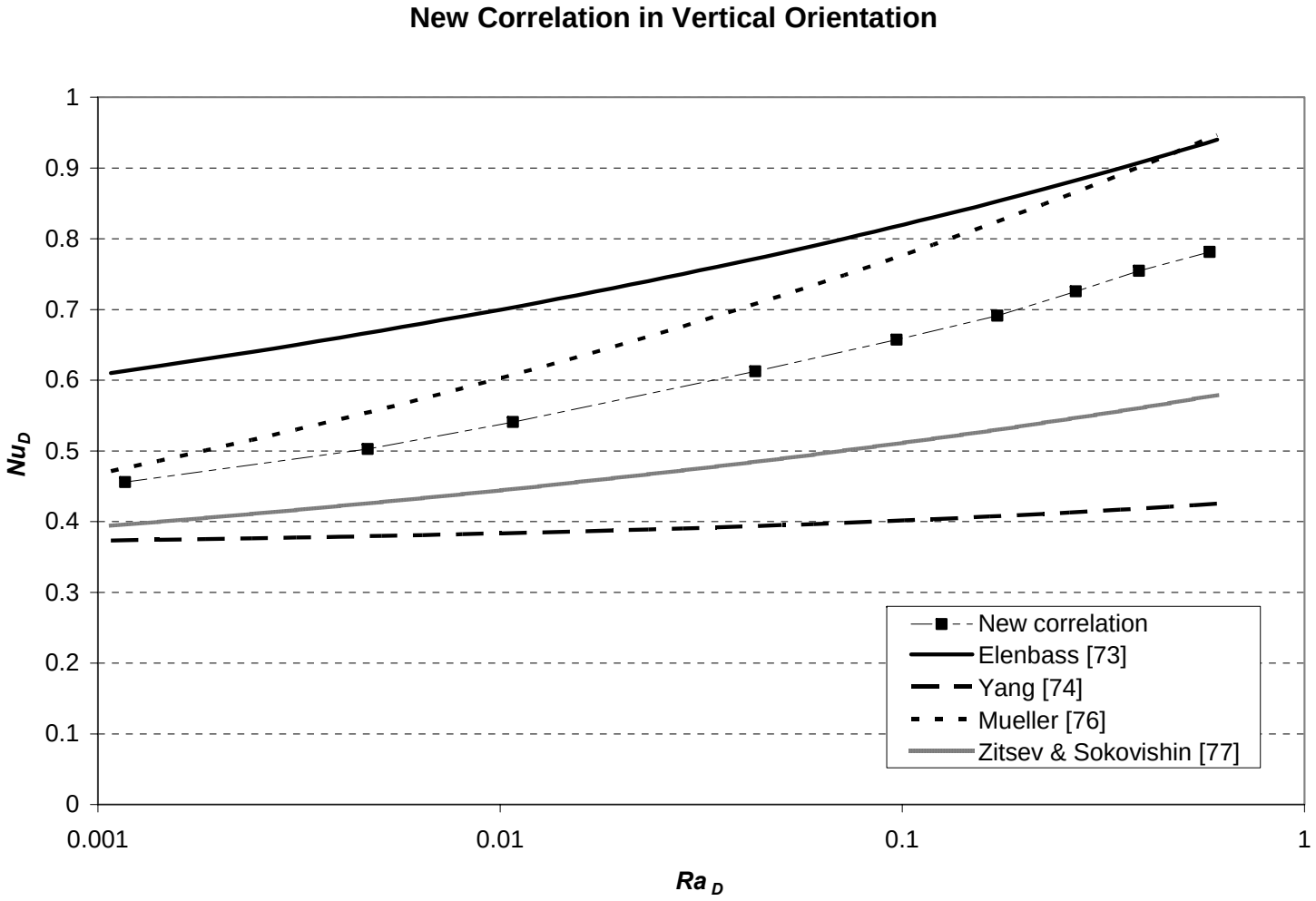

Figure 6-5 Comparison to the Existing Correlations in Vertical Orientation

6.3 SMA Wire Temperature Prediction Through New Correlation

The SMA constitutive and phase kinetic behaviors are directly controlled by the heat transfer rate to and from the wires, a detailed heat transfer model is needed to monitor and predict the temperature and the behavior of the SMA wires. The new correlation is developed based on experimental results; it then helps to predict SMA wire temperature when giving the diameter and the inclination angle of the SMA wire.

Assuming a short SMA wire is a section of a sufficiently long SMA wire, when it is heated by a current and reaches a steady state, there is no conduction along the axial direction of the SMA wire due to the uniform temperature distribution along the SMA wire. The heat transfer equation of this short section of SMA wire is in the form:

$$I^2 R_{SMA} = hA_s\left(T - T_\infty\right) + \varepsilon\sigma A_s\left(T^4 - T_\infty^4\right) \tag{6-4}$$

Following the flowchart in **Figure 6-6**, the temperature of the SMA wire can be determined.

For example: a 0.5 *mm* diameter SMA wire is inclined 50^0 to the horizontal in 1 *atm* air pressure. According to **Equation 6-3**, Nu_D-Ra_D becomes:

$$Nu_D = 1.0314 \cdot Ra_D^{0.1128} \tag{6-5}$$

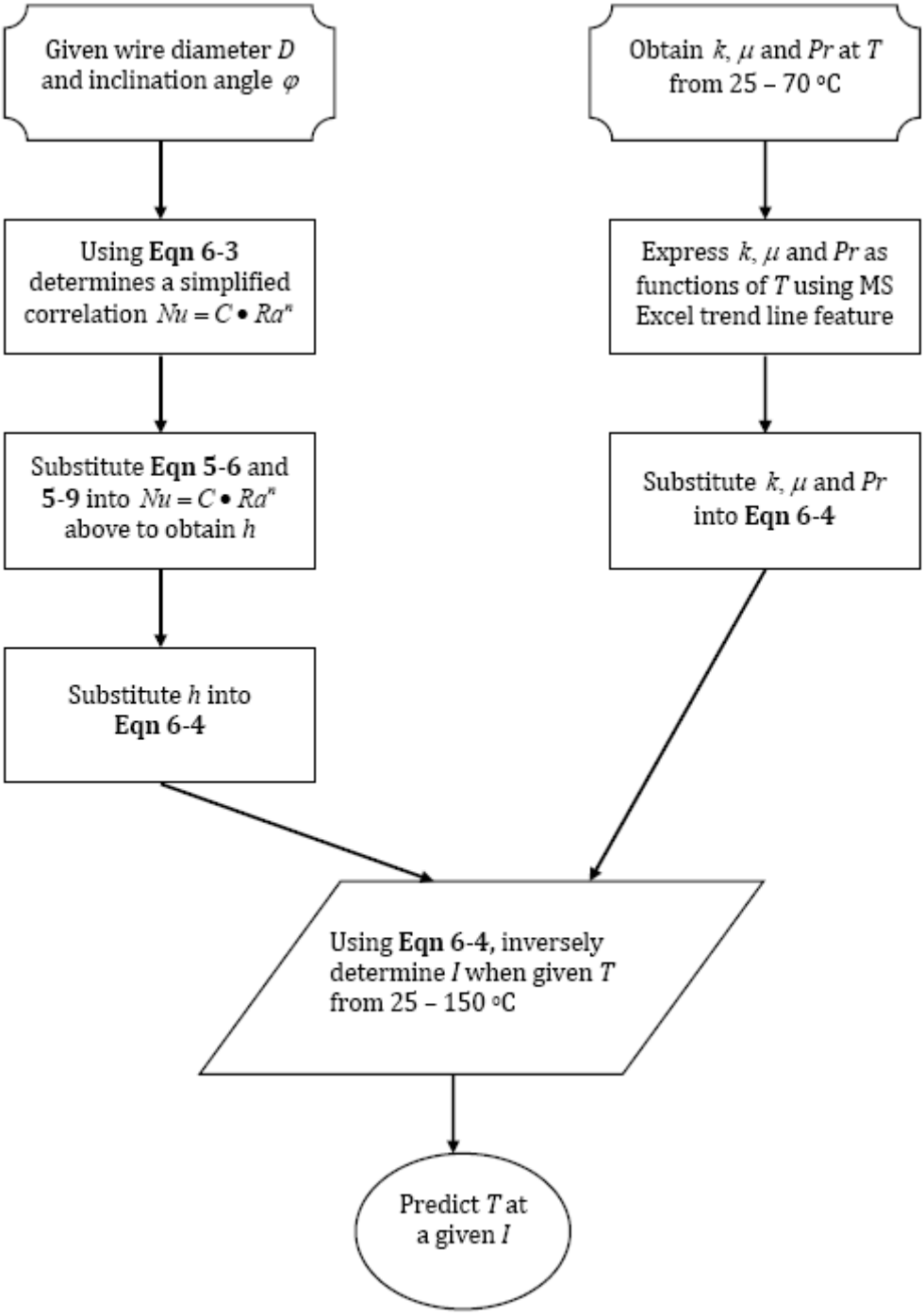

Figure 6-6 Flowchart to Determine SMA Wire Temperature

Substitute **Equation 5-6** and **5-9** into **Equation 6-5**, **Equation 6-5** becomes:

$$\frac{hD}{k} = 1.0314\left(\frac{g(T_{SMA}-T_{\infty})D^3P^2}{\mu^2 T_{\infty}R^2Z^2\left(\frac{T_{SMA}+T_{\infty}}{2}\right)^2}\cdot \Pr\right)^{0.1128} \tag{6-6}$$

The heat transfer coefficient is:

$$h = \frac{1.0314\cdot k}{D}\left(\frac{g(T_{SMA}-T_{\infty})D^3P^2}{\mu^2 T_{\infty}R^2Z^2\left(\frac{T_{SMA}+T_{\infty}}{2}\right)^2}\cdot \Pr\right)^{0.1128} \tag{6-7}$$

Substitute **Equation 6-7 into Equation 6-4**, the heat transfer equation of the SMA wire becomes:

$$I^2R_{SMA} = \frac{1.0314\cdot k}{D}\left(\frac{g(T_{SMA}-T_{\infty})D^3P^2}{\mu^2 T_{\infty}R^2Z^2\left(\frac{T_{SMA}+T_{\infty}}{2}\right)^2}\cdot \Pr\right)^{0.1128} \cdot \pi Dl(T_{SMA}-T_{\infty}) + \varepsilon\sigma\pi Dl(T_{SMA}^4-T_{\infty}^4) \tag{6-8}$$

The resistance of a unit length of 0.5 *mm* diameter SMA wire is 4.3 *Ω/m* **[87]**, from Dynalloy, Inc. The length of this short section of SMA wire is assumed to be 1 *cm*. So its resistance is $R_{SMA} = 0.043\ \Omega$.

The values of *k,* μ and *Pr* **[93]** change with temperature, which are tabulated in **Table 6-9**.

Table 6-9 The Values of *k*, μ and *Pr* at Different Temperature (25 – 70 ^0C)

T_m (K)	μ kg/(m.s)	k W/(m.K);	Pr
298	1.849 x 10^{-05}	0.02551	0.7296
303	1.872 x 10^{-05}	0.02588	0.7282
308	1.895 x 10^{-05}	0.02625	0.7268
313	1.918 x 10^{-05}	0.02662	0.7255
318	1.941 x 10^{-05}	0.02699	0.7241
323	1.963 x 10^{-05}	0.02735	0.7228
333	2.008 x 10^{-05}	0.02808	0.7202
343	2.052 x 10^{-05}	0.02881	0.7177

Use Microsoft Excel "add trend line" feature, μ, k and Pr can be expressed as functions of T_m in the forms:

$$\mu = 0.9228 \cdot (5\times10^{-8} \cdot T_m + 5\times10^{-6}) \quad (6\text{-}9)$$
$$R^2 = 0.9999$$

$$k = 1.04 \cdot (7\times10^{-5} \cdot T_m + 0.0037) \quad (6\text{-}10)$$
$$R^2 = 1$$

$$\mathrm{Pr} = 5\times10^{-7} \cdot T_m^2 - 0.0006 \cdot T_m + 0.8645 \quad (6\text{-}11)$$
$$R^2 = 1$$

$P = 1atm = 1.013 \times 10^5\ Pa$. T_∞ is assumed to be 296 K (23 ^0C). g, R and Z are constant, $g = 9.8\ m/s^2$, $R = 0.287\ kJ/(kg{\cdot}K)$, $Z = 1$. $\varepsilon = 0.63$, $\sigma = 5.67\times10^{-8}\ W/(m^2{\cdot}K^4)$.

Substitute **Equation 6-9, 6-10 and 6-11**, g, R and Z into **Equation 6-8**, the results of T_{SMA} vs I can be tabulated as in **Table 6-10** and plotted as in **Figure 6-7**:

Similarly, when a 0.381 *mm* diameter SMA wire is inclined from horizontal at 35^0, the correlation becomes:

$$Nu_D = 1.0764 \cdot Ra_D^{0.1138} \quad (6\text{-}12)$$

Its unit length resistance is 8.3 *Ω/m.* **[87]**

When a 0.254 *mm* diameter SMA wire is inclined from horizontal at 65^0, the correlation becomes:

$$Nu_D = 0.9684 \cdot Ra_D^{0.1086} \quad (6\text{-}13)$$

Its unit length resistance is 18.5 *Ω/m.* **[87]**

T_{SMA} vs I in both cases are also tabulated in **Table 6-10** and plotted as in **Figure 6-7**. As shown in **Figure 6-7**, since a thinner diameter SMA wire has a larger electrical resistance to heat the SMA wire to a same temperature, the thinner SMA wires need less current.

6.4 Summary of Results and Discussion

The experimental results have been presented and discussed in this chapter. The raw data was processed and presented in the form of tables and figures. A new heat transfer correlation was developed based on the empirical data. The comparisons of the new correlation to the existing correlations were discussed and the analysis showed the

discrepancies were attributed to the temperature distortion on the sample SMA wire. At the end of this chapter, three examples were cited to describe the prediction of SMA wire temperature by applying the new correlation.

Table 6-10 T_{SMA} vs Carrying Current I (P = 1 *atm*)

T_{SMA} (K)	I (A) D = 0.5 *mm* $\varphi = 50^0$	I (A) D = 0.381 *mm* $\varphi = 35^0$	I (A) D = 0.254 *mm* $\varphi = 65^0$
298	0.137	0.094	0.057
303	0.273	0.187	0.114
313	0.445	0.305	0.186
323	0.577	0.396	0.241
333	0.690	0.474	0.288
343	0.791	0.543	0.330
353	0.884	0.607	0.369
363	0.972	0.668	0.405
373	1.056	0.725	0.440
383	1.135	0.779	0.473
393	1.213	0.832	0.504
403	1.287	0.883	0.535
413	1.360	0.933	0.565

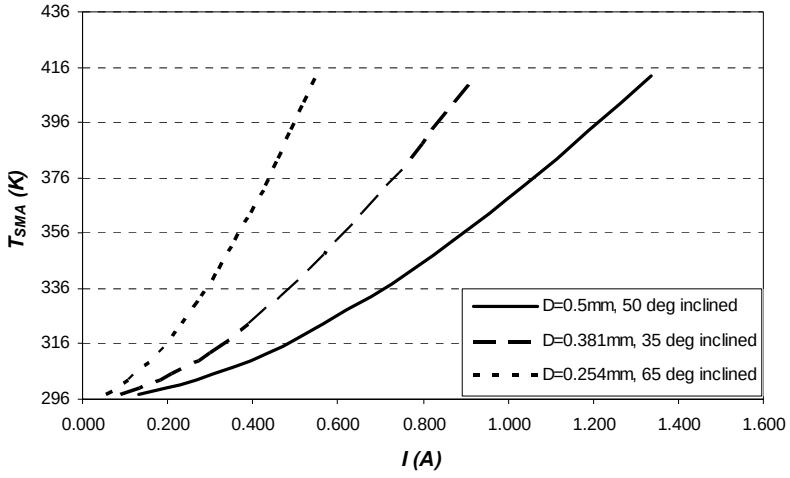

Figure 6-7 T_{SMA} vs Carrying Current I (P = 1 *atm*)

Chapter 7

Conclusion and Recommendations

7.1 Conclusion

There are five major conclusions following the experiment and the discussion around the temperature measurement of SMA wire and the natural convective heat transfer model for SMA wire.

7.1.1 The Carrying Current's Influence on Temperature Readings

The carrying current affects the temperature readings by adding a "spurious voltage" ΔV to the thermo electro-motive force (EMF) of the thermocouple which is spot welded onto the SMA wire. The "spurious voltage" is a result of the ohmic drop between two thermocouple legs due to the carry current which are actually at two different locations on the SMA wire. The magnitude of ΔV is dependent on the spatial offset between the two thermocouple legs, Δx, and the carrying current I. When the direction of the carrying current is reversed, ΔV becomes negative. The carrying current's influence on temperature reading can be eliminated by three methods: 1, the pulse shut off method; 2, the reverse current and average method and 3, the improved two-step spot welding thermocouple method.

7.1.2 Two-Step Spot Welding Thermocouple

The two-step spot welding method can spot weld the thinnest E-type 40 AWG thermocouple wires onto the SMA wire with the smallest junction and effectively negate the influence of the carrying current on the temperature readings, which has been successfully applied in a pending patent **[94]**. Unlike the conventional method, in which a thermocouple bead is made on a thermocouple welder, and then the bead is spot welded onto the SMA wire using a capacitor current discharge welder, the two-step spot welding thermocouple spot welds the thermocouple wires directly onto the SMA wire. With the aid of a microscope, the two-step spot welding method takes good control of the thin thermocouple wires and the SMA wire, precisely adds the second thermocouple wire on the spot where the first thermocouple wire is welded on the SMA wire. As a result, the junction size and the distance between the sense point of thermocouple and the SMA wire are both the smallest that can be obtained, yet are big enough to offset the carrying current's influence on the thermocouple readings.

7.1.3 Infrared Thermal Imaging is a Good Supplement

Infrared thermal imaging is a good supplement to thermocouples in verifying the occurrence of temperature distortion. Infrared thermal imaging cannot be the primary method to determine the temperature of SMA wire and to model convection heat transfer for SMA wires with confidence because of radiosity effect from the surroundings, the SMA wire tends to move during the phase transformation which greatly changes the

temperature readings, and the IR software is unable to provide recordable data which are required in modeling heat transfer (by the current IR camera: ThermaCAM S60). But as an invasive method, infrared thermal imaging has an advantage which can give the temperature of the SMA wire without having a sensor contact the SMA wire. An infrared camera can take the thermal pictures of the SMA wire and the thermocouple in the two-step spot welding method. By comparing the temperature at the location where the thermocouple is attached to the locations elsewhere on the SMA wire in the thermal image, the infrared thermal imaging can verify if there is a temperature distortion on the SMA wire and how big the distortion is.

7.1.4 Temperature Distortion Error in New Correlation's Verification

The new correlation in this work was verified in the horizontal and vertical orientations. The verification in the vertical orientation is acceptable as the new correlation is positioned in the middle of the existing correlations: lower than Elenbass **[73]** and Mueller **[76]**; but higher than Zitsev & Sokovishin **[77]** and Yang **[74]** In the horizontal orientation, the new correlation agrees with the existing correlations from Tsubouchi & Masuda **[69]**, Morgan **[70]**, Churchill & Chu **[71]** and Raithby & Hollands **[72]** in the Rayleigh number range: $0.001 < Ra_D < 0.05$; but is higher than these correlations in the Rayleigh number range: $0.05 \leq Ra_D < 0.6$. This discrepancy is likely due to the temperature distortion that the thermocouple brings to the SMA wire when the air pressure increases and the temperature distortion becomes larger.

7.1.5 SMA Wire Temperature Prediction Through New Correlation

Based on the present experimental results, a new correlation can be determined as: $Nu_D = (-0.0033 \cdot \varphi + 1.158) \cdot Ra_D^{(-0.0003 \cdot \varphi + 0.1195)}$. For a given SMA wire with a diameter D and an inclination angle φ, the new correlation can be used to determine the convective heat transfer coefficient of the SMA wire h. When a current I passes the SMA wire and reaches a steady state, the temperature of the SMA wire can be predicted through the heat transfer equation: $I^2 R_{SMA} = hA_s(T - T_\infty) + \varepsilon\sigma A_s(T^4 - T_\infty^4)$.

7.2 Recommendations

The recommendations to this work are in three aspects: to improve the two-step spot welding thermocouple technique on 250 μm diameter SMA wire; to improve the thermocouple measurement that can minimize the temperature distortion and to develop a correlation of SMA wire based on electrical resistance instead of temperature.

7.2.1 Improve Two-Step Spot Welding

The two-step spot welding thermocouple technique works well on a 500 μm diameter SMA wire, but it becomes harder when working on a 250 μm diameter SMA wire. The difficulty on a 250 μm diameter SMA wire is the smaller size of the SMA wire makes it harder to control the welding spot on the SMA wire and to find a proper power on the welder.

7.2.2 Improve Thermocouple Method to Minimize Temperature Distortion

Temperature distortion leads to big errors in heat transfer model. The infrared thermal imaging can identify the distortion, but it can not accurately model this temperature distortion due to the inherent drawbacks as described in the Chapter 3. The temperature distortion can be decreased by improving the thermocouple measurement as suggested by Nakabeppu **[21]**.

7.2.3 Develop a Correlation of Temperature and Resistance

The current work is based on temperature measurement to model heat transfer. Because of the drawbacks with the temperature measurement, invasive or non-invasive, especially working on thin wires, there are still some errors when measuring the temperature of SMA wires for heat transfer modeling. If changes in electrical resistance as a result of change in SMA temperature can be accurately measured, this maybe a more reliable method of modeling heat transfer.

Appendix A
Ring Terminal Brings SMA Wire Temperature Down

When the ring terminal is crimped on the SMA wire, the SMA wire temperature can decrease. This is demonstrated in the infrared picture depicted in **Figure A-1**. The ring terminal is at the right side of IR picture. The color on the SMA wire close to the ring terminal is deep yellow in the IR picture, which represents a lower temperature, while the SMA wire on the other side is bright yellow in the IR picture which represents higher temperature. Through the line analysis across the SMA wire on the research software, we can find that the maximum temperature on each line decreases from 96 ^{0}C to 84.7 ^{0}C when the line moves toward to ring terminal. This proves that there is a temperature distribution on the SMA wire when the ring terminal is connected because the maximum temperature on each line represents the SMA wire temperature at the point where the line crosses.

The picture in **Figure A-1** was taken on a 500 μm diameter SMA wire which was suspended in air at 1 *atm*. The fact that the SMA wire close to the ring terminal has a lower temperature shows that the ring terminal's temperature is lower than the SMA wire. This is easy to understand because the ring terminal itself does not generate heat. It obtains heat from the SMA wire through conduction and then it dissipates the heat to the environment through convection and radiation. Due to the larger surface of the ring terminal, it has a higher heat dissipation rate than the SMA wire and hence acts as a heat sink. Analysis of the IR picture shows that the voltage measurement lead should be placed at least 15 *mm* away from the ring terminal in order to eliminate its influence.

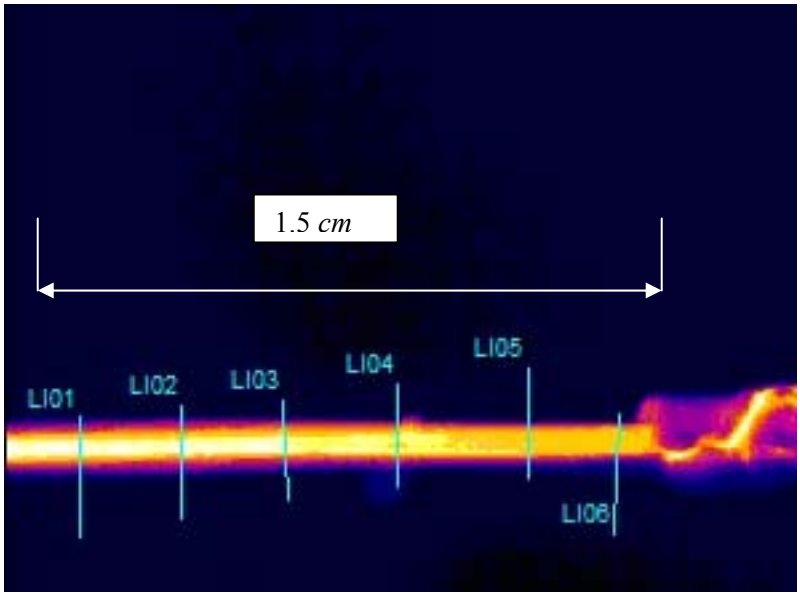

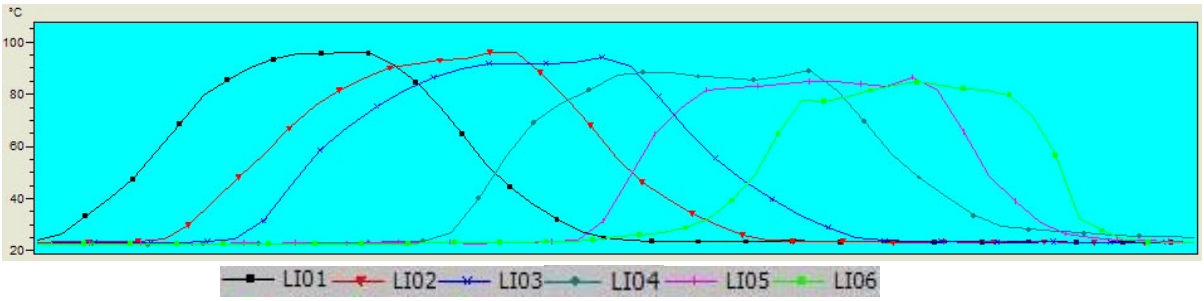

Label	Value [°C]	Min	Max	Max - Min	Avg	Stdev
Image		21.9	101.1	79.1		
LI01		23.1	96.0	72.9	43.1	27.1
LI02		23.0	96.1	73.1	44.2	27.1
LI03		22.6	94.0	71.4	46.0	27.7
LI04		22.4	89.2	66.8	45.1	26.5
LI05		22.6	86.6	63.9	41.1	25.4
LI06		22.6	84.7	62.1	38.4	23.5

Figure A-1 Thermal Gradient After a Ring Terminal is Crimped on SMA Wire

Appendix B
Uncertainty Analysis

The uncertainty analysis based on the accuracy of all the equipment used in the test apparatus is provided in this section.

B.1 Uncertainty Analysis Method

The uncertainty analysis method used in this work is adapted from the experiment uncertainty analysis of Wheeler and Ganji **[95]**. In their analysis, they think if a result R is the function of n measured variables $x_1, x_2, x_3, ..., x_n$ in an experiment as:

$$R = f(x_1, x_2, x_3, ..., x_n) \tag{B-1}$$

Then a small change in R, δR can be expressed by the variables $x_1, x_2, x_3, ..., x_n$, in a differential formula:

$$\delta R = \delta x_1 \frac{\partial R}{\partial x_1} + \delta x_1 \frac{\partial R}{\partial x_1} + \cdots + \delta x_n \frac{\partial R}{\partial x_n} = \sum_{i=1}^{n} \delta x_i \frac{\partial R}{\partial x_i} \tag{B-2}$$

If R is a calculated result based on measured x_i's, the values of the δx_i's can be replaced by the uncertainty in the variables, which can be denoted by w_{xi}'s and δR can be replaced by the uncertainty in the result, denoted by w_R, as:

$$w_R = \delta R \tag{B-4}$$

The maximum uncertainty in R can be estimated by forcing all terms on the right-hand side of **Equation B-2** to be positive as:

$$w_R = \sum_{i=1}^{n} \left| w_{xi} \frac{\partial R}{\partial x_i} \right| \tag{B-5}$$

The uncertainty that is produced by **Equation B-5** might be very high because the variables w_{xi} can be positive simultaneously. So a better estimate for the uncertainty is given by:

$$w_R = \left[\sum_{i=1}^{n} \left(w_{xi} \frac{\partial R}{\partial x_i} \right)^2 \right]^{1/2} \tag{B-6}$$

If the result R is dependent only on a product of the measured values:

$$R = C x_1^a x_2^b \cdots x_n^N \tag{B-7}$$

The **Equation B-6** can be expressed as:

$$\frac{w_R}{R} = \left[\left(a \frac{w_1}{x_1} \right)^2 + \left(b \frac{w_2}{x_2} \right)^2 + \cdots + \left(N \frac{w_n}{x_n} \right)^2 \right]^{1/2} \tag{B-8}$$

Equation B-8 is a better form since the fractional error in the result R is related directly to the fractional errors in the individual measurements.

B.2 Uncertainty in Measured Values

In this experiment, there are six measured values, temperature T, voltage V, current I, pressure P, dimension d and l. Each of them has an uncertainty in measurement.

B.2.1 Temperature *T*

The temperature is measured by E-type thermocouples and is read through the Keithley 2700 / 7700 with an internal junction on the module. According to the data from Keithley Instrument, Inc, the uncertainty in the temperature reading is ± 1 ^{0}C, or

$$\frac{\delta T}{T} = \pm\left(\frac{1^{0}C}{T(^{0}C)}\right) \tag{B-9}$$

B.2.2 Voltage *V*

The uncertainty of voltage measurement depends on the voltage reading and the measurement that the range of measurement that the readings fall in. Referring the Keithley 2700 / 7700 specification, the uncertainty of voltage V is as following:

$$\frac{\delta V}{V} = \pm\left(3.0\times10^{-5} + \frac{3.5\times10^{-7}}{V(V)}\right) \text{ in the range of 100 } mV \tag{B-10}$$

$$\frac{\delta V}{V} = \pm\left(3.0\times10^{-5} + \frac{7.0\times10^{-6}}{V(V)}\right) \text{ in the range of 1 } V \tag{B-11}$$

$$\frac{\delta V}{V} = \pm\left(3.0\times10^{-5} + \frac{5.0\times10^{-5}}{V(V)}\right) \text{ in the range of 10 } V \tag{B-12}$$

B.2.3 Current *I*

Current is obtained by measuring the voltage across the current shunt, so the uncertainty of current depends on the voltage reading of shunt; the uncertainty of voltage measurement and the uncertainty of shunt. The uncertainty of current is in the form as following, which is the result from Teertstra **[96]**

$$\frac{\delta I}{I} = \pm\left[\left(3.0\times10^{-5} + \frac{3.5\times10^{-6}}{V_{shunt}(V)}\right)^2 + 0.0014^2\right]^{1/2} \tag{B-13}$$

B.2.4 Pressure *P*

The air pressure in the bell jar is measured using a Varian CeramiCel pressure gauge, which senses the pressure and outputs a voltage signal. The uncertainty of the pressure depends on the uncertainty of the Varian CeramiCel pressure gauge and the uncertainty of voltage measurement. According to Teertstra **[96]**, the uncertainty of pressure has the following form:

$$\frac{\delta P}{P} = \pm\left[\left(\frac{1}{10^5 V_{pressure}(V)}\right)^2 + \left(3\times10^{-5} + \frac{5\times10^{-5}}{V_{pressure}(V)}\right)^2\right]^{1/2} \tag{B-14}$$

B.2.5 Dimension

The dimensions in the experiment are measured by an electronic digital caliper with a resolution of ± 0.005 *mm*. The uncertainties of the diameter, the length and the surface area of SMA wire are in the following forms:

$$\frac{\delta d}{d} = \pm \frac{0.005}{d(mm)} \tag{B-15}$$

$$\frac{\delta l}{l} = \pm \frac{0.005}{l(mm)} \tag{B-16}$$

$$\frac{\delta A}{A} = \pm \left[\left(\frac{0.005}{d(mm)} \right)^2 + \left(\frac{0.005}{l(mm)} \right)^2 \right]^{1/2} \tag{B-17}$$

B.2 The Inclination Angle φ

The inclination angle is measured using a plastic protractor which has an uncertainty of $\pm 0.5^0$. The uncertainty of angle is:

$$\frac{\delta \varphi}{\varphi} = \pm \frac{0.5^0}{\varphi(^0)} \tag{B-18}$$

B.3 Uncertainty in Calculated Values

Q_{rad} is the power input in vacuum: $Q_{rad} = VI_{vacuum}$, so the uncertainty of Q_{rad} is:

$$\frac{\delta Q_{rad}}{Q_{rad}} = \left[\left(\frac{\delta V_{SMA-vacuum}}{V_{SMA-vacuum}} \right)^2 + \left(\frac{\delta I_{SMA-vacuum}}{I_{SMA-vacuum}} \right)^2 \right]^{1/2} \tag{B-19}$$

When modeling heat transfer, the Nusselt number (Nu_D) and the Rayleigh number (Ra_D) are calculated by **Equation 5-6** and **5-9**, so the uncertainty of Nu_D and Ra_D are calculated by the following **Equation B-20** and **B-21**.

$$\frac{\delta Nu_D}{Nu_D} = \left[\begin{array}{l} \left(\frac{\delta V_{SMA}}{V_{SMA}} \right)^2 + \left(\frac{\delta I_{SMA}}{I_{SMA}} \right)^2 + \left(\frac{\delta V_{SMA-vacuum}}{V_{SMA-vacuum}} \right)^2 + \left(\frac{\delta I_{SMA-vacuum}}{I_{SMA-vacuum}} \right)^2 + \left(\frac{\delta d_{SMA}}{d_{SMA}} \right)^2 \\ + \left(\frac{\delta A_{SMA}}{A_{SMA}} \right)^2 + \left(\frac{\delta T_{SMA}}{T_{SMA}} \right)^2 + \left(\frac{\delta T_\infty}{T_\infty} \right)^2 \end{array} \right]^{1/2}$$

(B-20)

$$\frac{\delta Ra_D}{Ra_D} = \left[\left(2\frac{\delta P}{P} \right)^2 + \left(3\frac{\delta d}{d} \right)^2 + \left(\frac{\delta T_{SMA}}{T_{SMA}} \right)^2 + \left(\frac{\delta T_\infty}{T_\infty} \right)^2 + \left(2\frac{\delta T_m}{T_m} \right)^2 + \left(\frac{\delta T_\infty}{T_\infty} \right)^2 \right]^{1/2}$$

(B-21)

Because $T_m = \frac{T_{SMA} + T_\infty}{2}$, then $\frac{\delta T_m}{T_m} = \pm \left[\left(\frac{\delta T_{SMA}}{T_{SMA}} \right)^2 + \left(\frac{\delta T_\infty}{T_\infty} \right)^2 \right]^{1/2}$, so **Equation B-21** is actually in the form of:

$$\frac{\delta Ra_D}{Ra_D} = \left[\left(2\frac{\delta P}{P} \right)^2 + \left(3\frac{\delta d}{d} \right)^2 + 5\left(\frac{\delta T_{SMA}}{T_{SMA}} \right)^2 + 6\left(\frac{\delta T_\infty}{T_\infty} \right)^2 \right]^{1/2} \tag{B-22}$$

B.4 Uncertainty of Experimental Result

The uncertainties of the Nusselt number (Nu_D) and the Rayleigh number (Ra_D) can be calculated by the **Equation B-20** and **B-22**. The raw data, the results of Nu_D, Ra_D and their uncertainties are tabulated in **Table 6-1** to **Table 6-7.**

Appendix C

Conduction Wire Loss Via TC and Voltage Measurement Leads

Conduction wire loss through the thermocouple and the voltage measurement leads can be estimated by adding a thermocouple onto the testing SMA wire and comparing the power inputs in two cases at the same temperature.

Figure C-1 is the setup diagram to estimate the conduction wire losses via the thermocouple and the voltage measurement leads. The SMA wire test section between two voltage measurement leads in **Figure C-1** has a unique temperature when in heat equilibrium because it is 2.5 *cm* away from the terminal rings and it is 15 *cm* away from the power leads.

The experiment to estimate conductive wire losses needs to run two times: one with only one thermocouple TC1; the other one with two thermocouples TC1 and TC2. The experiment steps are as follows:

1. Setup the experiment as in **Figure C-1**
2. Spot welded the thermocouple "TC1" at the centre of the testing SMA wire (no TC2 at this time
3. Place the setup into the bell jar
4. Evacuate the bell jar by the mechanical pump and the diffusion pump until the pressure is below 10^{-7} *torr*
5. Turn on the power to heat the SMA to 100 ^{0}C

6. After the TC1 is stable at 100 ^{0}C for 1 minute, increase the pressure in the bell jar to 0.01 *torr*.

7. Adjust the current knob on the power supply to keep TC1 at 100 ^{0}C

8. After the TC1 is stable at 100 ^{0}C for 1 minute, increase the pressure in the bell jar to the pressure 33 *torr*, 66 *torr*, 100 *torr*, 200 *torr*, …,760 *torr* as in step 6

9. At each pressure, adjust the current knob on the power supply to bring TC1 to the temperature 100 ^{0}C, when the temperature 100 ^{0}C is stable for 1 minute, as in step 7

10. Spot weld TC2 in the same manner as TC1 at the location as shown in **Figure C-1**

11. repeat above steps from 3 to 9

12. compare the power inputs in the two cases

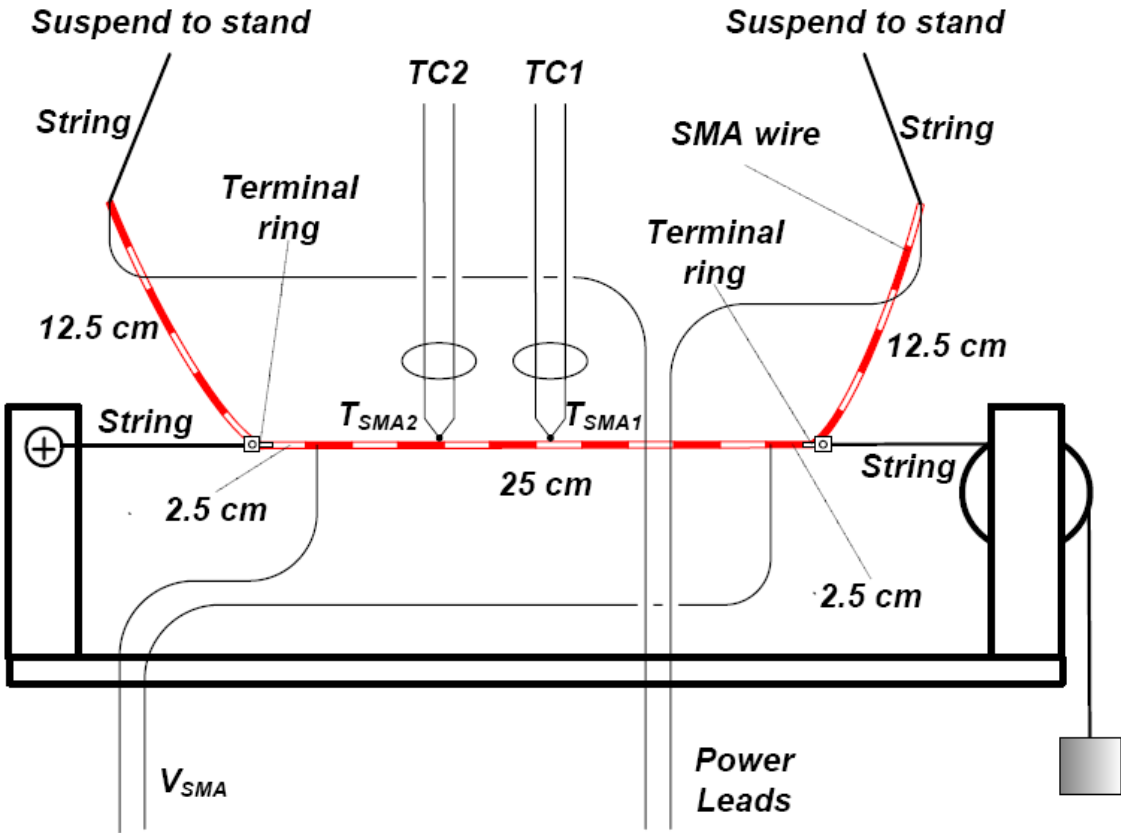

Figure C-1 SMA Wire Setup Diagram

The power inputs of the two cases in vacuum are compared in **Figure C-2**. A same power input of 0.0924 W is required in both cases to keep the SMA wire at 100 ^{0}C. This means that adding a second thermocouple doesn't increase the power input in order to keep the SMA wire test section at the same temperature 100 ^{0}C in vacuum. In other words, the conductive wire loss through thermocouple is very small and can be neglected in vacuum. Because the voltage measurement leads use the same size and type wire as thermocouple, the wire loss through the voltage measurement leads can also be neglected.

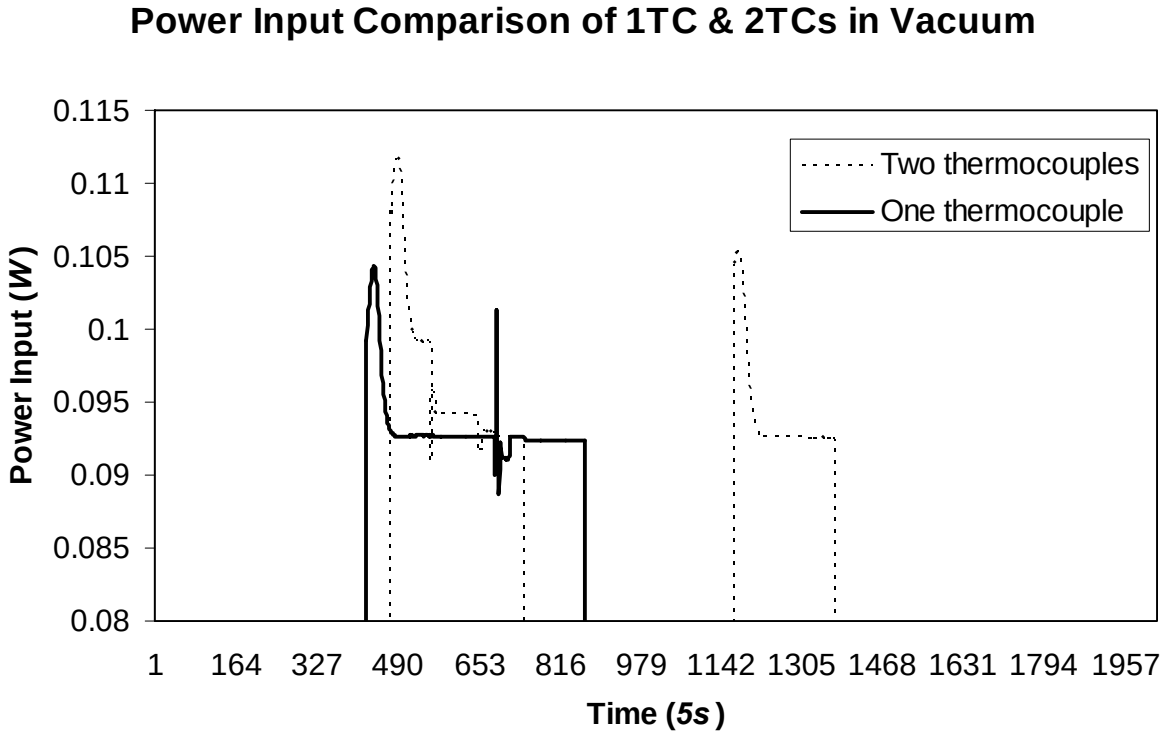

Figure C-2 Comparison of Power Input of 1TC and 2TCs in Vacuum

The power inputs in both cases of one thermocouple and two thermocouples are plotted in **Figure C-3**. It shows that the power input for one thermocouple agree with two thermocouples at all pressures, so adding a thermocouple onto the testing SMA wire doesn't need to increase the power input to keep the SMA wire test section at the same temperature 100 ^{0}C at all pressures.

This experiment concludes that the conductive wire losses via spot welded E-type 40 AWG thermocouple and constantan, 40 AWG voltage measurement leads are very small and can be neglected at all pressures in the experiment.

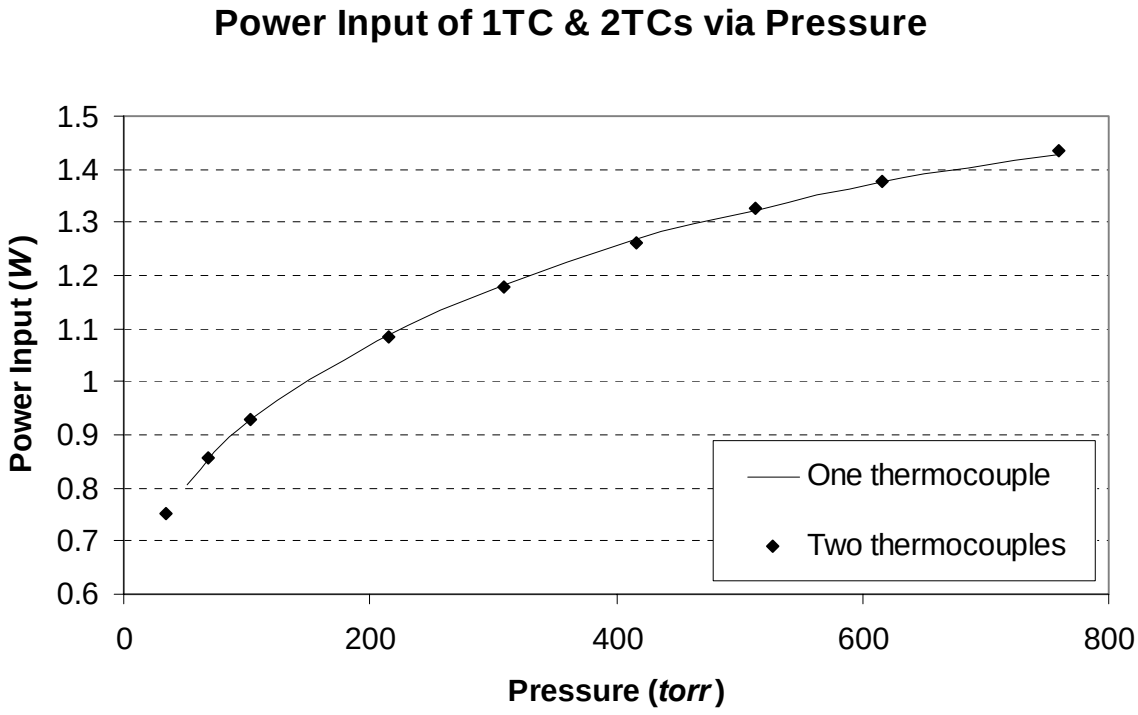

Figure C-3 Comparison of Power Input of 1TC and 2TCs at Pressures

References

[1] Otsuka, K., Wayman, CM., *Shape Memory Materials,* Cambridge, Cambridge University Press, 1998

[2] Kurdjumov, G. V., Khandros, L. G., "*First Reports Of The Thermoelastic Behaviour Of The Martensitic Phase Of Au-Cd Alloys*", *Doklady Akademii Nauk*, SSSR 66, 1949, pp 211–213

[3] Buehler, W. J., Gilfrich, J. V., Wiley, R. C., "Effects of low-temperature phase changes on the mechanical properties of alloys near composition TiNi", *Journal of Applied Physics,* 34, 1963, p 1475

[4] Schetky, L., "Shape-Memory Alloys", *Scientific American,* 241 pp 74-82

[5] Wayman, M., Harrison, J., "The Origins Of The Shape Memory Effect", *Journal of Minerals, Metals, and Materials,* 41 (99), 1989, pp 26–28

[6] Wu, M. H., Schetky, L. M., "Industrial Applications For Shape Memory Alloys", *Proceedings of the International Conference on Shape Memory and Superelastic Technologies,* Pacific Grove, California, 2000

[7] Doonkersloot, H. C., Vucht, V., "Martensitic Transformations in Au-Ti, Pd-Ti and Pt-Ti Alloys", *Journal of Less-Common Metals,* 20, 1970, pp 83–91

[8] Miyazaki, S., Mizukoshi, K., Ueki, T., Sakuma, T., Liu, Y., "Fatigue Life of Ti-50", *Science and Engineering,* 1999, pp 658–663

[9] Oulu University - http://herkules.oulu.fi/isbn9514252217/html/x317.html

[10] Sanders, B., Crowe, R., Garcia, E., "Defense Advanced Research Projects Agency – Smart Materials And Structures Demonstration Program Overview", *Journal of Intelligent Material Systems and Structures*, 15, 2004, pp 227–233

[11] Birman, V., "Review Of Mechanics Of Shape Memory Alloy Structures", *Applied Mechanics Reviews,* 50 (11), 1997, pp 629–645

[12] Johnson, A., "Non-explosive separation device", *U.S. Patent* 5,119,555, June, 1992

[13] Otsuka, K., Kakeshita, T., "Science And Technology Of Shape-Memory Alloys", *New developments, bulletin,* February, 2002

[14] Childs, Peter R. N., *Practical Temperature Measurement,* Butterworth-Heinemann, Oxford, London, 2001, p 7

[15] http://www.omega.com/prodinfo/temperaturemeasurement.html

[16] Steur, P.P.M., "The Interpolating Constant-volume Gas Thermometer And Thermal Anchoring", *Metrologia,* 36, 1999, pp 33-39

[17] Steur, P.P.M., Pavese, F., "He-3 Constant Volume Gas Thermometer As Interpolating Instrument: Calculations Of The Accuracy Limit Versus Temperature Range And Design Parameters", *Cryogenics,* 29, 1989, pp 135-138

[18] Edsinger, R.E., Schooley, J.F., "Differences Between Thermodynamics Temperature And (IPTS-68) In The Range 230^0C to 660^0C", *Metrologia,* 26, 1989, pp 95-106

[19] Michalski, L., Eckersdorf, K., Kucharski, J., *Temperature Measurement,* John Wiley & Sons Ltd, London, 1991, p 333

[20] Robertson, D., *United States Patent,* 3834237, 1972

[21] Nakabeppu, O., Suzuki, T., "Microscale Temperature Measurement By Scanning Thermal Microscopy", *Journal of Thermal Analysis and Calorimetry,* Vol. 69, 2002, pp 727–737

[22] Ishihara, A., Tang, K.C., Brewster, M.Q., "Temperature Measurement of a Burning Surface by a Thermocouple II", *American Institute of Aeronautics and Astronautics,* 2005-3576, 41st AIAA/ASME/SAE/ASEE Joint Propulsion Conference & Exhibit, Tucson, Arizona, 10 - 13 July, 2005,

[23] Shaukatullah, H., Claassen, A., "Effect of Thermocouple Wire Size and Attachment Method on Measurement of Thermal Characteristics of Electronic Packages", *Nineteenth Annual IEEE Semiconductor Thermal Measurement and Management Symposium,* Cat. No.03CH37437, 2003, pp 97-105

[24] Renken, W., *United States Patent,* 5746513, 1997

[25] Leath, C.W., *United States Patent,* 3476910, 1968

[26] Anon, C., "Thermocouple Attachment Method", *IBM Technical Disclosure Bulletin,* v 27, n 10A, March, 1985, p 5534

[27] Sobolik, K.B., Keltner, N.R., Beck, J.V., "Measurement Errors For Thermocouples Attached to Thin Plates. Application to Heat Flux Measurement Devices", *American Society of Mechanical Engineers, Heat Transfer Division, (Publication) HTD,* v 112, 1989, p 15-22

[28] Dunstan, P. S., Kennon, N. F., Middleton, L. A., Dunne, D. P., "Thermal Characteristics of a Nitinol Heat Engine", *Journal of Materials Science,* 21, 1986, pp 1637-1641

[29] Volkov, S.D., "The Use of Welded Thermocouples on Current Carrying Surfaces", http://www.laboratory.ru/articl/tech/at150e.htm (accessed Nov 30, 2005)

[30] Zanstra, P.E., "Welding Uniform Sized Thermocouple Junctions From Thin Wires", *Journal of Physics E (Scientific Instruments),* v 9, n 7, July, 1976, pp 526-528

[31] Wang, T. P., Martincavage, J., Bediones, D., "Precision Calibration of Thermocouples & RTD'S and a New Calibration Laboratory with Computerized Data Acquisition System", *ISA,* 1987, pp 107-128

[32] Maeno, Y., Haucke, H., Wheatley, J., "Simple Differential Thermometer Using a Thermocouple with a SQUID Detector", *AIP Conference Proceedings,* n 103, 1983, p 467

[33] Sawada, T., Nishiwaki, N., "Response of a Thermocouple to Transient Temperature Changes in a Metal to Which it is Attached", *International Journal of Mechanical Sciences,* v 33, n 7, 1991, pp 551-561

[34] Suyama, Y., Miyazato, M., Hamada, T., "An Evaluation Test on Calibration Accuracy of Type R Thermocouples by Comparison with a Platinum Resistance Thermometer", *Transactions of the Society of Instrument and Control Engineers,* v 33, n 4, April, 1997, pp 302-304

[35] Ancsin, J., "A Study of Thermocouple Stability, Reproducibility and Accuracy (Pt vs. Pt-Rh and Pt vs. Au)", *Metrologia,* v 28, n 4, November. 1991, pp 339-347

[36] Cengel, Y. A., Zing, P. T. L., Kalinski, M. J., "Use of Operational Amplifiers in Temperature Measurements with Thermocouples for Increased Accuracy and Resolution" *American Society of Mechanical Engineers, Fluids Engineering Division (Publication) FED,* v 44, 1986, pp 87-91

[37] Rego, G., Santos, L.M.N.B.F., Schroder, B., Marques, P.V.S., Santos, J.L., Salgado, H.M., "In Situ Temperature Measurement of An Optical Fiber Submitted To Electric Arc Discharges", *Photonics Technology Letters, IEEE*, Volume16, Issue 9, September, 2004, pp 2111-2113

[38] Childs, Peter R. N., *Practical Temperature Measurement,* Butterworth-Heinemann, Oxford, London, 2001, p146

[39] Nicholas, J.V., White, D.R., *Traceable Temperatures,* 2nd Edition, John Wiley & Sons, England, 2001, p 207

[40] Nicholas, J.V., White, D.R., *Traceable Temperatures,* 2nd Edition, John Wiley & Sons, England, 2001, p 250

[41] http://www.thermistor.com/pdf/qtmb.pdf

[42] http://sensing.honeywell.com/index.cfm?ci_id=140301&la_id=1&pr_id=145382

[43] Allison, S.W., Gillies, G.T., "Remote Thermometry With Thermographic Phosphors: Instrumentation and Applications", *Review of Scientific Instruments,* 68(7), 1997, pp 2615-2650

[44] Bradley, L.C., *Review of Scientific Instruments,* 24, 1953, p 219

[45] Czysz, P., Dixin, W.P., "Thermographic Heat Transfer Measurement", *Instruments and Control Systems,* 41, 1968, pp 71-76

[46] Czysz, P., Dixin, W.P., "Quantitative Heat Transfer Measurement Using Thermographic Phosphors", *SPIE Journal,* 1969, pp 77-79

[47] Tobin, K.W., Allison, S.W., Cates, M.R., Capss, G.J., Beshears, D.L., Cyr, M., Boel, B.W., "High-Temperature Phosphor Thermometry Of Rotating Turbine Blades", *AIAA Journal,* 28(8), 1990, pp 1485-1490

[48] Noel, B.W., Borella, H.M., Lewis, W., Turley, W.D., Beshears, D.L., Capps, G.J., Gates, G.J., Cates, M.R., Muhs, J.D., Tobin, K.W., "Evaluating Thermographic Phosphors In An Operating Turbine Engine", *Journal of Engineering for Gas Turbines and Power,* 113, 1991, pp 242-245

[49] Ervin, J., Murawski, C., Macarthur, C., Chyu, M., Bizzak, D., "Temperature Measurement of A Curved Surface Using Thermographic Phosphors", *Experimental Thermal and Fluid Science,* 11(4), 1995, pp 387-394

[50] Edge, A.C., Laufer, G., Krauss, R.H., "Surface Temperature-field Imaging Withlaser-induced Thermographic Phosphorescence", *Appl. Optics,* 39(4), 2000, pp 546-553

[51] Kusama, H., *Jpn. Appl. Phys.,* 15, 1976, p 2349

[52] Dever, M., Bugos, A., Dyer, F., Cates, M., Tobin, K., Beshears, D., Capps, G., "Measurement Of The Surface Of Textiles During Microwave Drying Using A Thermographic Phosphor", *Journal of Microwave Power and Electromagnetic Energy,* 25, 1990, pp 230-235

[53] Cambell, R.P., Molezzi, M.J., "Application Of Advanced Liquid Crystal Video Thermography To Turbine Cooling Passage Heat Transfer Measurement", *ASME Paper* 96-GT-225, 1996

[54] Lee, S.J., Yoon, J.H., "Temperature Field Measurement Of Heated Ventilation Flow In A Vehicle Interior", *International Journal of Vehicle Design,* 19, 1998, pp 228-243

[55] Simonich, J.C., Moffat R.J., "Liquid Crystal Visualization Of Surface Heat Transfer On A Concavely Curved Turbulent Boundary Layer", *Journal of Engineering for Gas Turbines and Power,* 106, 1984, pp 619-627

[56] Ireland, P.T., Jones, T.V., "The Response Time Of A Surface Thermometer Employing Encapsulated Thermochromic Liquid Crystals", *Journal of Physics E*., 20, 1987, pp 1195-1199

[57] Childs, Peter R. N., *Practical Temperature Measurement*, Butterworth-Heinemann, Oxford, London, 2001, p248

[58] Nicholas, J.V., White, D.R., *Traceable Temperatures*, 2nd Edition, John Wiley & Sons, England, 2001, p 367

[59] http://www.flirthermography.com/media/S60_datasheet.pdf

[60]http://www.flirthermography.com/english/accessories/accessory/1231/accessory_category_id/1035/

[61] http://www.exergen.com/industrl/spotlight/wiretemp/index.htm

[62] Borca-Tasciuc, T., Chen G., "Temperature Measurement Of Fine Wires By Photothermal Radiometry", *Rev Sci. Instrum.,* Vol. 68, No. 11, November, 1997, pp 4080-4083

[63] Moron, C., Aroca, C., SAnchez, M.C., Lbpez, E., Sanchez, P., "Local Temperature In Amorphous Ribbons During Current Annealing", *IEEE Transactions on Magnetics*, Vol. 30, No. I , January, 1994, pp 53-63

[64] Shimizu, Y., Ishii, J., Baba, T., "Reflectance Thermometry for Microscale Metal Thin Films", *Japanese Journal of Applied Physics*, Vol. 46, No. 5A, 2007, pp 3117–3119

[65] Iadicola, M. A., Shaw, J. A., "The Effect of Uniaxial Cyclic Deformation on the Evolution of Phase Transformation Fronts in Pseudoelastic NiTi Wire", *Journal of Intelligent Material Systems and Structures*, Vol. 13, February/March, 2002, pp 143-155

[66] Iadicola, M. A., Shaw, J. A., "An Experimental Setup for Measuring Unstable Thermo-mechanical Behavior of Shape Memory Alloy Wire", *Journal of Intelligent Material Systems and Structures,* Vol. 13, February/March, 2002, pp 157-166

[67] Chang, B. C., Iadicola, M. A., Shaw, J. A., "Thermodynamics of Shape Memory Alloy Wire: Modeling, Experiments, and Application", *Continuum Mech. Thermodyn.,* 18, 2006, pp 83–118

[68] Jaluria, Y., *Natural Convection Heat and Mass Transfer*, Pergamon, Oxford, U.K., 1980, p 87

[69] Tsubouchi, T., Masuda, H., "Heat Transfer By Natural Convection From Horizontal Cylinders at Low Rayleigh Numbers"*, Sci. Rep. Res. Inst., Tohoku University, Ser. B*, 19, 1967 – 1968, pp 205-219

[70] Morgan. V. T., *Adv. Heat Transfer*, 11, 1975, p 199

[71] Churchill. W., Chu, H. H. S., *Int. J. Heat Mass Transfer*, 19, 1976, p 1127

[72] Raithby, G. D., Hollands, K. G. T., *Trans. ASME, Ser. C, J. Heat Mass Transfer,* 98, 1976, p 72

[73] Elenbaas, W., "The Dissipation of Heat by Free Convection-Horizontal and Vertical Cylinders"*, Physica's Grav.,* vol. 9, 1942, pp 665–672

[74] Yang, S.M., "General Correlating Equations for Free Convection Heat Transfer from a Vertical Cylinder", *Proc. Int. Symposium on Heat Transfer*, Tsinghua University, Peking, 1985, pp 153–159

[75] Koch, W., "Uber Die Warmeabgaba Geheizter Rohre Bei Veerschiedener Neigung Der Rohrachse", *Gesundh Ing., Beih., Ser*. I, No. 22, 1927, pp 1-29

[76] Mueller, A. C., "Heat Transfer from Wires to Air in Parallel Flow", *Trans. Amer. Inst. Chem. Eng.* 38, 1942, pp 613-627

[77] Zaitsev, V. A., Sokovishin, Yu. A., *Heat and Mass Transfer-VI, vol. 1, part 3,* Minsk, 1980, pp 82–86

[78] Oosthuizen, P. H., *J. Heat Transfer* 98, 1976b, p 672

[79] Çengel, Y. A., *Heat Transfer: A Practical Approach*, McGraw-Hill, 2nd edition, p 563

[80] Siegel R., Howell, J.R., *Thermal Radiation Heat Transfer*, 4th edition, Taylor & Francis, 2002, p 16

[81] Çengel, Y. A., *Heat Transfer: A Practical Approach*, McGraw-Hill, 2nd edition, p 567

[82] Childs, Peter R. N., *Practical Temperature Measurement*, Butterworth-Heinemann, Oxford, London, 2001, p255

[83] Childs, Peter R. N., *Practical Temperature Measurement*, Butterworth-Heinemann, Oxford, London, 2001, p279

[84] Dutton, R. and Lee, E.C., "Surface Temperature Measurement of Current Carrying Objects", *Journal, Instrument Society of America,* vol 6 no 12, December, 1959

[85] Mulford, S.F., "Compensated Thermocouple" *US Patent no. 2,612,779*, October 7, 1952

[86] Kuribayashi, K., "Improvement of the Response of an SMA Actuator using a Temperature Sensor", *Int. J. Robot., Res.10,* 1991, pp 13–20

[87] http://www.dynalloy.com/TechData.html (accessed Aug 28 2009), Dynalloy, Inc. "Flexinol Technical and Design Data",

[88] Croarkin, M., Guthrie, W., Burns, G., Kaeser, M., and Strouse, G., "Temperature-Electromotive Force Reference Functions and Tables for the Letter-Designated Thermocouple Types Based on the ITS-90", *Natl. Inst. Stand. Technol. Monograph 175*; 1993, p 630 (available online at http://srdata.nist.gov/its90/main/, accessed Aug 28 2009)

[89] Gorbet, R.B., Wang, D.W.L, Morris, K.A., "Preisach Model Identification of a 2-Wire SMA Actuator," *Proceedings of the 1998 ICRA,* 1998, pp 2161-2167

[90] Çengel, Y. A., *Heat Transfer: A Practical Approach*, McGraw-Hill, 2nd edition, p 466

[91] Martynenko, O. G., Khramtsov, P. P., *Free-Convective Heat Transfer*, Springer-Verlag Berlin Heidelberg, 2005, pp 229-230

[92] Martynenko, O. G., Khramtsov, P. P., *Free-Convective Heat Transfer*, Springer-Verlag Berlin Heidelberg, 2005, p 244

[93] Çengel, Y. A., *Heat Transfer: A Practical Approach*, McGraw-Hill, 2nd edition, p 874

[94] *Thermocouple Measurement in a Current Carrying Path*, GM Ref. No. P005402, OLG Ref. No. GM1834PUS

[95] Wheeler, A.J., Ganji, A.R., Introduction To Engineering Experimentation, Prentice Hall, Inc., 1996, pp 159 - 161

[96] Teertstra, P., "Models and Experiments for Laminar Natural Convection from Heated Bodies in Enclosures," Department of Mechanical Engineering, University of Waterloo, Waterloo, Ontario, Canada, 2003, pp 192 - 200